

TECHNISCHE UNIVERSITÄT MÜNCHEN

Lehrstuhl für Technische Chemie II

**Catalytic methylenedianiline synthesis
on porous solid acids**

Michael Salzinger

Vollständiger Abdruck der von der Fakultät für Chemie der Technischen Universität München zur Erlangung des akademischen Grades eines

Doktors der Naturwissenschaften (Dr. rer. nat.)

genehmigten Dissertation.

Vorsitzender: Univ.-Prof. Dr.-Ing. Kai-Olaf Hinrichsen

Prüfer der Dissertation:

1. Univ.-Prof. Dr. rer. techn. Johannes A. Lercher

2. apl. Prof. Dr. rer. nat. habil. Peter Härter

Die Dissertation wurde am 25.08.2010 bei der Technischen Universität München eingereicht und durch die Fakultät für Chemie am 17.09.2010 angenommen.

*There is no sadder sight in the world
than to see a beautiful theory killed by a brutal fact.*

Thomas Henry Huxley (1825-95), brit. Zoologe

*For my parents
and always, for Sabine.*

Acknowledgements

First of all I want to thank Professor Johannes A. Lercher for giving me the chance to do my PhD thesis in his group and providing me with such an interesting and challenging research topic. While leaving me on a long line and allowing me to progress through the projects' obstacles according to my own plans and judgment, our discussions always offered fresh ideas, insights and new angles to tackle problems.

Thanks also to Xaver Hecht, for measuring N₂-physisorption and helping me to repair my setups again and again, Andreas Marx for making my computer run, Martin Neukamm for elemental analysis and Thomas Tafelmeier, Ulrike Ammari and Sabine Martinetz of the microanalytical laboratory for CHN analysis. Helen Lemmermöhle, Katharina Thies and Stefanie Maier must not be forgotten, because without them doing all organisations, nothing here could go about its course at all!

Many students did a great job and contributed to the present work. I would like to point out especially Matthias Fichtl, Jennifer Ludwig and Florian Hanus, who spent a lot of time in my laboratory and proofreading this work. Thank you!

Special thanks to all dear colleagues, present and past, who were working alongside me over these three years. While it would be impossible to mention everybody I want to stress out several special people. First of all I want to mention Chang Uk Lee, whom I met in our very first lecture at University and who is up until today one of my best friends and also my best man! Regrettably, he is currently in South Korea, doing his military service. I pray for his safe return and look forward to the day we meet again. Thanks also to Sebastian Baer (a.k.a. McGyver) one of my dearest friends since my first days at University, for providing distraction, T-shirts, cakes and many more useful things. Sarah Maier and Daniela Hartmann have also endured five years of studying alongside me and have furthermore decided to do their PhD thesis also at TC2. Thank you for countless hours of laughing and talking during the last eight years. Without Oliver Gobin and Tobias Förster to break the everyday routine in office 46303, three years of PhD would have definitely been less fun. And without Stephan Reitmeiers' constant urge to shut windows, all of us would have less to sweat (and laugh).

Last but not least I want to mention my parents Josef and Siglinde and my dear wife Sabine and give them very special thanks for all the love and invaluable support they gave me and, above all, for enduring me when I was in a bad temper, which might have happened form time to time...

Abbreviations

Å	Angström
AAS	atom absorption spectroscopy
Al	aluminium
BET	Brunauer-Emmet-Teller
Ca	calcium
CSTR	continuous stirred tank reactor
CTMABr	cetyltrimethylammoniumbromide
DFT	density functional theory
DMSO	dimethylsulfoxide
equ.	equivalent(s)
eV	electronvolt
FID	flame ionization detector
FTC	framework type code
GC/MS	gas chromatography – mass spectrometry
HMI	hexamethyleneimine
HPLC	high-pressure liquid chromatography
(k)J	(kilo)joule
K	kelvin
L	liter
MALDI	matrix-assisted laser desorption ionisation
MDA	methylenedianiline
(m)mol	(milli)mol
min	minute
mL	milliliter
mm	millimeter
µg	microgram
µm	micrometer
Na	sodium
OABA	<i>ortho</i> -aminophenylaniline
Pa	pascal

PABA	<i>para</i> -aminophenylaniline
PFR	plug flow reactor
Ph	phenyl
pMDA	poly-MDA
pPABA	poly-PABA
ppm	parts per million
rpm	rounds per minute
τ	residence time
TEM	transmission electron microscopy
TEOS	tetraethylorthosilicate
TMAOH	tetramethylammoniumhydroxide
TOF	time-of-flight
TOF	turn over frequency
TPAOH	tetrapropylammoniumhydroxide
TPD	temperature programmed desorption
TUM	Technische Universität München
wt %	weight percent
XRD	X-ray diffraction

TABLE OF CONTENTS

1	GENERAL INTRODUCTION.....	1
1.1	POLYURETHANES.....	2
1.2	METHYLENEDIANILINE (MDA) PRODUCTION.....	3
1.3	REACTION MECHANISM – STATE OF THE ART.....	6
1.3.1	<i>Non-catalytic condensation of aniline and formaldehyde to N,N'-diphenylmethylenediamine (aminal).....</i>	7
1.3.2	<i>Catalytic rearrangement of aminal to benzylanilines.....</i>	7
1.3.3	<i>Acid catalyzed rearrangement of benzylamine-intermediates into MDA.....</i>	8
1.4	ALUMINOSILICATES AS SOLID ACID CATALYSTS.....	10
1.4.1	<i>Zeolites.....</i>	10
1.4.2	<i>Mesoporous Aluminosilicates.....</i>	20
1.5	SCOPE OF THE THESIS.....	28
2	REACTION NETWORK AND MECHANISM OF THE SYNTHESIS OF METHYLENEDIANILINE OVER DEALUMINATED Y-TYPE ZEOLITES.....	35
2.1	INTRODUCTION.....	36
2.2	METHODS.....	38
2.3	RESULTS.....	42
2.3.1	<i>Catalyst characterization.....</i>	42
2.3.2	<i>Time concentration profiles.....</i>	44
2.3.3	<i>Temperature dependence.....</i>	50
2.3.4	<i>Reaction orders.....</i>	52
2.3.5	<i>Influence of aminal to aniline ratio.....</i>	52
2.4	DISCUSSION.....	54
2.4.1	<i>Reaction network and mechanism.....</i>	54
2.4.2	<i>Simulation of the reaction network.....</i>	59
2.5	CONCLUSION.....	72

3	ON THE INFLUENCE OF PORE GEOMETRY AND ACIDITY ON THE ACTIVITY OF PARENT AND MODIFIED ZEOLITES IN THE SYNTHESIS OF METHYLENEDIANILINE	75
3.1	INTRODUCTION.....	76
3.2	METHODS.....	78
3.2.1	<i>Materials</i>	78
3.2.2	<i>Characterization</i>	82
3.2.3	<i>Catalytic reaction</i>	83
3.2.4	<i>Modeling</i>	84
3.3	RESULTS.....	85
3.3.1	<i>Catalyst characterization</i>	85
3.3.2	<i>Catalytic reaction</i>	94
3.4	DISCUSSION.....	95
3.5	CONCLUSION.....	103
4	INVESTIGATIONS ON THE DEACTIVATION OF ALUMINO-SILICATE CATALYSTS DURING METHYLENEDIANLINE SYNTHESIS.....	108
4.1	INTRODUCTION.....	109
4.2	METHODS.....	113
4.2.1	<i>Materials</i>	113
4.2.2	<i>Characterization</i>	115
4.2.3	<i>Chemical pulping of deactivated zeolite</i>	115
4.2.4	<i>Catalytic reaction</i>	116
4.2.5	<i>Continuous lifetime testing setup</i>	118
4.3	RESULTS.....	120
4.3.1	<i>Catalyst characterization</i>	120
4.3.2	<i>Chemical pulping of deactivated zeolite</i>	124
4.3.3	<i>Catalytic reaction</i>	125
4.3.4	<i>Continuous lifetime testing</i>	125
4.4	DISCUSSION.....	130
4.5	CONCLUSION.....	134
5	SUMMARY/ZUSAMMENFASSUNG.....	137

Chapter 1

General Introduction

Methylenedianiline (MDA) is an important starting material for the production of polyurethanes. It is industrially produced from aniline and formaldehyde in an acid catalyzed process. Most commonly mineral acids, such as HCl, are applied as catalysts. As this poses plant engineering and environmental problems, it is of great commercial interest to replace mineral acids in the process by solid acid catalysts. Zeolites are among the most promising candidates for choice of such catalysts, as they provide strong Brønsted acidity, high thermal and mechanical stability and tailor able acid site density and porosity. However, first studies in this field revealed that the formation of MDA from aniline and formaldehyde over zeolite catalysts is heavily limited by pore diffusion and the catalysts tend to deactivate very fast. The aim of this study to reveal the reaction network and mechanism involved in the formation of MDA over solid acid catalysts to identify the critical parameters for the catalysts' activity and lifetime and to understand and describe the processes leading to catalyst deactivation. Distinct goal of the project is the development of a catalyst with high activity and improved lifetime behavior based on a profound understanding of the above mentioned reaction parameters.

1. Introduction

1.1 Polyurethanes

Polyurethanes are widely used for the production of elastic foams (mattresses, cushions, car seats, earplugs), rigid foams (insulation materials, water heaters, refrigerated transport), rigid and flexible moldings with compact skins, window frames and engineering moldings with high hardness and elasticity including high performance adhesives and sealants.¹ The consumption of polyurethanes in Western Europe amounts to 10.4 million metric tons per year.² China is already the biggest polyurethane market in the world, and forecast to grow at a remarkable 10% per year within the next 12 years, with downstream customer industries growing at similar rates.³

The first essential component of a polyurethane polymer is an isocyanate. The applied isocyanates can be classified as aromatic, such as diphenylmethane diisocyanate (MDI), and aliphatic, such as hexamethylene diisocyanate (HDI) or isophorone diisocyanates (IPDI).

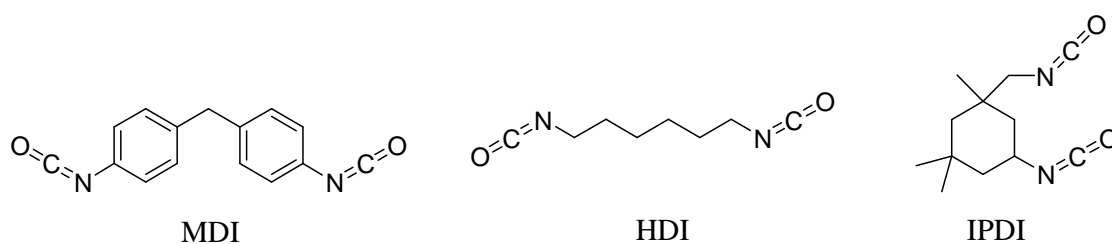


Figure 1: Isocyanates for the production of polyurethanes.

Volume wise, aromatic isocyanates account for the vast majority of global diisocyanate production, as the aromatically linked isocyanate group is significantly more reactive than the isocyanates linked by aliphatic chains. Furthermore, aromatic isocyanates are more economical to use. Aliphatic isocyanates are only applied if special properties are required for the final product. For example, light stable coatings and elastomers on polyurethane basis can only be obtained with aliphatic isocyanates.⁴ One of the key

precursors for the production of the most common aromatic diisocyanate, diphenylmethane diisocyanate (MDI), is 4,4'-Methylenedianiline (Diaminodiphenylmethane or MDA). MDI is produced from MDA by reaction with two equivalents of phosgene.

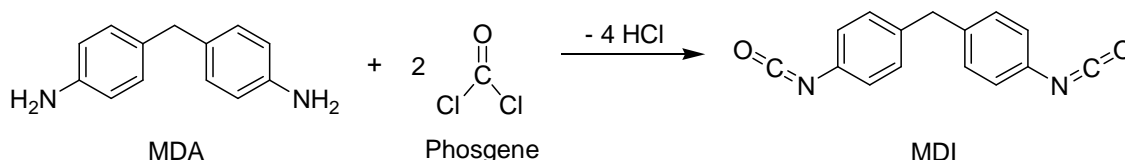


Figure 2: Synthesis of diphenylmethane diisocyanate (MDI) from methylenedianiline (MDA).

MDI is further converted to polyurethanes by reacting with polyols. This polymerization reaction is catalyzed by tertiary amines, such as dimethylcyclohexylamine, or organometallic compounds, such as dibutyltin dilaurate or bismuth octanoate.⁴⁻⁶

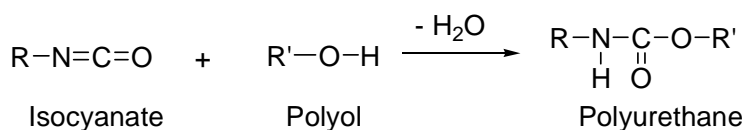


Figure 3: Generalized polyurethane formation reaction.

In 1999, 1.02 million metric tons of MDI were produced in U.S. and 1.08 million in Western Europe with an average annual growth rate of 7% in the U.S. and 5% in Western Europe in the past 5 years.⁷ In addition to the polyurethane production, about 4000 t of MDA are annually used as hardener for epoxy resins, hardener in adhesives and intermediate in the manufacture of other high-performance polymers.⁸

1.2 Methylenedianiline (MDA) production

Industrial amounts of MDA are produced by the condensation of aniline with formaldehyde to *N,N'*-diphenylmethylenediamine (further referred to as "aminal") and a

following rearrangement reaction catalyzed by hydrochloric acid. The reaction is currently performed by adding formaldehyde to stoichiometric amounts of hydrochloric acid and aniline at 60-80°C in an agitated reactor.⁹ The reaction mixture is then heated to 100-160°C for about 1 h to complete the rearrangement reaction. The stoichiometric amount of HCl is needed as the resulting amine is forming hydrochlorides. MDA is yielded as the major component of a technical mixture with a varying content of tri- and polymers with varying substitution patterns (*ortho* and *para*), which is processed to polyurethane without further purification. The presence of 2,4'-MDA and MDA polymers is not only not hindering the ongoing conversion, but is vital for the properties of the resulting polyurethane.

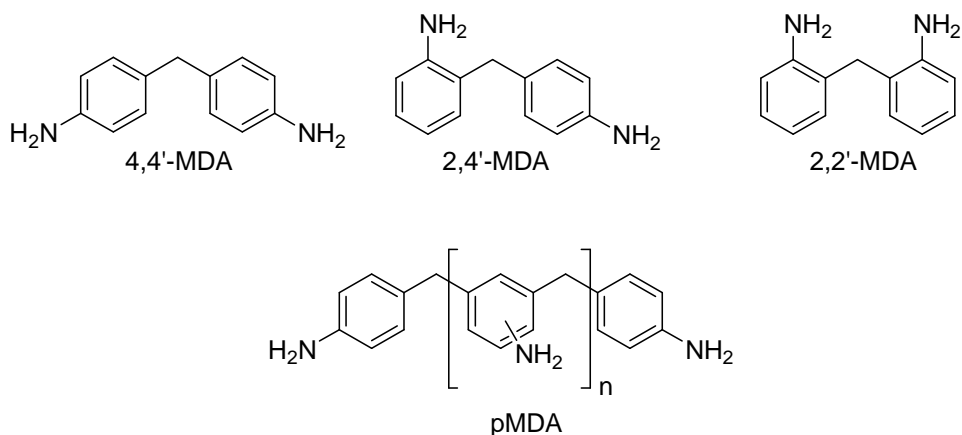


Figure 4: MDA isomers.

The use of hydrochloric acid as catalyst in this reaction causes several problems, including the handling of hydrochloric acid, which corrodes storage and disposal containers and requires the construction of important parts of using special and expensive materials that can resist such corrosion. Furthermore, a large environmental problem is caused by the necessity of neutralizing the hydrochlorides prior to further conversion to MDI. This process does not only consume stoichiometric amounts of NaOH, but also forms about 590 kg of aniline-contaminated sodium chloride per ton of MDA. The separation of this phase is often a difficult and undesirable energy-consuming process. An overview of the process is shown in Figure 5.^{10,11}

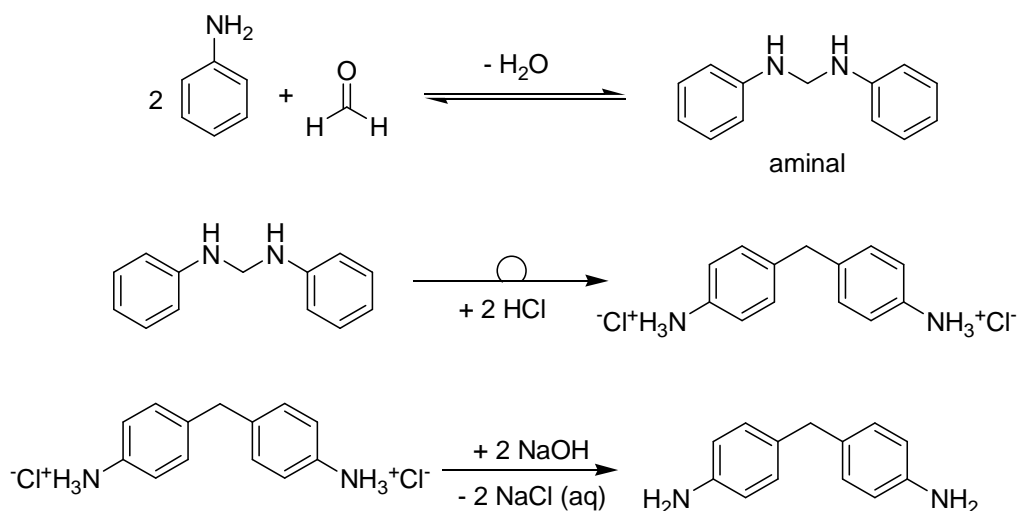


Figure 5: Formation of aminal, hydrochloride and MDA.

Due to these major drawbacks, which are aligned to the use of HCl as catalyst, it is of considerable commercial interest to substitute the mineral acid by a solid acid catalyst. Moreover, a solid catalyst could be regenerated, lowering the total cost of raw materials. Numerous efforts have been made during the last years to replace liquid mineral acids, such as HCl, by solid catalysts. Ion-exchanged resins, clays, intermetallic compounds and zeolites are only some of the materials that have been proven to be possible catalysts for the process.¹²⁻¹⁹

However, intermetallic compounds present a serious problem for the synthesis of MDA: a considerable amount of *N*-methylated-MDA (6.1-8.6% of reaction products), is produced during the reaction. *N*-methylated-MDA is a very noxious byproduct in MDA synthesis because it can not be transformed into MDI through the reaction with phosgene.²⁰ Having only one isocyanic group per mole, *N*-methylated MDA interrupts the polymerization chain and the free acidity of the *N*-methylated amine lowers the stability of the polyurethane polymer.

The productivities reported for ion-exchange resins (styrene-divinylbenzene containing sulfonic groups and tetrafluoroethylene-perfluorovinylether containing sulfonic groups (Nafion)) are not adequate for industrial development, although their selectivity to MDA was found to be very high. The maximum performance of 4.95 and

2.47 g(MDA)/g(catalyst) is still very poor in comparison with zeolites (260 g(MDA)/g(zeolite)).²¹

Zeolites can achieve higher aminal conversion, higher activity and better selectivity to MDA in comparison to other solid acid catalysts.¹¹ Thus, zeolites such as FAU, BEA, silylated BEA and ERB-1 have shown a clear improvement for the reaction.^{12,13} Previously, Perego *et al.*¹⁰ have screened various solid acid catalysts. They confirmed that zeolites seem to be the most promising alternatives in terms of activity and stability to catalyze this reaction. According to the large dimension of the aromatic molecules involved in the reaction, one can deduce that mesoporous materials or large pore zeolites should be good candidates to catalyze this reaction. Corma *et al.*¹¹ have also suggested that this process could be controlled by diffusion. They have claimed that the use of delaminated zeolites, such as ITQ-2, ITQ-6 and ITQ-18, causes a significant gain in activity. It has been found that ITQ-2 exhibits a much lower rate of deactivation than other zeolites and aluminosilicates tested so far. The improved catalyst lifetime is attributed to the molecular diffusion and faster desorption of products inherent to a process taking place in the outer shell of the catalyst. It is noticeable that the structured external surface of ITQ-2 has an important influence in the product selectivity.

1.3 Reaction Mechanism – state of the art

The reaction network and mechanism of the formation of MDA from aniline and formaldehyde over solid acid catalysts has, to the best of our knowledge, not been studied in detail so far. In literature¹⁰⁻¹², the reaction network is roughly divided into three main steps:

1. The uncatalyzed formation of aminal by condensation of aniline with formaldehyde.
2. The acid catalyzed rearrangement reaction of the aminal to intermediate benzylaniline species.
3. The acid catalyzed rearrangement of the intermediates to MDA isomers.

1.3.1 Non-catalytic condensation of aniline and formaldehyde to *N,N'*-diphenylmethylenediamine (aminal)

N-phenylaminomethanol is formed by the reaction of aniline with formaldehyde. The *N*-phenylaminomethanol then forms a Schiff base by loss of water. The excess aniline will react with the Schiff base to form the aminal, which is stable up to 50 °C in the absence of an acid catalyst. As it hinders the activity of the applied catalyst, the water produced in this step is removed before further reaction.

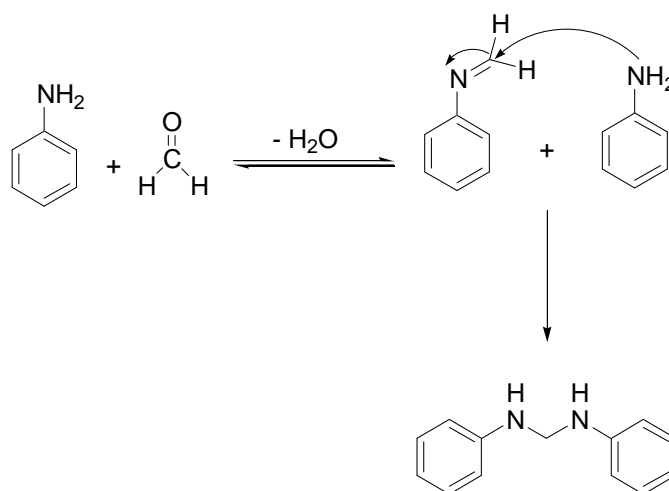


Figure 6: Reaction of aniline with formaldehyde.

1.3.2 Catalytic rearrangement of aminal to benzyanilines

The following rearrangement step requires an acid catalyst, such as a zeolite. The amino-group of the aminal is protonated by a Brønsted acid, resulting in the dissociation of the aminal into a molecule of aniline and a carbocation, which can react by an electrophilic substitution with an aromatic compound (e.g. aniline) and form the *para* and *ortho*-aminobenzylanilines PABA and OABA.⁹

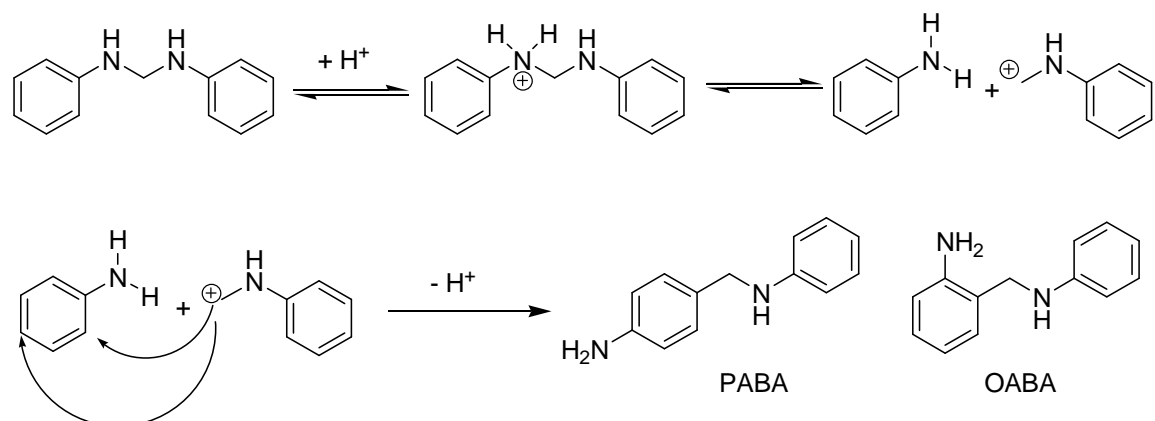


Figure 7: Reaction mechanism for the rearrangement of aminal into PABA and OABA.

The formation of PABA and OABA is very rapid. While the concentration of PABA and OABA in the reaction mixture grows quickly, the concentration of aminal decreases drastically. The formation of PABA is favoured, according to the lowest steric hindrance of the *para*-position compared to the *ortho*-position.⁹

1.3.3 Acid catalyzed rearrangement of benzylamine-intermediates into MDA

The benzylamines themselves are converted to MDA isomers in a further acid catalyzed rearrangement reaction. According to Perego *et al.*⁹, the reaction proceeds *via* a benzylic carbenium ion, which reacts with aniline yielding MDA. It is proposed that the catalyst protonates the secondary amine and splits the PABA and OABA into two molecules, aniline and a *p*-aminobenzyl carbenium ion in case of PABA or a *o*-aminobenzyl carbenium ion in case of OABA. The reactive carbenium ions attack either the electron rich *ortho* or *para* position of aniline, producing the different isomers of MDA (2,4'-MDA, 4,4'-MDA and small traces of 2,2'-MDA). According to the steric hindrance, 4,4'-MDA is the favoured product. This reaction is considered to be the rate determining step. However, the existence of these carbenium ions is not clarified at the present time.

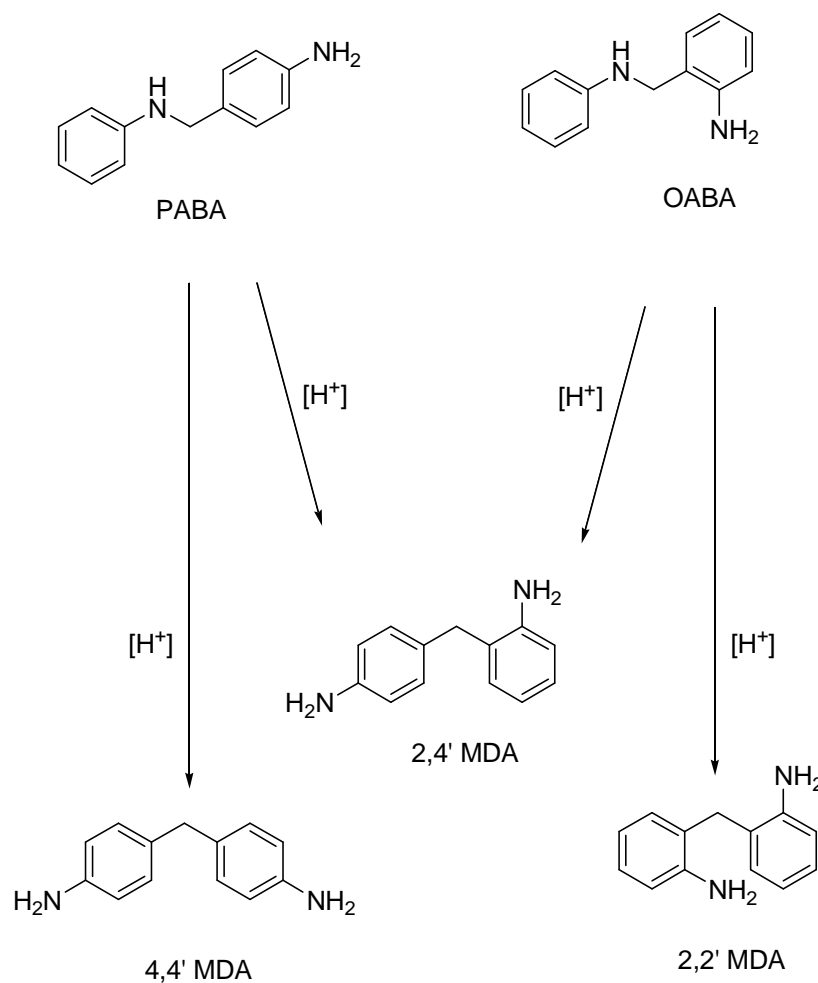


Figure 8: Rearrangement of PABA and OABA into MDA isomers.¹²

The most important variables affecting the product distribution are the molar ratio of aniline to aminal and the temperature. High concentrations of aminal and high reaction temperatures favor the formation oligomeric MDA species. On the other hand, the choice of catalyst seems to have little influence on the final product distribution. Only BEA-type zeolites display an increased selectivity to 2,4'-MDA. However, the reason for this behavior is not fully understood until now, though some theories state a correlation between 2,4'-MDA formation and the density of strong Brønsted acid sites.¹²

All authors agree that the reaction is limited by pore diffusion of the bulky reactant species through the micropores, if zeolites are applied as catalysts, as the pores themselves are of similar size as the reactants. In order to bypass this limitation, the use

of mesoporous materials, such ITQ-2 and MCM-41¹¹ or nanosized materials with large external surface¹², was proposed.

The main problem of all solid acid catalyst tested so far is deactivation. None of the proposed catalysts showed lifetimes that would make an industrial process based on a solid acid catalyst feasible. However, the processes leading to catalyst deactivation are not understood so far.

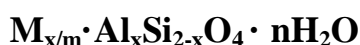
1.4 Aluminosilicates as solid acid catalysts

1.4.1 Zeolites

General Introduction

Zeolites are crystalline microporous (alumino-)silicates of natural or synthetic origin with highly ordered structures and *micropores* of molecular dimensions (pore diameter <20 Å). They occur naturally in the vugs of basaltic lava, in volcanic deposits from saline, alkaline lakes and non-marine tuff beds. The term zeolite was coined in 1756 by Axel Fredrik von Cronstedt.²² He found that the material stilbite can produce a large amount of steam from water which had been adsorbed previously by the material. Therefore, he named the material “zeolite”, from the Greek words *zeo*, meaning “to boil”, and *lithos* for “stone”.

The general empirical formula for a zeolite’s composition is:

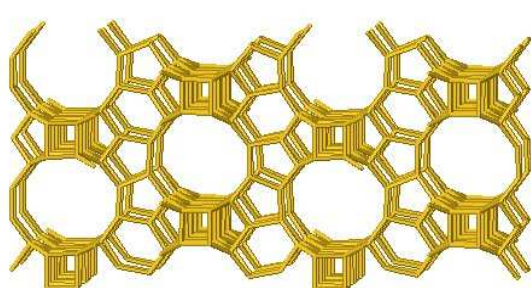
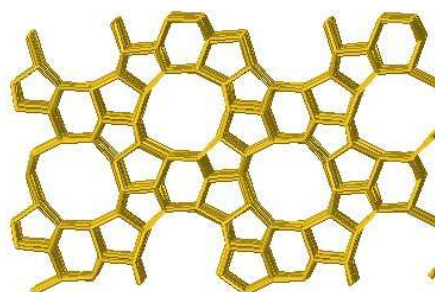


where m is the valence of the cation M , n is the water content and x the Al content ($0 \leq x \leq 1$). The structure of a zeolite is composed of a three-dimensional supporting network filled with loosely bound exchangeable cations and adsorbed phase. The building blocks of the underlying network are TO_4 tetrahedral. The central T atom is most commonly a silicon or aluminum atom, or more rarely a phosphorus, titanium, gallium or iron atom. Thus, the framework of a zeolite is made of aluminium and silicon tetrahedral with the restriction that, according to Lowenstein’ rule, two AlO_4 tetrahedral will never lie side by side.²³

Zeolites are industrially produced since the middle of the 1950s and have then mainly been used as adsorbents and ion exchangers. In 1959, Y-type zeolite (a synthetic faujasite) was first used as catalyst by Union Carbide. In 1972, Mobil Oil (foremost Socony) developed a whole new family of pentasil materials. The most important of these pentasils is ZSM-5. In the 1980s, zeolites were used to replace phosphates in washing agents. Today, zeolites find wide application in catalysis (FCC cracking, hydroisomerization), water purification, detergents for washing agents and construction (additive to asphalt concrete or Portland cement).

Common Properties

The backbone structure of a zeolite is constructed of TO_4 tetrahedral units linked by shared oxygen corners, yielding a network-like pattern. This pattern replicates periodically, giving rise to well-organized arrays of channels that comprise topological characteristics specific to the zeolites.²⁴ The resulting framework does not depend on specific cations, adsorbent phase, chemical composition, or physical and mechanical properties of the zeolite crystals. Following the rules set up by the Commission on Zeolite Nomenclature of the International Union of Pure and Applied Chemistry,²⁵ a distinct framework type is labeled by a framework type code (FTC) denoted by three capital letters. FTCs are assigned and curated by the Structure Commission of the International Zeolite Association (IZA).²⁶ The search for novel framework is up until now an actively pursued research area. Currently, 191 distinct framework types have been approved by IZA, including 5 frameworks approved in the first half of 2009 and 10 others in 2008.^{26,27}

**BEA****MFI**

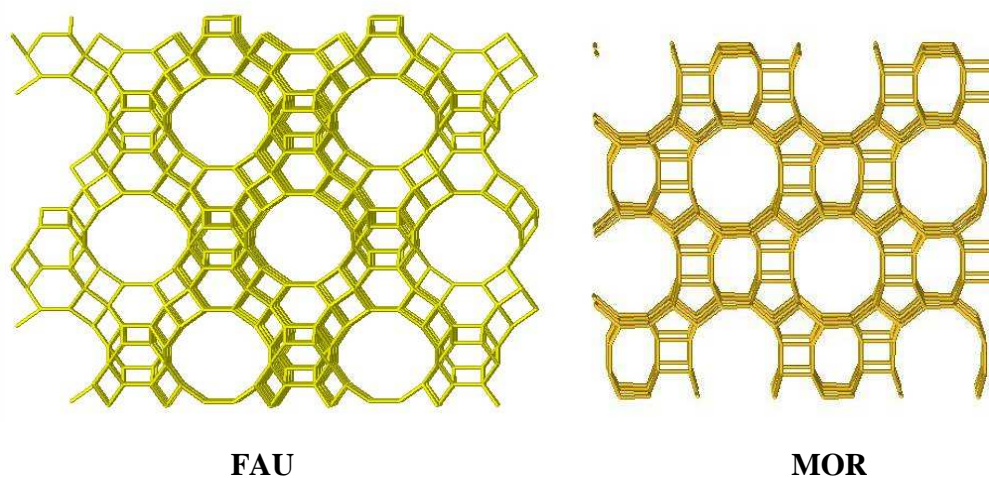


Figure 9: Several zeolite frameworks.²⁸

By replacing a silicon atom with a net +III charge in the framework by an aluminum atom, which only carries a +III charge, a net negative charge is introduced to the framework. To compensate this charge, a wide variety of cations, such as H^+ , Na^+ , K^+ , Ca^{2+} , etc. are held in the pores and cages of a zeolite.²⁹ These cations do not only allow zeolite crystals to be used in ion-exchange processes, but they also create a strong Brønsted acid site if a proton is used as counter ion. The oxobridges on the other hand exhibit Lewis base properties.

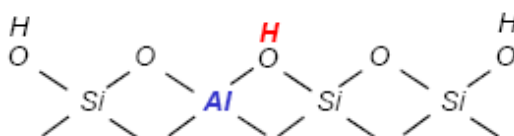


Figure 10: Brønsted acid site generated by substitution of Si with Al.³⁰

For Brønsted acidity both the density and actual strength of the acid sites are important in catalysis. While sites of different strength may be able to catalyze different reactions - e.g. only very strong Brønsted acid sites are active in fluid catalytic cracking³¹ - the density of such sites is directly correlated with the catalyst's actual activity. Brønsted acidity is influenced by both the chemical composition and by the lattice structure of the zeolite (topography). The density of acid sites is directly related to the Si/Al ratio: The lower the ratio of Si/Al, the higher the concentration of acid sites.

On the other hand, as the density of aluminum atoms in the framework increases, the actual strength of the Brønsted acid sites decreases. Quantum chemical calculations indicate that this effect has its origin in the lower electronegativity of aluminum *versus* silicon atoms in the vicinity of a given Al-OH group.³²

Apart from their acidity, which can be tailored in both acid strength and site density to meet the requirements of an application, zeolites offer a second interesting property related to their structure. Zeolites have a highly ordered crystal structure with regular pores being present. These micropores (3 -20 Å for common zeolites) are of similar size as common reactant molecules, endowing these molecular sieves with a special property known as shape selectivity. This refers to the selectivity achieved in heterogeneous catalysis reactions, which depends specifically on the pore diameter or framework architecture of the microporous material and the size of the reactants. One distinguishes between three types of shape selectivity:

- Reactant selectivity: Only starting materials below a certain size can enter into the interior of the zeolites' pore system and undergo the catalytic reaction at the active sites in the micropores.
- Product selectivity: Only products of a certain size and/or shape can exit from the pore system. Larger products are retained and converted again until a smaller product is formed, which is then able to exit the pore system.
- Restricted transition state selectivity: This form of shape selectivity depends on the fact that chemical reactions often proceed *via* intermediates. Only those intermediates that are geometrically fitting into the zeolite cavities can be formed during catalysis, exit the pore system and turn into the desired product.

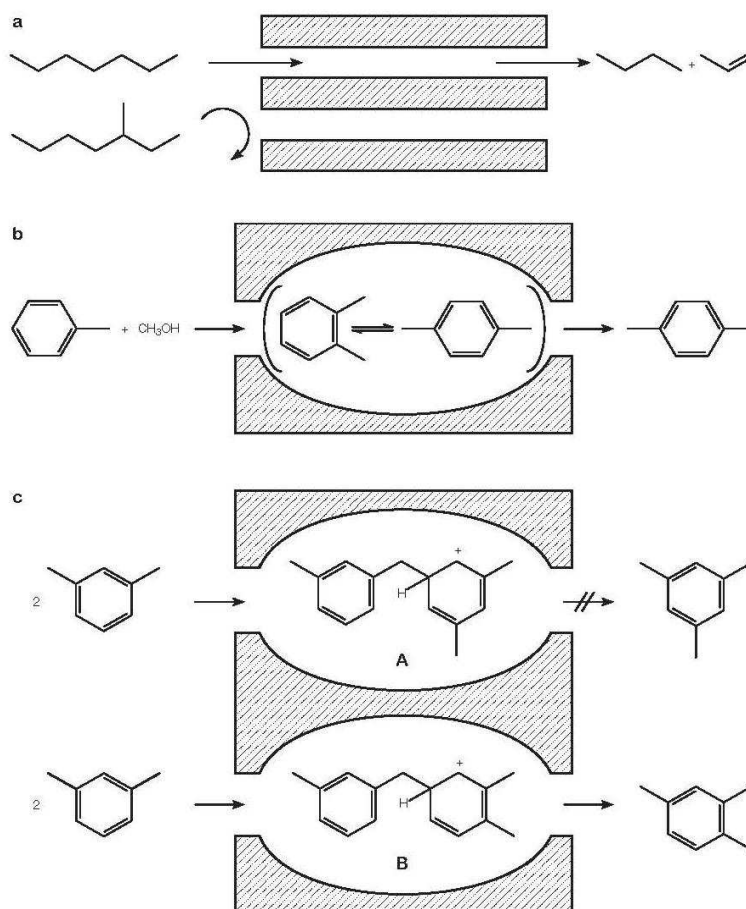


Figure 11: Shape selectivity of zeolites; a) reactant selectivity; b) product selectivity; c) restricted transition state selectivity.³³

In the following pages, the frameworks and properties of the zeolites and other aluminosilicates, which were applied in this thesis, are discussed in more detail.

BEA-type zeolite

Zeolite Beta, a large pore, high-silica zeolite was first reported in a US Patent issued to Mobil Oil Corporation in 1967. It has been demonstrated to be useful in several hydrocarbon conversion processes, such as cracking, hydrocracking, dewaxing, dealkylation and isomerization of n-alkanes.^{34,35} Zeolite Beta crystallizes in a tetragonal structure with 12-membered ring channels ($6.6 \times 6.7 \text{ \AA}$) in one room direction, which are crossed with a second type of 12-membered ring channels ($5.6 \times 5.6 \text{ \AA}$) in a second direction. Figure 12 shows a model of zeolite Beta, viewed along the 100 plane. One set of 12-membered pores is running perpendicular to the projection plane, opening “out of the sheet”, while the second set of 12-membered pores is running from left to right within the projection plane. As these two pore systems are interconnected, they can be regarded as “*communicating vessels*”, in which reactants can easily pass from one pore to another.

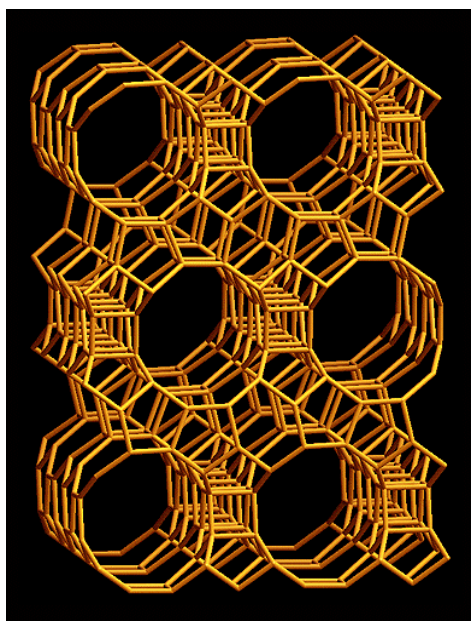


Figure 12: Model of the zeolite Beta pore structure viewed along (100).²⁸

MFI-type zeolite

MFI-type zeolite is a highly porous material and has an intersecting two-dimensional pore structure. It has two types of pores, straight 10-membered ring channels ($5.1 \times 5.5 \text{ \AA}$) and intersecting 10-membered ring channels ($5.3 \times 5.6 \text{ \AA}$) which are not straight but sinusoidal. This two-dimensional pore structure allows molecules to move from one point in the catalyst to anywhere else in the particle.

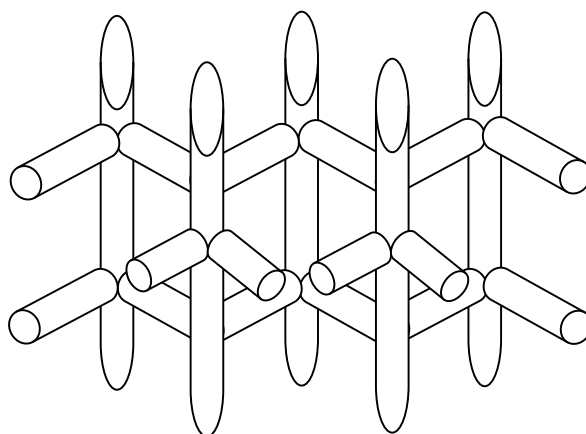


Figure 13: Schematic pore structure of ZSM-5.

ZSM-5 is one of most important zeolites with structure type MFI. It is also one of the most versatile catalysts ever found. It was discovered in 1972 by researches of Mobil Oil (foremost Socony),³⁶⁻³⁸ who were looking for novel zeolite materials based on pentasils. The new materials discovered by this group were named ZSMs, -Zeolite Socony Mobile-, after the type of material (zeolites) and the company which discovered them (Socony and later Mobil Oil). The abbreviation ZSM is followed by a running number, simply giving the chronological order of their discovery.

As ZSM-5 is a zeolite with a high Si/Al ratio, it displays strong acidity, resulting in high activity in processes catalyzed by strong Brønsted acids, such as isomerization. Therefore, zeolite ZSM-5 is widely used in the petroleum industry as a heterogeneous catalyst for hydrocarbon isomerization reactions.³⁹

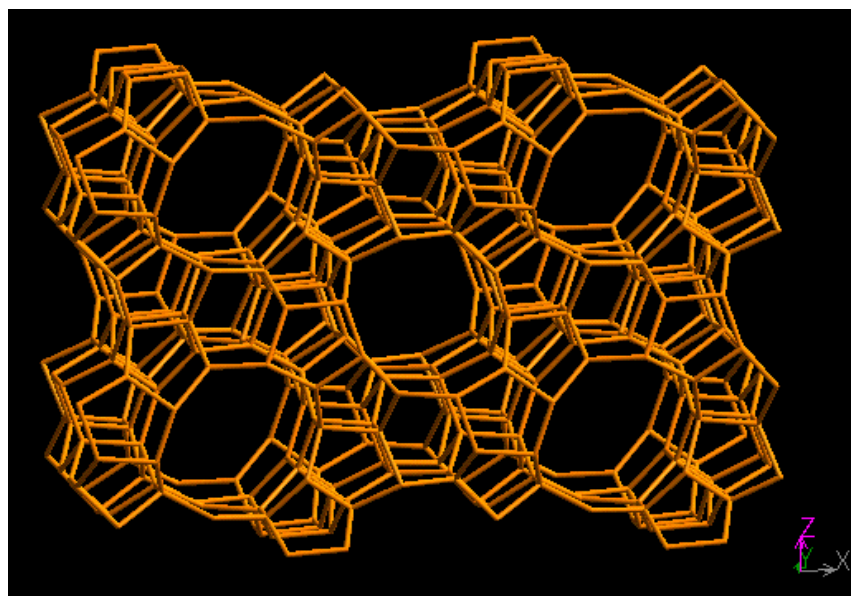


Figure 14: Model of the MFI pore structure viewed along (010).²⁸

FAU-type zeolite

The abbreviation FAU refers to the small family of rare natural silicate minerals of faujasites, namely *faujasite-Na*, *faujasite-Ca* and *faujasite-Mg*. Faujasite was first discovered in 1842 by M. Damour in Sasbach am Kaiserstuhl and is named for Barthélemy Faujas de Saint-Fond, a French geologist and volcanologist.⁴⁰ Apart from this rare natural form, synthetic zeolites X and Y have an identical structure.

The faujasite framework consists of sodalite cages connected through hexagonal prisms. The pores are arranged perpendicular to each other. The pores, which are formed by 12-membered rings, have a relatively large diameter of 7.4 Å. The inner cavity (supercage) has a diameter of 12 Å and is surrounded by 10 sodalite cages. Zeolite Y has a void fraction of 48 % and thermally decomposes at 793 °C.⁴¹ Depending on the silica-to-alumina ratio of their framework, synthetic faujasite zeolites are divided into X and Y zeolites. In X zeolites that ratio is between 2 and 3, while in Y zeolites it is 3 or higher. The stability of the zeolite increases with the Si/Al ratio of the framework. It is also affected by the type and amount of cations located in non-framework positions. For catalytic cracking, zeolite Y is often used in a Lanthanum-exchanged form.⁴²

By using thermal, hydrothermal or chemical methods, some of the alumina can be removed from the Y zeolite framework, resulting in high-silica Y zeolites with increased stability. Both common Y-type and USY-type (ultra stable Y) zeolites are used as catalysts in fluid catalytic cracking and hydrocracking to convert high-boiling fractions of petroleum crude to more valuable gasoline, diesel and other products. Zeolite Y has superseded zeolite X in this field because, due to the higher Si/Al ratio, it is both more active and more stable at high temperatures. It is also used in hydroisomerization units as a platinum/palladium support to increase the octane number of reformulated refinery products.⁴²

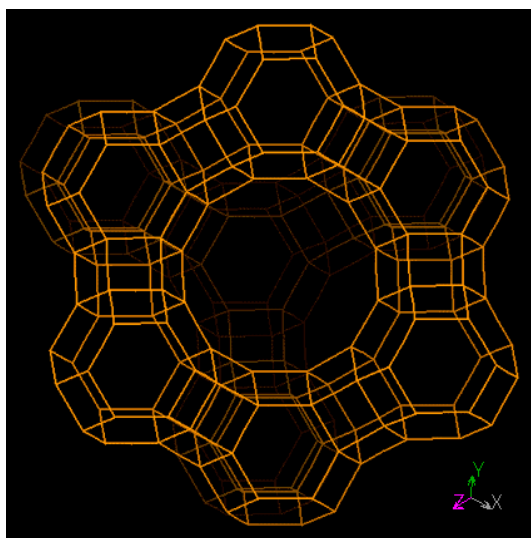


Figure 15: Model of the zeolite FAU pore structure viewed along (100).²⁸

MOR-type zeolite

Mordenite is a naturally occurring mineral that can be found e.g. in India, Canada, USA and Central Europe. It was first described by Henry How in 1864. He named it after the small community of Morden in Canada where it was first discovered.⁴³

Mordenite-type Zeolite (MOR) has orthorhombic crystal structure with straight 12-membered ring channels ($6.5 \times 7.0 \text{ \AA}$) and crossed slit shaped 8-membered ring channels ($2.8 \times 5.7 \text{ \AA}$). Synthetic mordenite finds some application in the petrochemical industry as catalyst for isomerization reactions.

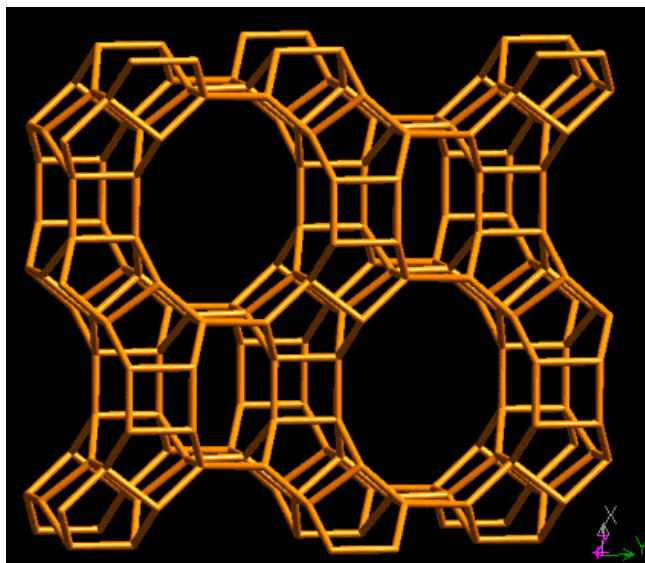


Figure 16: Model of the zeolite MOR pore structure viewed along (001).²⁸

MCM-22 framework

MCM-22 has an MWW-type framework consisting of a two dimensional sinusoidal channel system within hexagonal sheets, accessible through 10-membered ring apertures. One of these pore systems is defined by two-dimensional, sinusoidal channels ($4.0 \text{ \AA} \times 5.5 \text{ \AA}$), while the other consists of larger supercages, whose inner free diameter (7.1 \AA) is defined by a 12-membered ring with an inner height of 18.2 \AA . These coexisting pore systems may provide opportunities for a wide variety of catalytic applications in the petrochemical and refining industry.⁴⁴ MCM-22 with mid-strong acidity may also obtain a high catalytic activity and selectivity for alkylation of toluene with methanol. By swelling and following delamination, the MWW layers of MCM-22 can be separated, thus producing mesoporous materials, such as MCM-36 and ITQ-2.

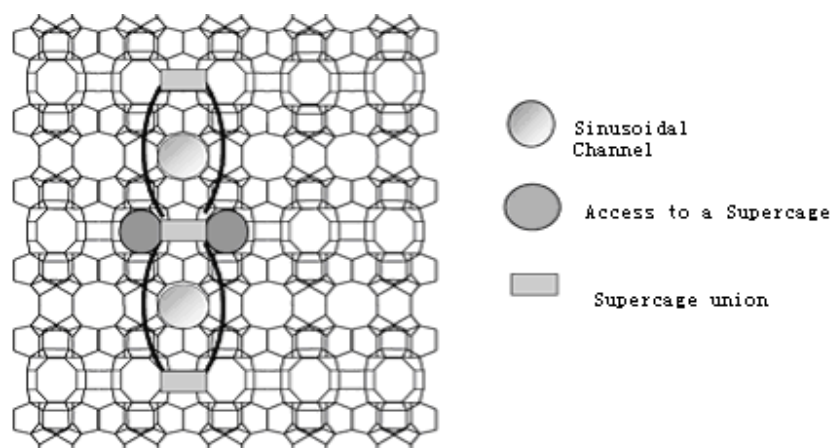


Figure 17: Proposed structural model for MCM-22.⁴⁴

1.4.2 Mesoporous aluminosilicates

General Introduction

While the use of zeolites as solid acid catalysts provides the above mentioned advantages of tailorable acidity (both density and strength), regular structure and thereby shape selectivity, high thermal and mechanical stability and rather low costs, their application as catalysts regularly faces one problem: mass transport limitation. As most reactant molecules are of similar size as the zeolites' pores themselves (which is indeed vital for shape selectivity), diffusion of these molecules through the pores is very slow, resulting in pore diffusion limitation.¹⁰⁻¹² This limitation can be bypassed or overcome by the application of aluminosilicates with larger pores are applied. Their pore diameters are then in the range of 2 – 50 nm and are referred to as *mesopores*. There are numerous possibilities to create mesoporous aluminosilicates, of which the most important are:

- The application of amorphous aluminosilicates, which are already mesoporous, but unordered after their synthesis. They can for example be prepared by co-condensation of silicon- and aluminumalkoxides without the addition of any structure directing additives (SDA).
- The generation of mesopores in a preformed zeolite framework by dealumination by steaming.

- The generation of mesopores in a preformed zeolite framework by desilication by alkaline leaching.
- Delamination of a layered zeolite precursor.
- Synthesis of ordered aluminosilicates, such as SBA-15, MCM-41 or KIT-6.

While amorphous aluminosilicates are easy and cheap to synthesize, their unordered structure and relatively low acid site density makes them rather poor catalysts for acid catalyzed processes, as was already shown in previous work.^{11,12} The generation of mesopores by steaming is a well established technique and is applied in technical scale for the preparation of USY catalysts from common zeolite Y by treatment with steam, leading to dealumination of the zeolite framework. As vast amounts of Al are removed from the zeolite framework (Si/Al ration increases from 2.5 up to 40) during this treatment, holes and cavities, which act as mesopores, are created.⁴⁵⁻⁴⁷

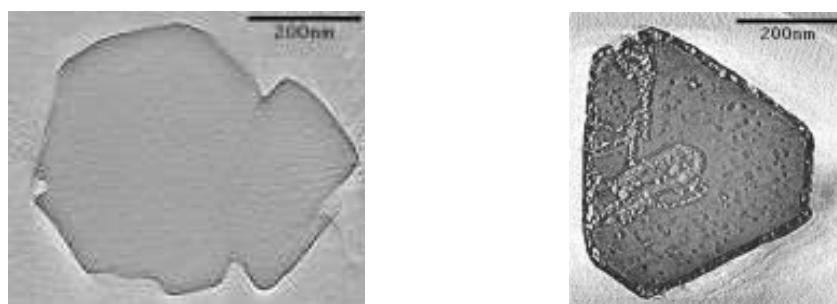


Figure 1.18: *left: 3D TEM reconstruction of a parent Na-Y crystal, right: 3D TEM reconstruction of a steamed Na-USY crystal.*⁴⁷

Very similar effects can be achieved by removing Si instead of Al from the framework by treatment with NaOH. The advantage of this method is that desilication, in contrast to dealumination, does not result in a loss of acid site density.⁴⁸

The delaminated materials ITQ-2 and MCM-36 are both prepared from MCM-22 and will be discussed in more detail later.

Ordered mesopores materials have attracted special attention in many fields, including adsorption, separation and catalysis since the discovery of M41S by Mobil's researchers in 1992.^{49,50} For the synthesis of such materials, it is necessary to preform a liquid crystal

from an organic template (e.g. Cetyltrimethylammoniumsalts CTMA in case of MCM-41 or polymers such as P123 in case of SBA-15 and KIT-6), which is then serving as a matrix around which the (alumino-)silicate grows. After complete condensation of the silica material under hydrothermal conditions, the organic template is removed by calcination.

Such aluminosilicates exhibit large uniform pore size, high surface area, high thermal and hydrothermal stability and relatively high acid strength. Therefore, materials such as Al-MCM-41, Al-SBA-15, Al-KIT-6, possess great potential for acid catalyzed reactions involving large reactant molecules. The large pores of those materials could alleviate diffusion problems present even in the best zeolites.

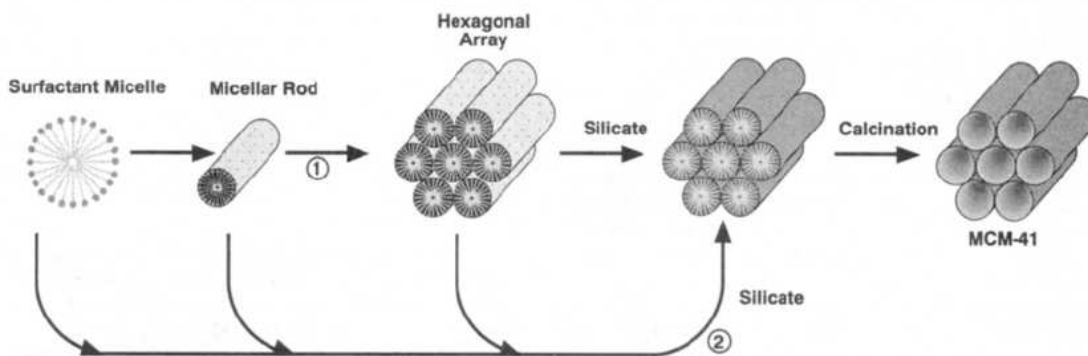


Figure 1.19: Possible mechanistic pathways for the formation of MCM-41: (1) liquid crystal phase initiated and (2) silicate anion initiated.⁵⁷

Delaminated materials: ITQ-2 and MCM-36

Both ITQ-2 and MCM-36 are prepared by delamination of the MWW-layers of a MCM-22 precursor (MCM-22(P)). While the MWW layers are randomly orientated in ITQ-2, they are neatly stacked and supported by silica “pillars” in case of MCM-36, thus generating regular mesopores between the layers. In a MCM-22(P) material, the MWW layers are already formed, but organic template (hexamethyleneimine HMI) trapped between the layers prevent them from condensing and thereby forming the final MCM-22 framework, which was already described earlier. Upon calcination of MCM-22(P), the organic template is removed and the MWW layers can condense and form MCM-22. However, it is possible to replace the HMI template by an even larger one

(Cetyltrimethylammonium-ions CTMA^+), thus further separating the MWW layers. This CMTA exchanged precursor is commonly referred to as swollen MCM-22. It is now possible to separate the layers completely by ultrasonic treatment, which yields the randomly oriented MWW layers in form of ITQ-2. Under milder delamination conditions followed by pillaring with Tetraethylorthosilicate (TEOS), the neatly stacked MWW-layers of MCM-36 are produced.⁵¹

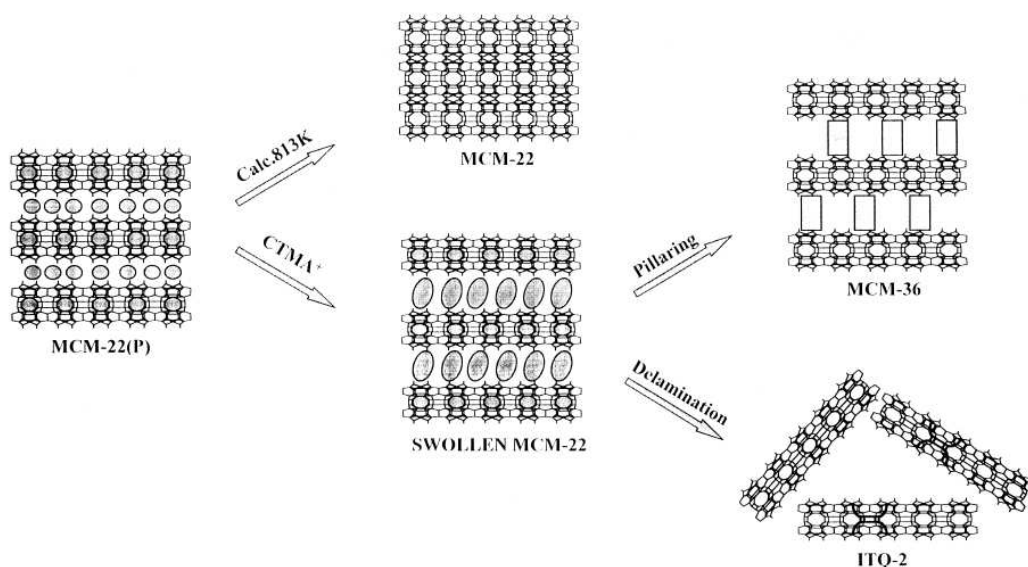


Figure 1.20: Synthesis of MCM-22, MCM-36 and ITQ-2 from MCM-22(P).⁵²

The first synthesis of ITQ-2 has been reported by Corma *et al.*⁵³. The material has been named ITQ after the Instituto de Tecnología Química, where it has been developed. It consists of very thin sheets of MWW-layers ($\approx 25 \text{ \AA}$ thick), leading to an extremely high external surface area of $700 \text{ m}^2/\text{g}$. These thin sheets consist of a hexagonal array of “cups” penetrating into the sheet from both sides. Because of the delamination of the MCM-22(P) precursor layers, the large cylindrical supercages of MCM-22 were halved and an increasing number of now half-open supercages (“cups”) are present in a hexagonal array on the sheets’ surface. These cups have an aperture of 7.0 \AA , formed by a 12-membered ring. The cups are 7.0 \AA deep and meet at the center of the sheet, forming a double 6-membered ring window that connects the cups, bottom to bottom, resulting in a smooth 10R pore system around the cups inside the layer.⁵³ Thus, reaction sites located previously in the supercages are more easily accessible, even for larger molecules. The

ITQ-2 structure is therefore more active for reactions controlled by diffusion through micropores than the parent MWW-type framework.

It was shown that, for example, that ITQ-2 exhibits increased catalytic activity in relation to the precursor zeolite in the cracking of *tri*-isopropylbenzene and gas oil, and also relative to other zeolites in the liquid-phase condensation of naphthalene with *para*formaldehyde to dinaphthylmethane. Recently, it was found that the *Friedel–Crafts* alkylation of biphenyl with propylene in gas phase over ITQ-2 can be considered a clean reaction to obtain only alkylated products, without other lateral reactions.⁵⁴

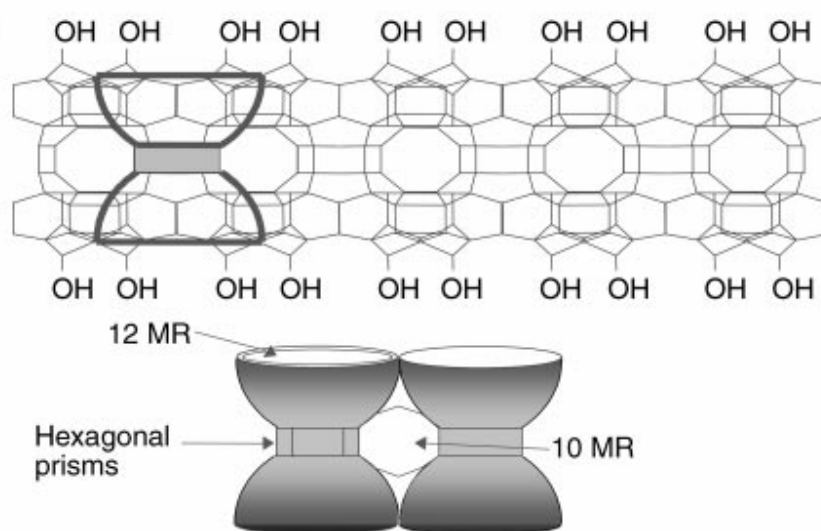


Figure 1.21: Proposed structural model for ITQ-2.⁵³

MCM-36 is a pillared molecular sieve with defined mesopores generated by expansion of the MCM-22 inter-layers *via* swelling and pillaring. MCM-36 contains mesopores with diameters between 2 and 4 nm and sinusoidal, 10-membered ring channels in the intact layers. As shown in Figure 21, the mesoporous region is located between the microporous layers of the MCM-22 and has the properties of a medium-pore zeolite. These attributes make MCM-36 a unique mesoporous material: it constitutes the first example of a zeolite-based pillared molecular sieve.⁵⁵ It is known that MCM-36 is an active, selective and stable solid acid catalyst for alkylation of isobutene with 2-butene. It has also been

shown that MCM-36 is very active for the alkylation of benzene with propylene to produce cumene.⁵⁶

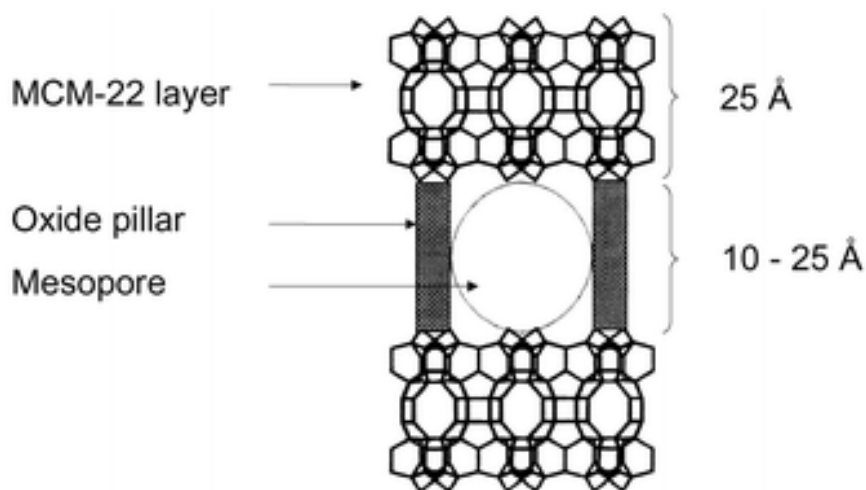


Figure 1.22: Model of the MCM-36 structure.⁵⁵

Framework MCM-41

MCM-41 is a direct descendant of M41S, the first ordered mesoporous material. It was developed by the same group in 1992.⁵⁷ MCM-41 is a completely ordered mesoporous material, not containing any micropores. It displays a honeycomb-like structure of hexagonally arranged uniform mesopores (~3 nm in diameter) running through a matrix of amorphous silica.

Due to its high specific surface area (approximately 1,000 m²/g) and mesopore volume (up to 1.0 cm³/g), high thermal and hydrothermal stability, its acidity and hydrophobicity and the possibility of controlling its pore size by adjusting the synthesis conditions MCM-41 has attracted the attention of scientists. Pinnavaia *et al.*⁵⁸ have shown that the well-defined mesoporous MCM-41 silicas may be readily harnessed to achieve selective oxidation (using in-built titanium ions and H₂O₂ as the key agents) of quite bulky molecules. Armengol *et al.*⁵⁹ have demonstrated that it is possible to alkylate large molecules, such as 2,4-di(*t*-butyl)phenol with cynamil alcohol giving rise to 6,8-di(*t*-butyl)-2-phenyl-2,3-dihydrobenzopyrab over Al-MCM-41.

However, because the O-Al-O angle is more rigid than the O-Si-O angle, Al-MCM-41 materials are less structurally ordered than their pure silica version and are highly similar to amorphous alumina, especially at high Al-contents.⁶⁰

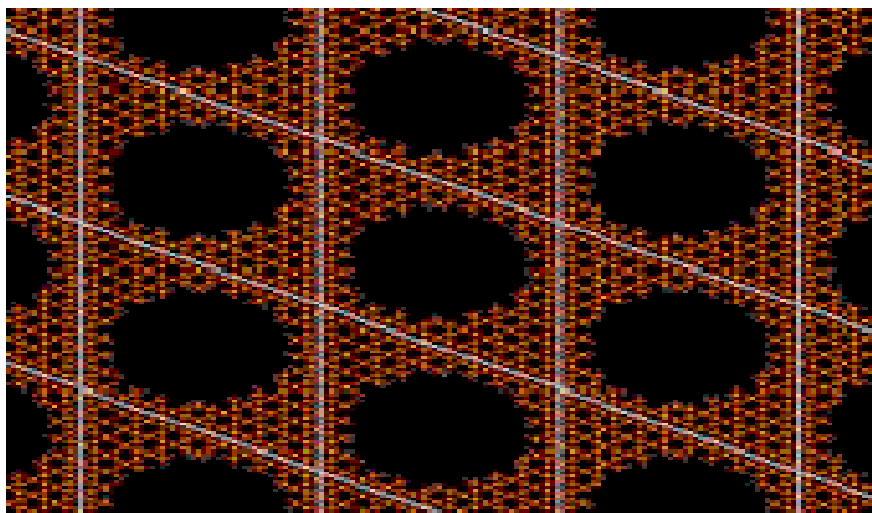


Figure 1.23: *Structural representation of MCM-41.*⁵⁷

Framework SBA-15

The structure of SBA-15 (Santa Barbara Amorphous number 15) consists of a hexagonal arrangement of cylindrical mesoporous tubes of 2 - 10 nm in diameter, which is similar to the structure of the honeycomb-like MCM-41 silica except for random interconnection of the tubes by micropores in the pore walls. It was first synthesized in 1998 by researchers of the University of California in Santa Barbara.^{61,62} SBA-15 can be prepared over a wide range of uniform pore sizes (from 46 to 300 Å) and pore wall thicknesses (of 31 to 64 Å) at low temperature (35° to 80°C), using a variety of poly(alkyleneoxide)triblock-copolymers and by the addition of cosolvent organic molecules. SBA-15 has attracted considerable attention because of its high structure regularity, thick inorganic walls, large pore diameter, excellent thermal and hydrothermal stability, its low-cost and non-toxic template, and because of the simple and reproducible synthesis. In addition to that, one of the interesting properties of SBA-15 is the coexistence of meso- and micropores.

Incorporation of Al into SBA-15 materials has been extensively studied due to their great potential in acid-catalyzed reactions for large molecules. A. Vinu *et al.*⁶³ have studied the alkylation of *m*-cresol with *iso*-propanol over different aluminosilicates. Al-SBA-15 (Si/Al=45) was found to be the most active catalyst in this study, showing 73.5% *m*-cresol conversion under the optimized reaction conditions.

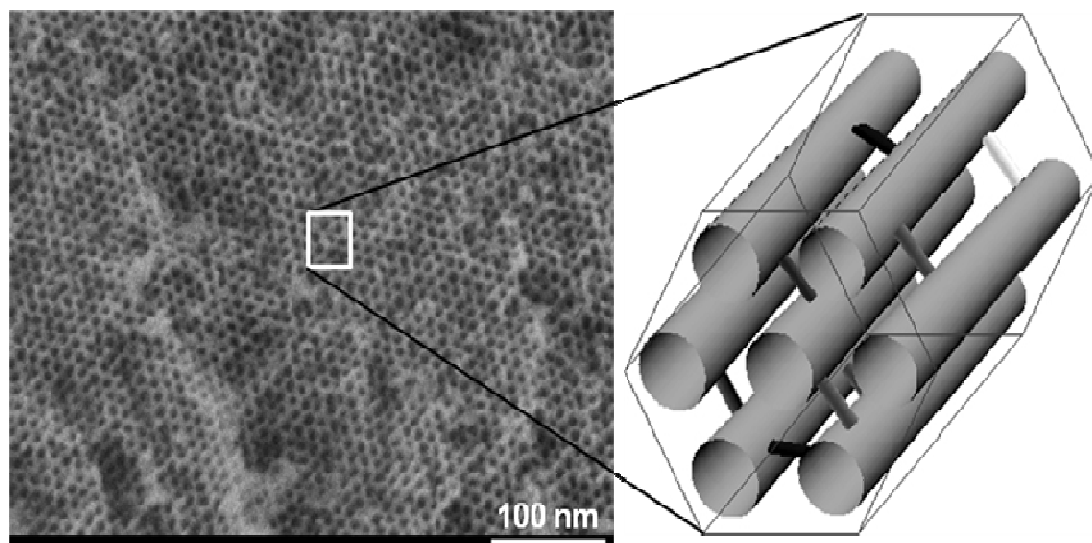


Figure 1.24: Pore structure of SBA-15.⁶⁴

Framework KIT-6

KIT-6, which is synthesized under very similar conditions as SBA-15 was first synthesized at the *Korea Advanced Institute of Science and Technology* in 2004. KIT-6 exhibits a three-dimensional cubic $Ia3d$ symmetric structure with two intertwined chiral pore systems. Due to this unique 3D channel network, highly opened spaces for direct access to guest species without pore blockage are present in the KIT-6 framework.⁶⁵ KIT-6 possesses large readily tunable pores with thick pore walls, high hydrothermal stability, high specific surface area and large mesopore volume. This material is expected to be superior to other mesoporous structures (in particular MCM-41 and SBA-15) with one or two-dimensional channels due to faster diffusion of reactants and products during reaction in the interconnected mesopores.

Prabhu *et al.*⁶⁶ have reported that Al-KIT-6 is a potential catalyst for selective O-acylation of phenol with acetic acid in the vapour phase with the aim of obtaining *ortho*- and *para*-hydroxyacetophenone, which is an important raw material for the production of pharmaceuticals, insecticides and perfumes.

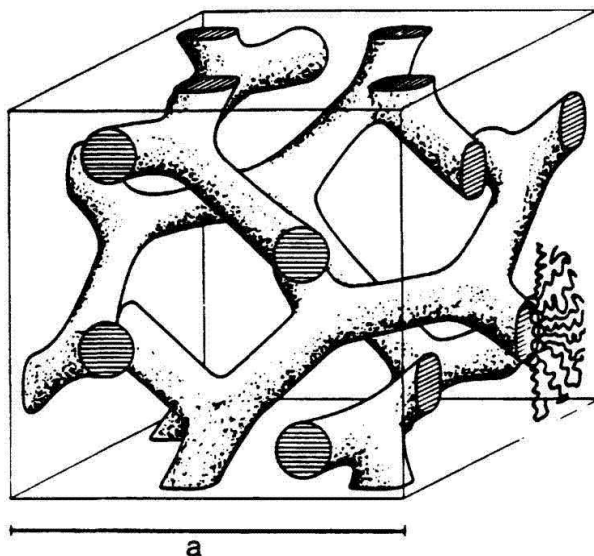


Figure 1.25: Proposed structural representation for KIT-6.⁶⁷

1.5 Scope of the Thesis

As described previously, it is of considerable commercial interest to replace HCl as catalyst in methylenedianiline production by a solid acid catalyst. However, all efforts in this direction have failed until now because of the low activity of solid acid catalysts for this process and their rapid deactivation. Recently, the application of delaminated materials (ITQ-2)¹¹ or small crystalline zeolites¹² was proposed in order to increase the catalysts' activity. However, deactivation of these materials under process conditions is still a major problem. It is the objective of our work to develop an aluminosilicate catalyst that displays both high activity and increased lifetime.

However, it is vital to understand the reaction mechanism and network in order to design an improved catalyst. It is likewise necessary to understand the processes leading to catalyst deactivation, if one is to design a material that can avoid or slow down this

deactivation. Therefore we divided the project “*Novel acid catalysts for methylenedianiline production*” into four main stages:

Stage 1 – Identification of the reaction mechanism and network -

In the first stage of the project, it is our aim to understand the reaction network and mechanism involved in the formation of methylenedianiline over a solid acid catalyst. In order to achieve this, we will collect time concentration profiles of the reaction in a batch reactor at different temperatures and starting concentrations. From this kinetic data, we can deduct activation energies and reaction orders of key steps in the reaction network. By the identification of all major reactants, intermediates and products found during the reaction, we should be able to suggest a valid model reaction network and mechanism.

Stage 2 – Catalyst screening -

Once the reaction mechanism is basically understood, it is important to understand how different catalysts affect the reaction in terms of product distribution and reaction rates. Therefore we will test a broad variety of commercially available aluminosilicate catalysts in a test reaction in order to determine which properties of a catalytic material are vital for its activity, selectivity and lifetime. Ideally, this data should further support and refine the established reaction mechanism of *Stage 1*.

Stage 3 – Deactivation -

The main problem of all catalysts tested so far is deactivation. However, there is no consensus in literature to what species is causing this deactivation and how it is formed, or even if deactivation might be caused by gradual decomposition of the catalytic material itself. It is our aim to identify the processes and substances leading to catalyst deactivation. The reaction mechanism and network of *Stage 1 and 2* should present a good starting point for these investigations. The construction of a continuous setup for lifetime testing will be necessary at this stage.

Stage 4 – Synthesis, Characterization and Testing of improved catalysts –

Based on a substantiated understanding of the reaction and deactivation mechanisms, we can identify the parameters that distinguish a catalyst with high activity and improved lifetime (such as framework type, pore size, acid strength and density). Then, the final step is to synthesize, characterize and test a first generation of promising materials that meet these requirements. Once the most effective of these new materials is identified, the synthesis of a second generation of improved catalysts is the final and ideal goal of this work.

References:

- [1] D. Dieterich, K. Uhlig, *Ullmann's Encyclopedia of Industrial Chemistry* **1991**, Vol. A21, VCH Weinheim, Germany, 665.
- [2] Bundesministerium für Verkehr, Bau und Stadtentwicklung, Ökologisches Baustonformationssystem,
[http://wecobis.iai.fzk.de/cms/content/site/wecobis/Home/Grundstoe/Kunststoe/GS/Polyurethan GS](http://wecobis.iai.fzk.de/cms/content/site/wecobis/Home/Grundstoe/Kunststoe/GS/Polyurethan%20GS), retrieved March **2010**.
- [3] *Polyurethane in China Market Report*, PU World, Shanghai, **2007**.
- [4] R. Becker, L. Thiele, J.C. Salamone (ed), "Polyurethane catalysis" in *Polymeric Materials Encyclopedia* **1996**, 9, CRC Press Inc., New York, 6940.
- [5] A.L. Silva, J.C. Bordabo, *Catal. Rev.* **2004**, 46(1), 31.
- [6] M.S. Vratasanos, J.C Salamone, "Polyurethane catalysis" in *Polymeric Materials Encyclopedia* **1996**, 9, CRC Press Inc., New York, 6947.
- [7] TDI/MDI, *Chem Systems Report 98/99 S8*; Process Evaluation/Research Planning Program, Chem Systems, San Francisco, **1999**.
- [8] P. Galloway, *Chem. Rev.* **1994**, 4(2), 20.
- [9] C. Perego, A. de Angelis, A. Carati, C. Flego, R. Millini, C. Rizzo, G. Bellussi, *Appl. Catal. A* **2006**, 307, 128.
- [10] A. de Angelis, P. Ingallina, C. Perego, *Ind. Eng. Chem. Res.* **2004**, 43, 1169.
- [11] A. Corma, P. Botella. C. Mitchell, *Chem. Commun.* **2004**, 2008.
- [12] T. Kugita, S. Hirose, S. Namba, *Catal. Today* **2006**, 111, 275-279.
- [13] J.L. Nafzinger, L.A. Rader, I.J. Seward, *US Patent 4,554,378*, **1985**.
- [14] R. A. Prater, N. N. Shah, *US Patent 4,294,987*, **1981**.
- [15] C. Perego, A. de Angelis, O. Farias, A. Bosetti, *US Patent WO 02/20458*, **2002**.
- [16] M. Clerici, G. Bellussi, U. Romano, *US Patent, 5,241,119*, **1993**.
- [17] F.F. Frulla, A.A. R. Sayigh, H. Ulrich, P.J. Whitman, *US Patent 4,039,580*, **1977**.
- [18] F.F. Frulla, A.A. R. Sayigh, H. Ulrich, P.J. Whitman, *US Patent 4,039,581*, **1977**.
- [19] F.F. Frulla, A.A. R. Sayigh, H. Ulrich, P.J. Whitman, *US Patent 4,092,343*, **1978**.
- [20] H. Ulrich, *Chemistry and Technology of Isocyanates*, Wiley, New York, **2001**.
- [21] F. Merger, G. Nestler, *EU Patent 0043933*, **1981**.

- [22] A.F. Cronstedt, *Om en obekant bärg art, som kallas Zeolites*, Akad. Handl. 18, Stockholm, **1756**, 120.
- [23] S.M. Auerbah, K.A. Corrado, P.K. Dutta, *Handbook of Zeolite Science and Technology*, Marcel Dekker, New York, **2003**.
- [24] L.B. McCusker, F. Liebau, G. Engelhardt, *Pure Appl. Chem.* **2001**, 73, 381–394.
- [25] R.M. Barrer, *Pure Appl. Chem.* **1979**, 51, 1091–1100.
- [26] C. Baerlocher, L.B. McCusker, Database of Zeolite Structures: <http://www.iza-structure.org/databases/>, **2010**.
- [27] S. Yang, M. Lach-hab, I.I. Vaisman, E. Blaisten-Barojas, *J. Phys. Chem. C* **2009**, 113, 21721.
- [28] C. Baerlocher, L.B. McCusker, D.H. Olson, *Atlas of Zeolite Framework Types, Sixth Revised Edition*, Elsevier, **2007**.
- [29] J. Weitkamp, L. Puppe, *Catalysis and zeolites: Fundamentals and Applications*, Springer, Berlin, **1999**.
- [30] J.A. Lercher, *Industrielle Chemische Prozesse I*, Technische Universität München, **2010**.
- [31] A. Corma, V. Gonzalez-Alfaro, A. Orchilles, *Appl. Catal. A* **1995**, 129(2), 203.
- [32] R.J. Farrauto, *Fundamentals of Industrial Catalytic Processes*, **1997**.
- [33] J. Hagen, *Industrial Catalysis*, Wiley, Weinheim, Germany **2006**.
- [34] R.L. Wadlinger, G.T. Kerr, E.J. Rosinski, *US Patent* 3,308,069, **1967**.
- [35] J. Weitkamp, R. Kumar, S. Ernst, *Chem.-Ing.-Tech.* **1989**, 61(9), 731.
- [36] S.A. Butter, A.T. Jurewicz, W.W. Kaeding, *US Patent* 3,894,107, **1975**.
- [37] C.D. Chang, W.H. Lang, A.J. Siivestri, *US Patent* 3,894,106, **1975**.
- [38] C.D. Chang, A.J. Silvestri, R.L. Smith, *US Patent* 3,928,483, **1975**.
- [39] D.W. Werst, E.E. Tartakovsky, E.A. Piocos, A.D. Trifunac, *J. Phys. Chem.* **1994**, 98(40), 10249.
- [40] M. Damour, *Annales des Mines* **1842**, 4(1), 395.
- [41] J.A. Hriljac, M.M. Eddy, A.K. Cheetham, J.A. Donohue, G.J. Ray, *Journal of Solid State Chemistry* **1993**, 106, 66.
- [42] J. Scherzer, *Catal. Rev.* **1989**, 31, 215.

-
- [43] A. Alberti, P. Davoli, G. Vezzalini, *Zeitschrift für Kristallographie* **1986**, 175, 249.
- [44] P. Frontera, F. Testa, R. Aiello, S. Candamano, J.B. Nagy, *Micro. Meso. Mater.* **2007**, 106, 107.
- [45] J. Scherzer, J.L. Bass, F.D. Hunter, *J. Phys. Chem.* **1975**, 79(12), 1194.
- [46] J. Scherzer, J.L. Bass, F.D. Hunter, *J. Phys. Chem.* **1975**, 79(12), 1200.
- [47] A.H. Janssen, A.J. Koster, K.P. De Jong, *Angew. Chem. Int. Ed.* **2001**, 40(6), 1102.
- [48] J.C. Groen, S. Abelló, L.A. Villaescusa, J. Pérez-Ramírez, *Micro. Meso. Mat.* **2008**, 114, 93.
- [49] C.T. Kresge, M.E. Leonowicz, W.J. Roth, J.C. Vartuli, *US Patent* 5,102,643, **1992**.
- [50] C.T. Kresge, M.E. Leonowicz, W.J. Roth, J.C. Vartuli, J.S. Beck, *Nature* **1992**, 359, 710.
- [51] R. Schenkel, J.-O. Barth, J. Kornatowski, J.A. Lercher, *Stud. Surf. Sci. Catal.* **2002**, 142, 69.
- [52] A. Corma, V. Fornes, J.M. Guil, S. Pergher, T.L.M. Maesen, J.G. Buglass, *Micro. Meso. Mat.* **2000**, 38, 301.
- [53] A. Corma, V. Fornes, J.M. Guil, S. Pergher, T.L.M. Maesen, J.G. Buglass *Micro. Meso. Mat.* **2000**, 38, 301.
- [54] A. Corma, H. Garcia, J. Miralles, *Micro. Meso. Mat.* **2001**, 43, 161.
- [55] Y. J. He, G.S. Nivarthi, F. Eder, K. Seshan, J.A. Lercher *Micro. Meso. Mat.* **1998**, 25, 207.
- [56] C.T. Kresge, W.J. Roth, K.G. Simmons, J.C. Vartuli, *US Patent* 5,229,341, **1993**.
- [57] J.S. Beck, J.C. Vartuli, W.J. Roth, M.E. Leonowicz, C.T. Kresge, K.D. Schmitt, C.T.-W. Chu, D.H. Olson, E.W. Sheppard, S.B. McCullen, J.B. Higgins, J.L. Schlenkert, *J. Am. Chem. Soc.* **1992**, 114, 10834.
- [58] T.J. Pinnavaia, W. Li, W. Zhang, R.T. Yang, *J. Catal.* **1997**, 172, 488.
- [59] E. Armengol, M.L. Cano, A. Corma, H. Garcia, M.T. Navarro, *Chem. Comm.* **1995**, 519.

- [60] S.M. Auerbah, K.A Corrado, P.K. Dutta, *Handbook of Zeolite Science and Technology*, Dekker, New York, **2003**.
- [61] D. Zhao, J. Feng, Q. Huo, N. Melosh, G.H. Fredrickson, B.F. Chmelka, G.D. Stucky, *Science* **1998**, 279, 548.
- [62] D. Zhao, Q. Huo, J. Feng, B.F. Chmelka, G.D. Stucky, *J. Am. Chem. Soc.* **1998**, 120, 6024.
- [63] A. Vinu, G.S. Kumar, K. Ariga, V. Murugesan, *J. Mol. Catal. A* **2005**, 235, 57.
- [64] F. Kleitz, *Ordered Nanoporous Materials: Synthesis, Characterization and Functionalization Methods*, Laval University, Quebec, Canada, **2003**.
- [65] T.W. Kim, F. Kleitz, B. Paul, R. Ryoo, *J. Am. Chem. Soc.* **2005**, 127, 7601.
- [66] A. Prabhu, L. Kumaresan, M. Palanichamy, V. Murugesan, *Appl. Catal. A* **2009**, 360, 59.
- [67] O.C. Gobin, *SBA-16 Materials*, Semesterarbeit, Laval University, Ste-Foy, Quebec, Canada, **2006**.

Chapter 2

Reaction network and mechanism of the synthesis of methylenedianiline over dealuminated Y-type zeolites

The reaction network and mechanism of the synthesis of methylenedianiline (MDA) from the condensation product of aniline and formaldehyde (aminal) on microporous acidic materials has been elucidated. The first step of the reaction, the decomposition of the aminal to N-benzylanilines, is limited by film diffusion, the second and significantly slower step, the acid catalyzed rearrangement of these intermediates to MDA, is controlled by microkinetics on mesoporous dealuminated Y-type zeolites. In contrast, the second step of the reaction network is limited by pore diffusion on zeolite BEA as an example for non-mesoporous materials. Based on time-concentration profiles collected by gas chromatography, we were able to determine the reaction orders of the initial decomposition of the aminal to one and two for the following rearrangement of para-aminobenzylaniline to 4,4'-MDA. From the kinetic data we deduced an S_N2 -type reaction mechanism and a complex reaction network, which is able to simulate the observed concentration profiles. Furthermore the influence of the aniline to formaldehyde ratio of the starting material on the final product distribution was examined and found to be negligible.

2. Reaction Network and Mechanism of the Synthesis of Methylenedianiline over dealuminated Y-type zeolites

2.1 Introduction

Methylenedianiline (MDA) is an important starting material for the production of methylenediisocyanate for polyurethane synthesis.¹ The most interesting production route for MDA starts from the condensation of aniline and formaldehyde followed by an acid catalyzed rearrangement reaction. Industrially mineral acids, such as HCl, are applied as catalysts. This does not only pose plant engineering problems by the handling of highly corrosive material, but also environmental problems. When HCl is used as catalyst, MDA is yielded in the hydrochloride form and has to be neutralized with NaOH prior to further conversion. HCl is actually spent in stoichiometric amounts and a large amount of waste containing NaCl contaminated with aniline is created.

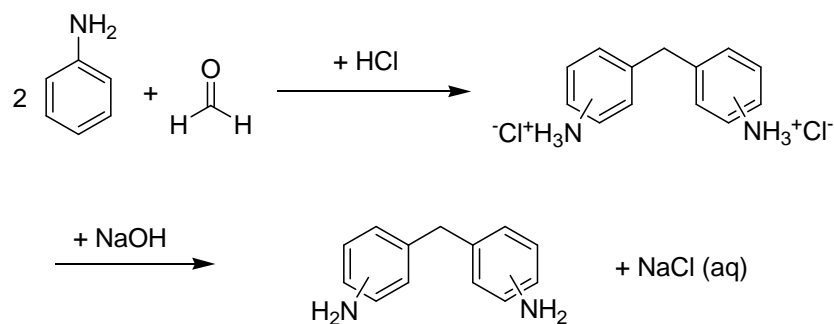


Figure 2.1: Current industrial process for MDA production.

Therefore, it is of great interest to replace the mineral acid in the process by a solid acid catalyst. Zeolites are very interesting in that respect, as their acidity and structure can be tailored to achieve maximum activity and lifetime.² Several studies and a great number of patents have been published on the use of zeolites in the production of MDA from aniline and formaldehyde.³⁻⁸

All agree that the activity of zeolite catalysts is limited by diffusion processes and that catalyst deactivation by clogging of pores is a major problem. To counteract these problems, mesoporous and delaminated structures as well as nano-sized zeolite crystals were proposed. In stark contrast to these solutions driven by intuition, the reaction network and the mechanism of the formation of MDA over a zeolite catalyst have not been explored and described in detail in literature. This understanding of the involved reaction network and the underlying reaction mechanism is vital for designing novel acid catalysts for the synthesis of MDA beyond intuition.

Corma *et al.* propose that the condensation product of aniline with formaldehyde (aminal) is subject to a series of rearrangement reactions in the presence of a Brønsted acid. The three MDA isomers (4,4'-MDA; 2,4'-MDA; 2,2'-MDA) and oligomers thereof are yielded *via para* and *ortho*-aminobenzylaniline (PABA and OABA).³ As the reaction is believed to be diffusion limited, only a fraction of the acid sites is accessible to the aminal, which is converted into MDA as shown in Scheme 2. Kugita *et al.* tested this hypothesis by applying a beta zeolite (Si/Al 15) with different crystallite sizes to the reaction. It was shown, that smaller crystallites displayed higher activity in the reaction, as more acid sites close to the particle surface are accessible to the reacting molecules.⁴

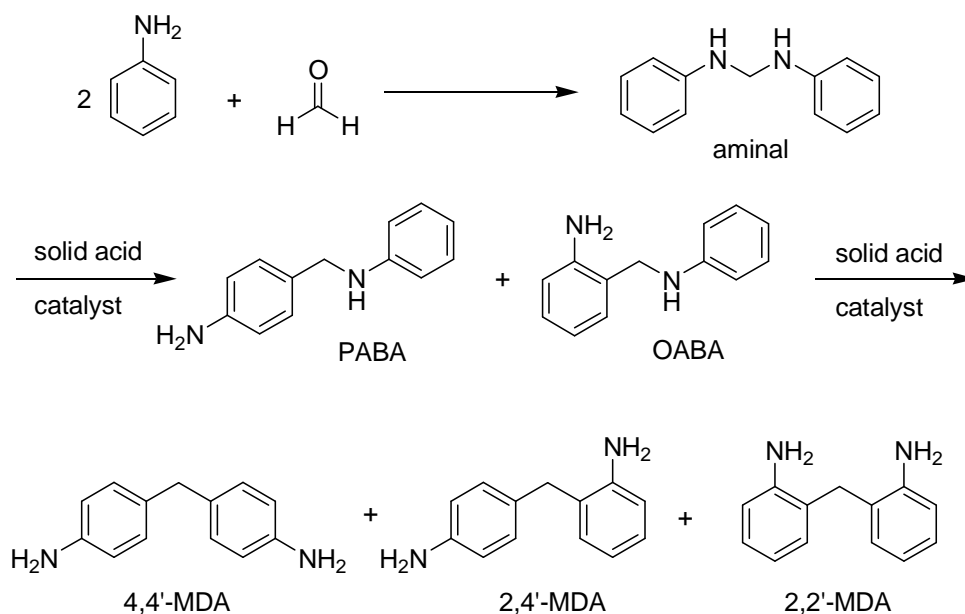


Figure 2.2: Proposed reaction network for the MDA synthesis over zeolite catalysts.^{3,6}

We decided, therefore, to explore the kinetics and the reaction network of MDA synthesis starting from the aminal on various well characterized zeolite catalysts in order to deduce a reliable reaction network and establish the overall reaction mechanism.

2.2 Methods

The aminal solution, which was used as starting material for all further reactions, was prepared as follows. In a 1 L round bottom flask 600 mL of aniline (6.58 mol, Sigma, purity $\geq 99.5\%$) were heated to 50°C under vigorous stirring. 100 mL of formalin (1.32 mol formaldehyde, Sigma, 37% wt of formaldehyde in water, stabilized with methanol) were added dropwise. After addition, stirring was continued at 50°C for 1 h. Water and methanol were removed in a Rotavapor. Concentration and purity of the resulting solution of 1 equ. of aminal in 3 equ. of aniline, which is ready for use in the test reactions, was verified by ^1H - and ^{13}C -NMR, as well as gas chromatography.

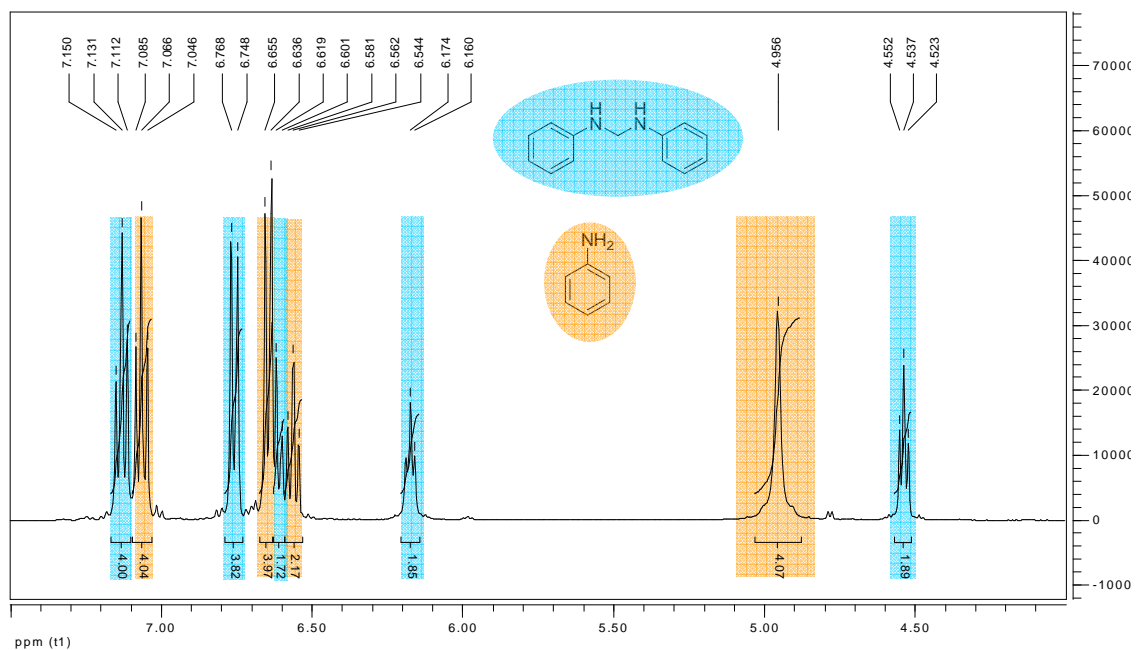


Figure 2.3: ^1H -NMR (300K; DMSO-d_6 , 400 MHz) of aminal solution with an aniline/aminal ratio of 2. Aminal signals in blue, aniline signals in orange.

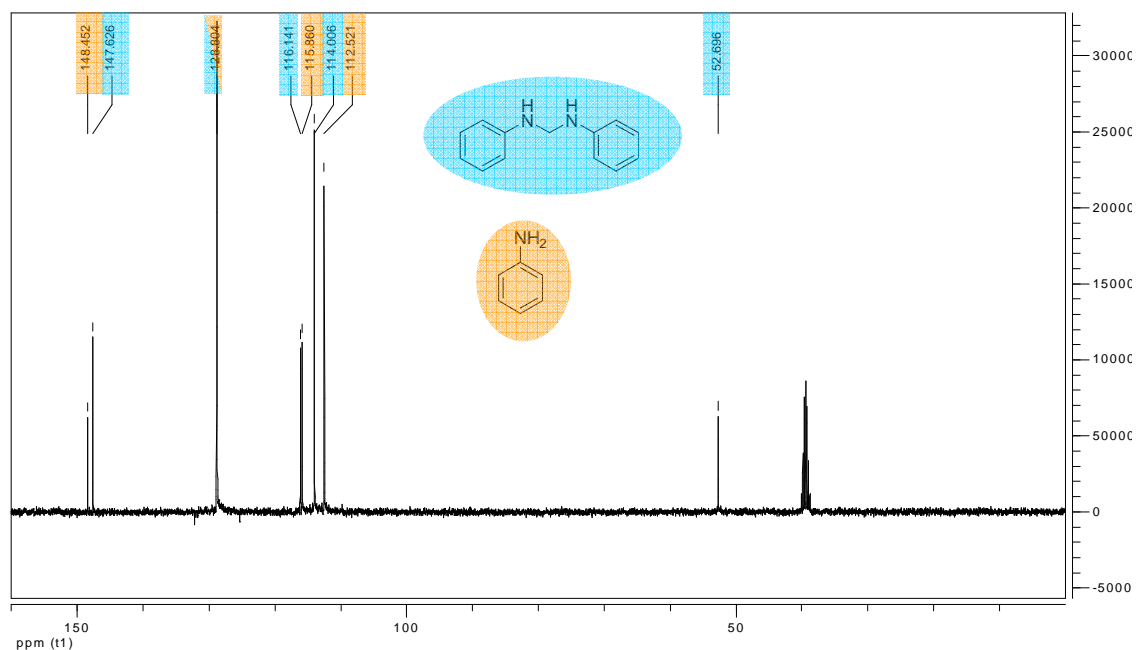


Figure 2.4: ^{13}C -NMR (300K; DMSO-d_6 , 400 MHz) of amination solution with an aniline/amination ratio of 2. Amination signals in blue, aniline signals in orange.

For the test reaction, 10 mL of the amination solution were placed in a three necked round bottom flask equipped with a reflux condenser and heated to the desired temperature. After the set temperature was reached, 0.50 g catalyst were added. 100 μL of sample were taken from the reaction mixture after defined time intervals and diluted with 0.9 mL of acetonitrile (Sigma, purity $\geq 99.5\%$), containing 1 mL of diphenylmethane (Fluka, purity $\geq 99\%$) per 100 mL of acetonitrile as internal standard. After removal of the catalyst by filtration through a syringe filter (Minisart SRC; 0.20 μm , $d = 4$ mm) the sample was analyzed by GC.

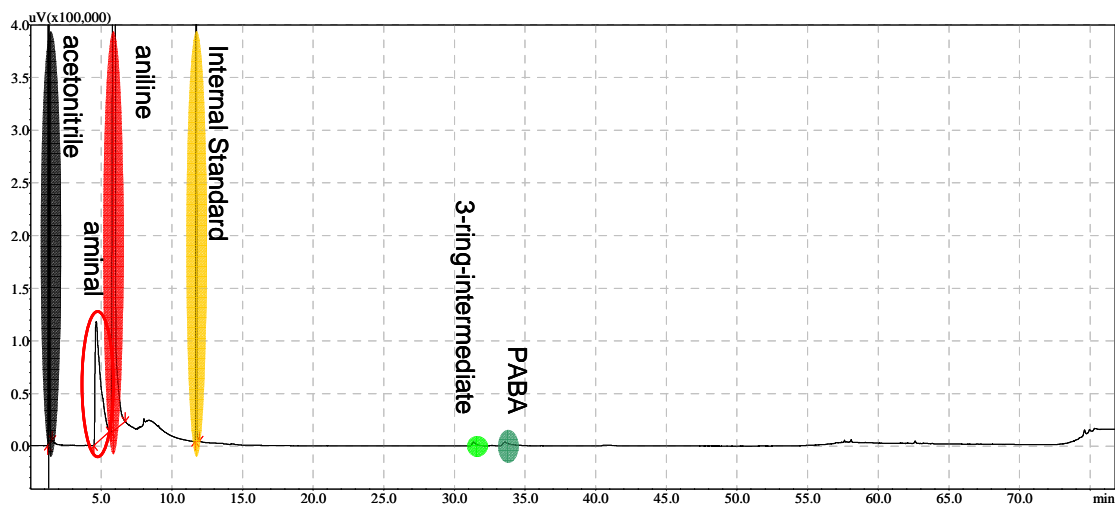


Figure 2.5: GC elugram of the reaction mixture directly before catalyst addition.

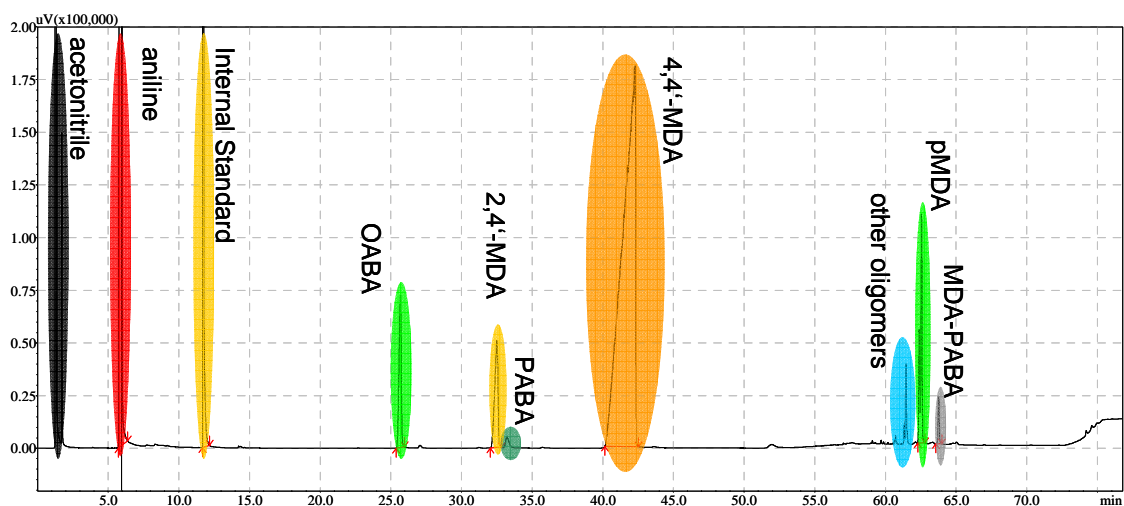


Figure 2.6: GC elugram of the reaction mixture shortly before complete reaction.

In order to calculate the activation energies for the key steps of the reaction network the test reaction was carried out at temperatures between 60 and 150°C. The initial rates for the decomposition of the aminal, the formation of PABA and OABA and the formation of 4,4'-MDA were determined. The rate of PABA decomposition at a PABA concentration of 0.10 mol/mol aniline was applied for the calculation of the apparent activation energy of the PABA decomposition.

For the determination of the reaction order of the decomposition of the aminoral, a defined amount of catalyst (10 mg H-CBV 760 or 200 mg of H-BEA 25) was contacted with 5.0 g of a solution containing different concentrations of aminoral in aniline at 70°C (80°C in case of H-BEA 25). In order to obtain the reaction order of the PABA decomposition, a defined amount of catalyst (20 mg CBV 760 or 200 mg of H-BEA 25) were added to 4.0 g of a solution containing different concentrations of PABA in aniline at a reaction temperature of 70°C (80°C in case of H-BEA 25). The initial decomposition rates of aminoral and PABA conversion were derived at conversions below 10%.

In order to investigate the influence of the aniline concentration, reaction mixtures with aniline to aminoral ratios ranging from 3 to 20 have been prepared. 15.0 g of these mixtures were reacted with 0.79 g of catalyst CBV 760 at 100°C. The composition of the reaction mixture was monitored by GC. When the reaction mixture reached a constant composition after 2-4 hours, the respective product distributions were determined.

For GC analysis a Shimadzu GC 2010, equipped with an Optima 35 MS column (length = 30 m, ID = 0.32 mm, film thickness 0.25 μm), a FID detector and an autosampler was available. A temperature profile beginning at 60°C, hold for 5 min, heating with an increment of 15 K min^{-1} to 170°C, holding for 40 min, heating with 25 K min^{-1} up to 300°C, holding for 15 min and heating with 25 K min^{-1} up to 350°C and holding this temperature for 2 min was applied. The injection volume was set to 1 μL with the Injection port heated to 280°C and a split ratio of 50. The instrument was calibrated to 4,4'-MDA, 2,4'-MDA, PABA, OABA and aminoral, the response factors for heavier products were assumed to be identical in first approximation and were estimated by closing the mass balance of the reaction.

As catalysts a dealuminated Y-type zeolite (CBV 760, Zeolyst), a parent Beta-type zeolite (H-BEA 25, Südchemie) and a set of Na-exchanged CBV 760 have been tested. The Na-exchanged CBV 760 samples were prepared from H-CBV-760 by ion exchange with NaNO_3 . Three partially exchanged samples were prepared by dispersing 6.0 g of CBV 760 in 90 mL of distilled water, containing 0.14 g (1.65 mmol), 0.54 g (6.35 mmol) or 0.90 g (10.6 mmol) NaNO_3 , at 80°C for 16 h under vigorous stirring. One completely exchanged sample was prepared according to the same procedure using a 0.2 M NaNO_3

solution and repeating the treatment two times. All samples were washed with 200 mL distilled water and dried over night at 80°C prior to use.

Nitrogen physisorption isotherms were measured using a PMI automated sorptometer at liquid nitrogen temperature (77 K), after outgassing under vacuum at 623 K for 4 h. The apparent surface area was calculated by applying the Brunauer–Emmett–Teller (BET) theory to the adsorption isotherms over a relative pressure range from 0.01 to 0.09. The micropore volumes were evaluated using the t-plot method⁹ according to Hasely.¹⁰ The mesopore volumes were determined by the cumulative pore volume of pores with diameters ranging from 2 – 50 nm according to the BJH method.¹¹ Because of the limitations of the PMI instrument, the isotherms were measured at relative partial pressures higher than 10^{-5} p/p⁰.

For temperature programmed desorption (TPD) experiments, approximately 50 mg of sample were activated for 1 h at 723 K in a six port parallel vacuum system (0.8 Pa). After activation, the samples were contacted with 1 mbar of NH₃ at 373K for 1 h, followed by degassing for 2 h at 373 K. For desorption, the samples were heated up to 1043 K with an increment of 10 K min⁻¹. Ammonia desorption was monitored by mass spectrometry (Pfeiffer QMS 200 Prisma). The amount of desorbed ammonia was determined by integration of the MS signal and calibration to a standard material (H-MFI 90; 360 μmol g⁻¹).

The elemental composition of the applied catalysts was determined by atomic adsorption spectroscopy in an Unicam M Series Flame-AAS equipped with an FS 95 autosampler and a GF 95 graphite furnace.

2.3 Results

2.3.1 Catalyst characterization

AAS analysis showed that the parent zeolite samples H-BEA 25 and H-CBV 760 have Si/Al ratios of 12.7 and 29.5, respectively. Both catalysts only contain negligible amounts of Na.

TPD of ammonia indicated acid site concentrations of 530 μmol g⁻¹ for H-BEA 25 and 348 μmol g⁻¹ for H-CBV-760. The sodium exchanged H/Na-CBV 760-X samples display

decreasing acid site concentrations of 282, 177 and 137 $\mu\text{mol g}^{-1}$ in line with increasing sodium concentration (see Table 1). The acidity of the completely Na-exchanged Na-CBV-760 is below the detection limit and its sodium content indicates complete ion exchange. XRD analysis verified that the structure of the ion exchanged Y-types was not damaged during ion exchange.

Table 2.1: *Elemental composition and acidity of the applied catalysts.*

Material name	Si/Al ratio	Na content wt. %	Acidity [$\mu\text{mol/g}$]	Na-exchange degree [%]
H-BEA 25	12.7	<0.01	530	0
H-CBV 760	29.5	<0.01	348	0
H/Na-CBV 760-1	25.8	0.18	282	19
H/Na-CBV 760-2	25.7	0.37	177	49
H/Na-CBV 760-3	23.6	0.50	137	61
Na-CBV 760	25.5	1.18	<10	100

Micro- and mesopore volume of H-BEA 25 and H-CBV 760 were determined by nitrogen physisorption. While H-BEA 25 has a micropore volume of $0.21 \text{ cm}^3 \text{ g}^{-1}$, mesopores were not found. H-CBV-760 showed a micropore volume of $0.28 \text{ cm}^3 \text{ g}^{-1}$ and also significant mesopore volume ($0.18 \text{ cm}^3 \text{ g}^{-1}$).

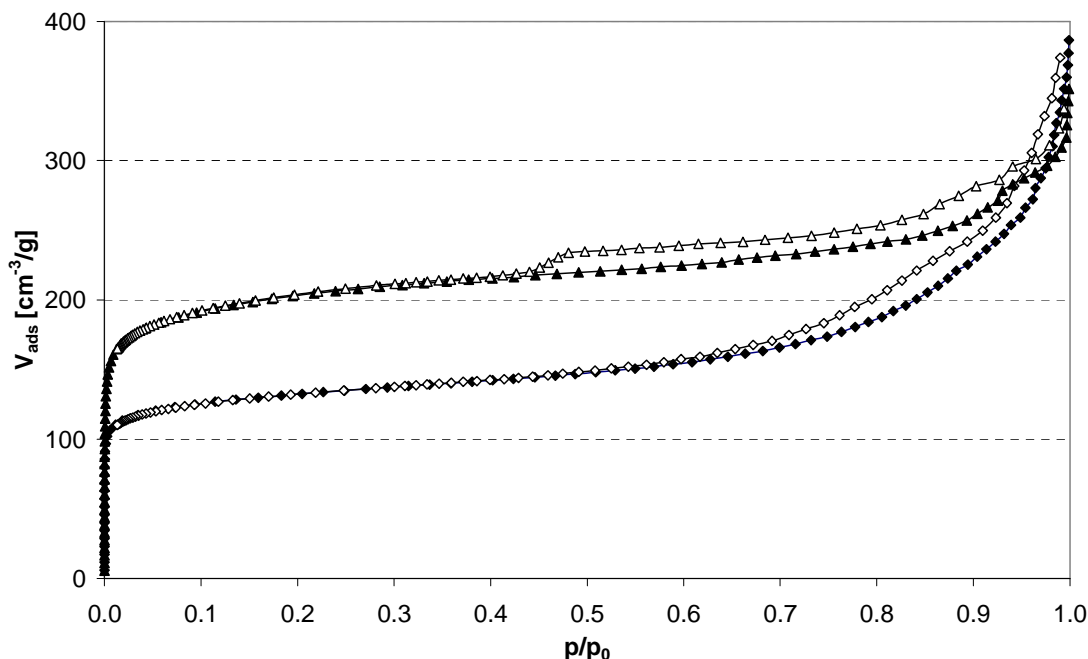


Figure 2.7: Nitrogen physisorption on H-BEA 25 (◆) and H-CBV 760 (▲).

2.3.2 Time concentration profiles

For the determination of the concentration profile of the reaction the test reaction was carried out at 100°C with 5% wt of CBV 760, a dealuminated Y-type zeolite (Si/Al 30), as catalyst. This catalyst was chosen from a variety of commercially available zeolite samples, because it displayed the highest activity for the desired reaction. A detailed study on the activity of different zeolites and aluminosilicates will be performed at the second stage of the project, once the reaction network and mechanism are established.¹⁵ The concentration of the aminal is rapidly decreasing from the initial concentration of 0.33 mol/mol aniline and is beneath detection limit 3 min after the start of the reaction. The concentrations of PABA and an oligomer are increasing fast at the beginning of the reaction and, after reaching a maximum after 8 and 15 min, respectively, decrease again. The concentration of OABA in the reaction mixture rises to a level of 0.011 mol/mol aniline and then decreases again very slowly. The concentration of a second oligomer reaches a maximum after about 60 min and decomposes slowly after that. The 4,4'-MDA concentration increases almost linearly over time until it reaches a constant level of about 0.26 mol/mol aniline at the end of the reaction. The concentrations of 2,4'-MDA and a

further oligomer are also gradually increasing until they reach a constant level of 0.014 and 0.012 mol/mol aniline, respectively at the end of the reaction.

At lower reaction temperatures the profiles look essentially the same, the reaction only proceeds significantly slower. While the reaction is finished after 300 min at 100°C, there are still significant amounts of intermediates (PABA, pPABA, ...) present after 1600 min of reaction time at 60°C. The composition of the reaction mixture at a certain reaction advancement number is almost identical.

When higher temperatures are applied the reaction is significantly faster. At 140°C the reaction is basically finished after 60 min. Again the composition of the reaction mixture is very similar at constant reaction advancement numbers, with two exceptions. Firstly, it is possible to convert OABA to 2,4'-MDA at higher temperatures. Therefore, the concentration of OABA is notably decreasing over time, while more 2,4'-MDA is formed. Secondly, higher temperatures seem to shift the product spectrum slightly towards oligomeric species.

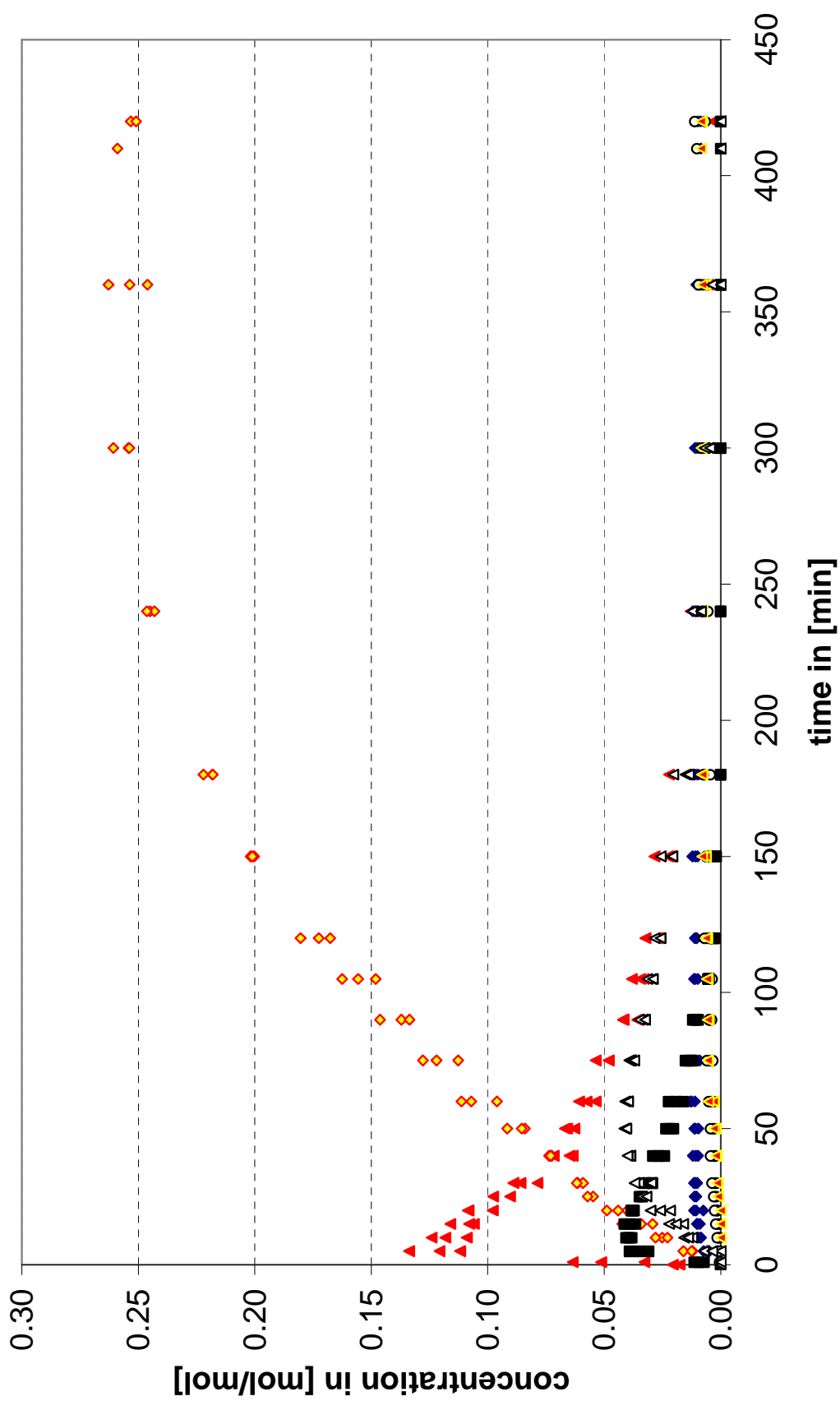


Figure 2.8: Time concentration profile of the synthesis of MDA from aminal at 100°C over a dealuminated Y-type zeolite (CBV 760); \blacktriangle PABA, \blacklozenge OABA, \blacklozenge 4,4'-MDA, \blacklozenge 2,4'-MDA, \blacksquare pPABA, \blacktriangledown MDA-PABA, \blacktriangle pMDA.

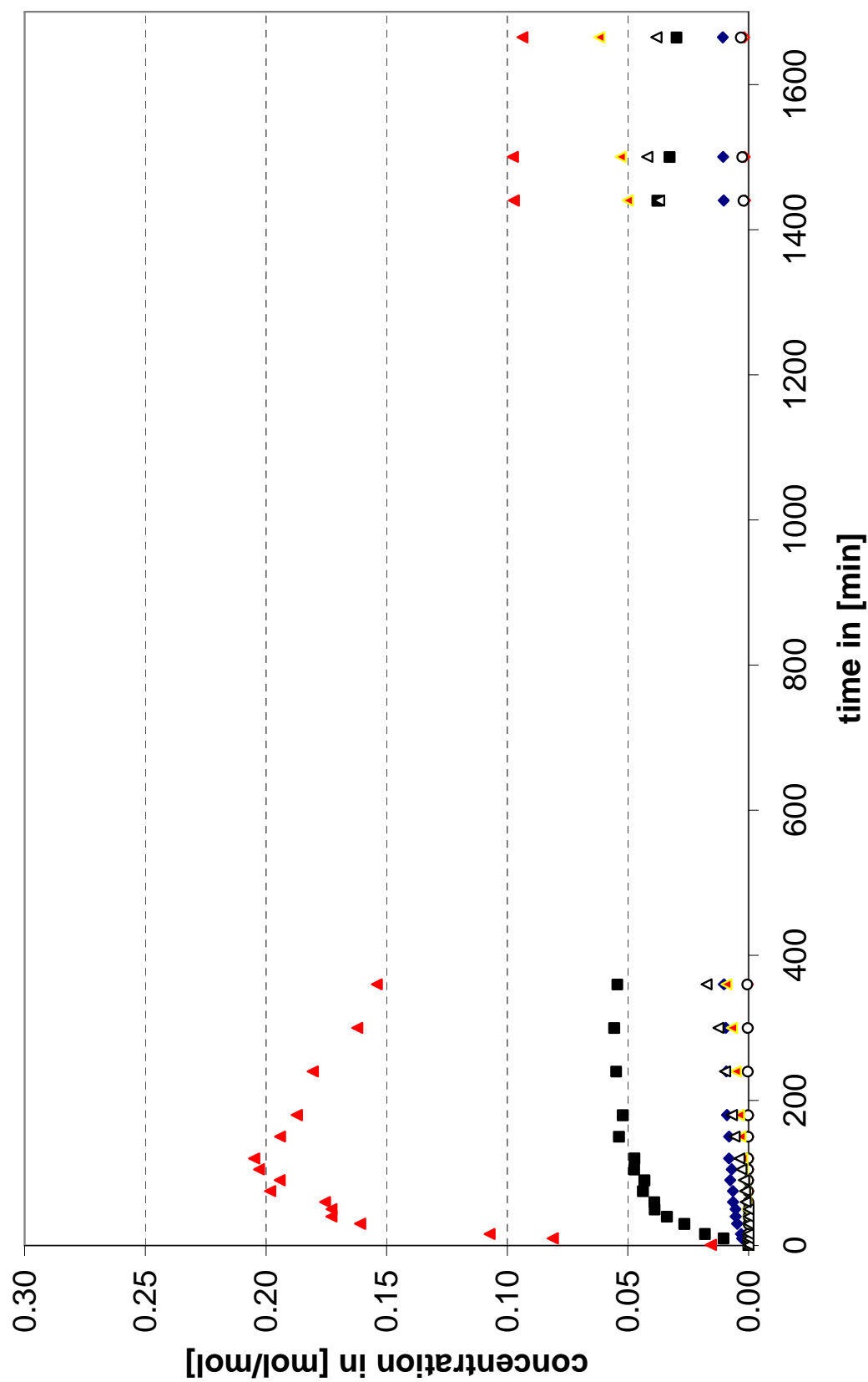


Figure 2-9: Time concentration profile of the synthesis of MDA from aminal at 60°C over a dealuminated Y -type zeolite (CBV 760); ▶ PABA, ◆ OABA, ◇ 4,4'-MDA, ○ 2,4'-MDA, ■ pPABA, ▷ MDA-PABA, ▶ pMDA.

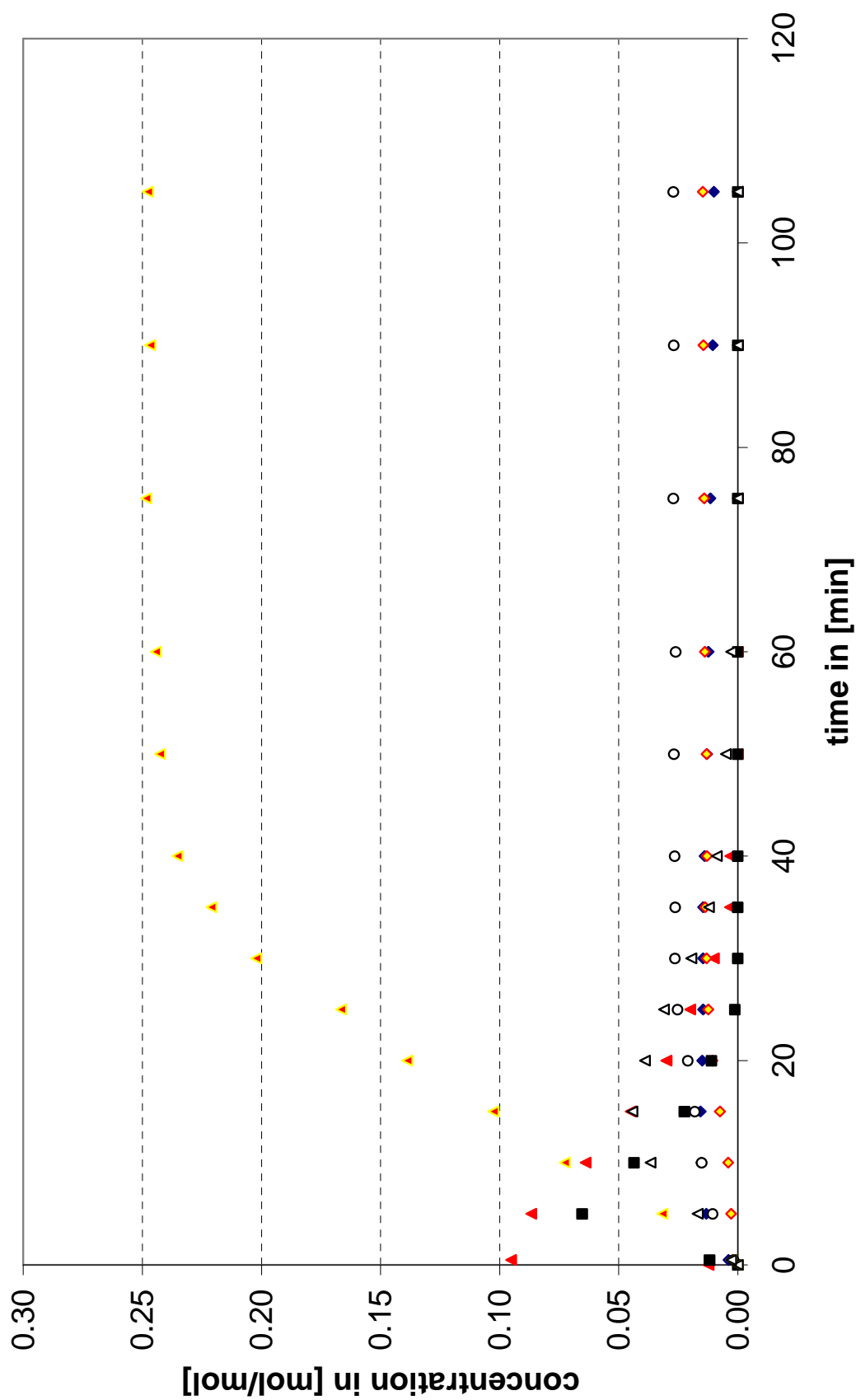


Figure 2.10: Time concentration profile of the synthesis of MDA from aminal at 140°C over a dealuminated Y-type zeolite (CBV 760); \blacktriangle PABA, \blacklozenge OABA, \circ 4,4'-MDA, \circ 2,4'-MDA, \blacksquare pPABA, \blacktriangledown MDA-PABA, \blacktriangleright pMDA.

The turnover frequencies (TOFs) of all applied catalysts were determined by normalizing the initial rates of 4,4'-MDA formation to the amount of catalyst in the reactor and its Brønsted acidity.

$$TOF[\text{min}^{-1}] = \frac{\text{rate of 4,4'-MDA formation } [\text{mol}_{4,4'\text{-MDA}} / (\text{mol}_{\text{aniline}} \cdot \text{min} \cdot \text{g}_{\text{cat}})]}{\text{acidity } [\text{mol}/\text{g}_{\text{cat}}] \cdot n_{\text{aniline}} [\text{mol}]} \quad (1)$$

While the fully ion exchanged Na-CBV 760 sample does not show activity towards MDA formation (due to its lack of Brønsted acidity), the pure proton form H-CBV 760, as well as the sodium exchanged H/Na-CBV-760-X, display constant TOFs of about 600 min^{-1} . The parent Beta type sample H-BEA 25 is significantly less active and reaches only a TOF of 24 min^{-1} .

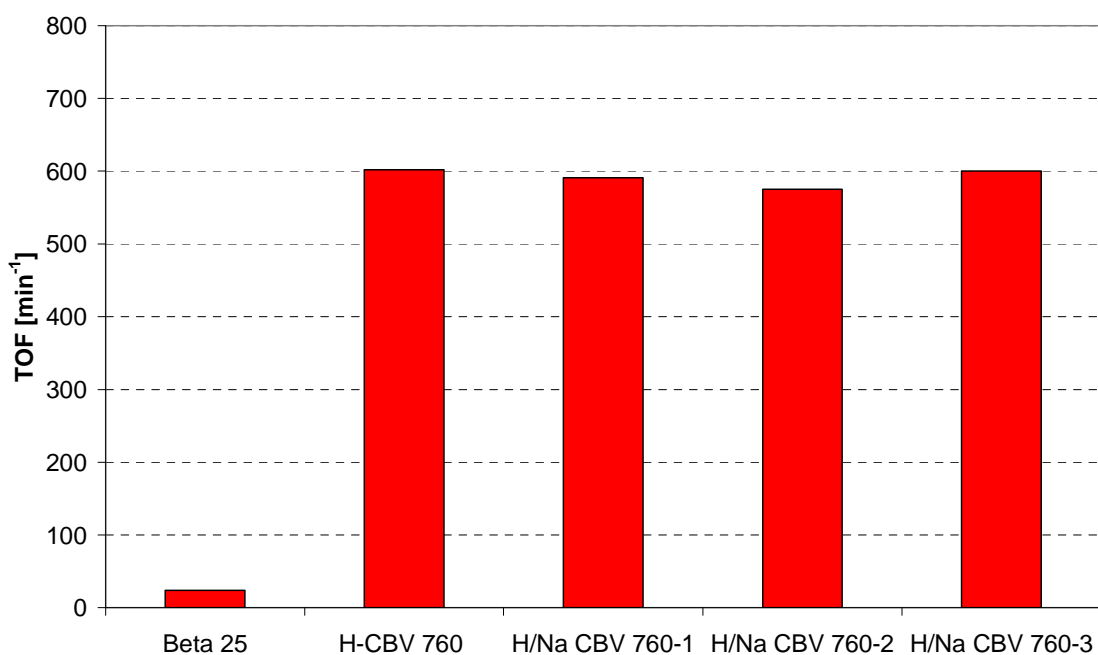


Figure 2.11: TOFs of H-BEA 25, H-CBV 760, H/Na-CBV 760-X.

2.3.3 Temperature dependence

The apparent activation energies over H-CBV 760 and H-BEA 25 were derived from of initial rates by the linear fits of the respective Arrhenius plots. For the decomposition of the aminal, an apparent energy of activation of 5 kJ/mol was found for both catalysts. For the formation of PABA a change of regimes is observed in case of H-CBV 760. At temperatures below 110°C, an activation energy of 37 kJ/mol was determined, while at temperatures exceeding 110°C, an activation energy of 12 kJ/mol was found. The same holds in principle also for the formation of OABA, where at temperatures beneath 90°C an activation energy of 80 kJ/mol was measured, while at temperature over 90°C the apparent activation energy was determined to 6 kJ/mol. For the decomposition of PABA and the formation of 4,4'-MDA 69 kJ/mol and 72 kJ/mol, respectively, were found. For H-BEA 25 the apparent activation energy for PABA formation was 32 kJ/mol over the whole temperature range. The OABA formation showed a similar change of regimes as over H-CBV 760. At temperatures below 80°C an activation energy of 155 kJ/mol was determined, while at temperatures exceeding 80°C an activation energy of 24 kJ/mol was found. For both the decomposition of PABA and the formation of 4,4'-MDA 37 kJ/mol were found over H-BEA 25.

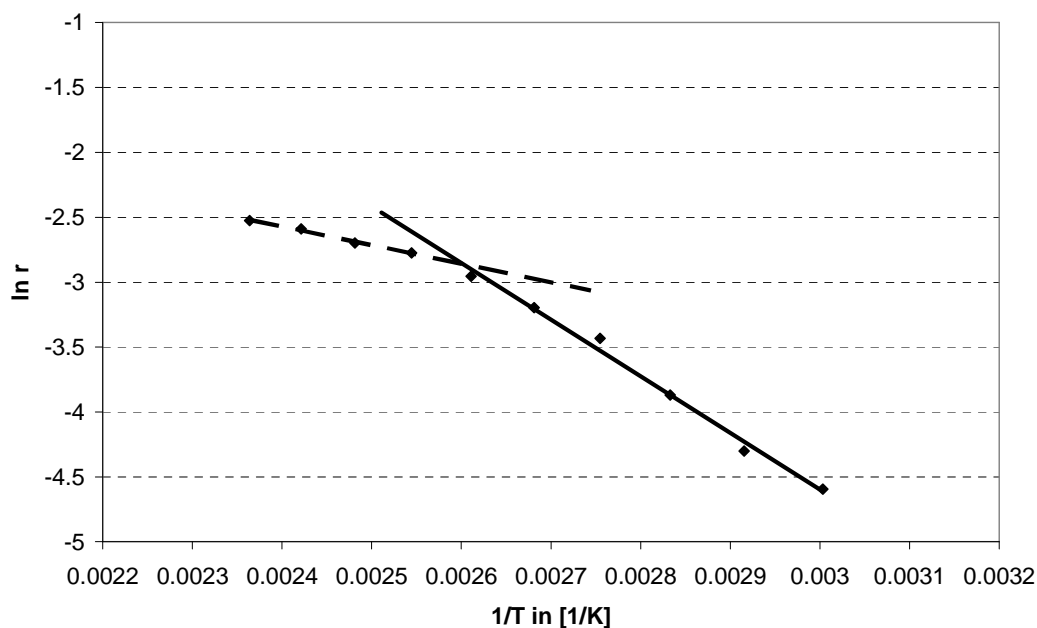


Figure 2.12: Arrhenius plot of the initial rates of formation of PABA, linear fit for dashed line $y = -1431x + 0.862$, $R^2 = 0.992$; linear fit for full line $y = -4368x + 8.503$, $R^2 = 0.992$.

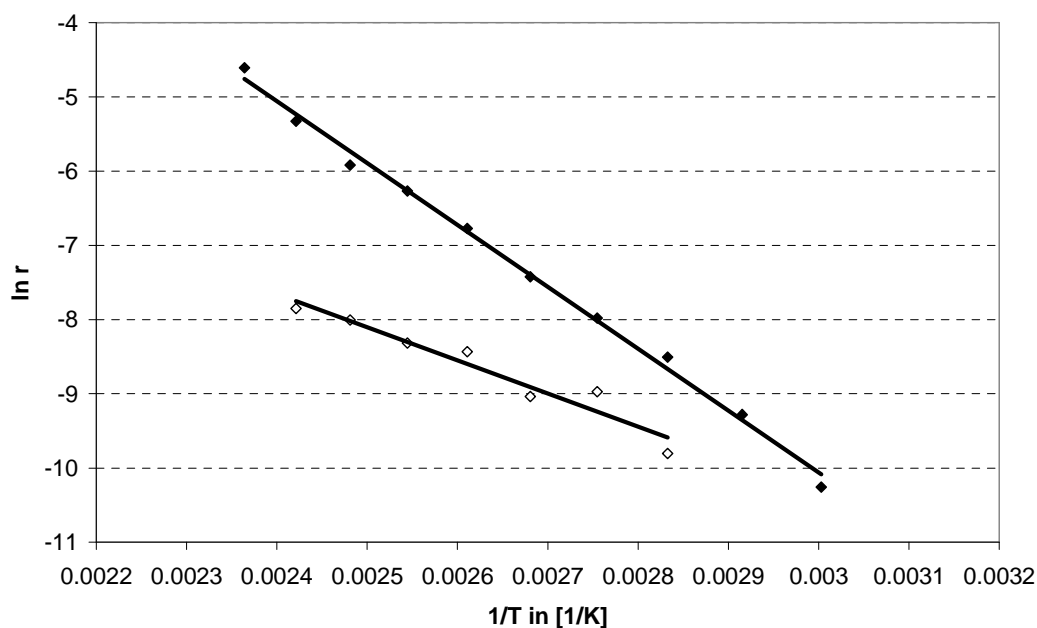


Figure 2.13: Arrhenius plot of the initial rates of decomposition of PABA over H-CBV 720 (full symbols) and H-BEA 25 (hollow symbols). Linear fit for H-CBV 720: $y = -8338x + 14.95$, $R^2 = 0.996$; linear fit H-BEA 25: $y = -4464x + 3.07$, $R^2 = 0.938$.

2.3.4 Reaction orders

A double logarithmic plot of the initial rates of PABA decomposition *versus* its initial concentrations yields straight lines with slopes of 1 for the aminal and 2 for PABA for CBV 760 as well as 1 and 1.5 for H-BEA 25, respectively (Fig. 2.14).

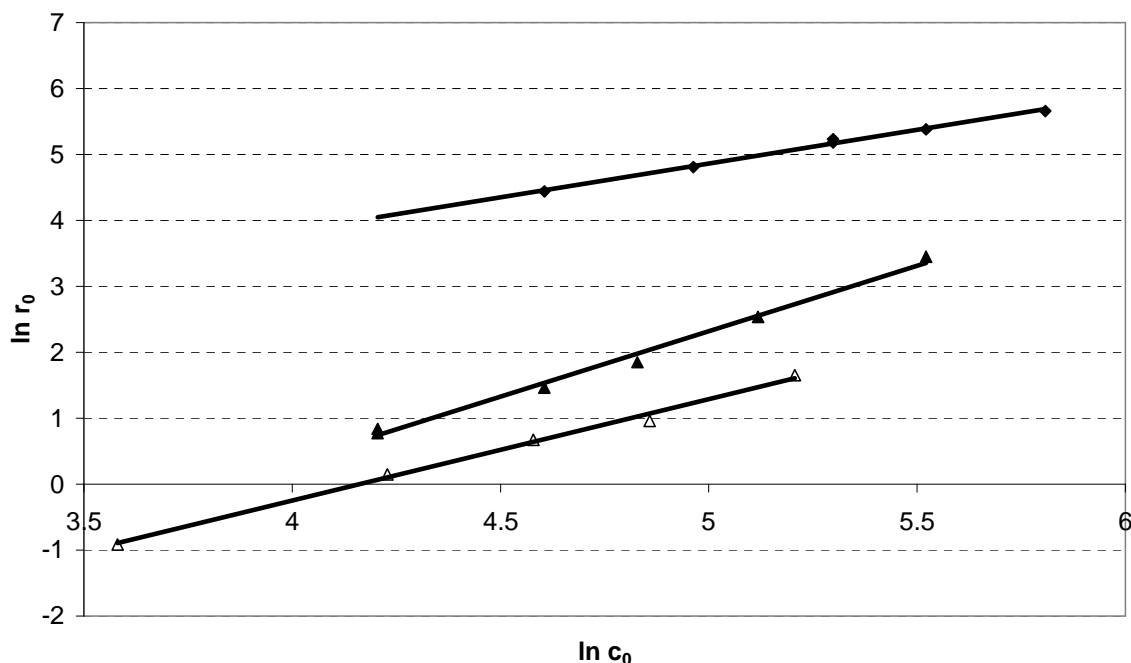


Figure 2.14: Determination of reaction orders over H-CBV 760 (full symbols) and H-BEA 25 (hollow symbols) for aminal (\blacklozenge) and PABA (\blacktriangle) decomposition, linear fit for aminal $y = 1.023x - 0.252$, $R^2 = 0.993$; linear fit for PABA H-CBV 760 $y = 2.002x + 7.677$, $R^2 = 0.995$; linear fit for PABA H-BEA 25 $y = 1.540x + 8.020$, $R^2 = 0.995$.

2.3.5 Influence of aminal to aniline ratio

A further aspect of the reaction being subject to controversial discussion in literature is the influence of the aminal to aniline ratio in the starting material on the final product distribution. While some publications state that a higher excess of aniline decreases the concentration of oligomers in the reaction product^{3,4}, others claim that next to none influence of aniline concentration on the product distribution has been found.⁸

Fig. 2.15 shows the determined product distributions from reaction mixtures with different aniline to aminal ratios. The 4,4'-MDA yield was constant at about 82% for all

concentrations. Also the yield of pMDA and isomers thereof is constant at 5-6%. Only the 2,4'-MDA yield is constantly rising from 4.5% up to 7%, while the OABA yield decreases from 2% to 1%. Furthermore, the yields of the intermediate MDA-PABA is constantly decreasing, because the reaction rate increases with decreasing aminal concentration, due to the higher catalyst to substrate ratio.

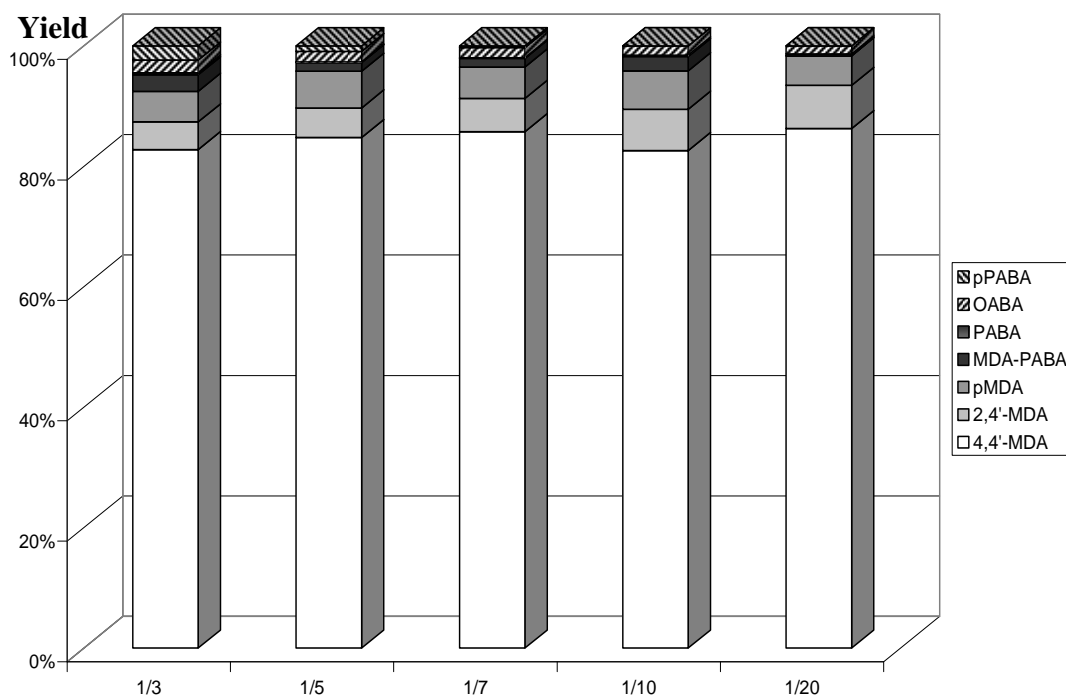


Figure 2.15: Product distribution for different aminal to aniline ratios after 4 h of reaction time.

2.4 Discussion

2.4.1 Reaction Mechanism and Network

The first step of the reaction network, the decomposition of the aminal, is by far the fastest step in the reaction network. This was to be expected as the aminal is the most reactive compound involved in the reaction. In fact the observed reaction order of one and an apparent activation energy of 5 kJ/mol suggests that the first observable step in the reaction network is the film diffusion of the aminal to the outer surface. The decomposition of the aminal, to e.g., PABA, is too fast to be measured itself. The following steps of reaction network, e.g., the decomposition of PABA is significantly slower and can, thus, be monitored.

All compounds showing a positive initial slope in the time concentration profile are primary products formed directly from the aminal. Therefore, PABA and OABA are both primary products, but the formation of PABA is strongly favored due to stronger steric hindrance in the *ortho* position. Also pPABA and the 3-ring aminal are primary products. Literature suggests that the aminal is cleaved on protonation on an acid site and the resulting highly reactive carbenium ion attacks the next available nucleophile.²

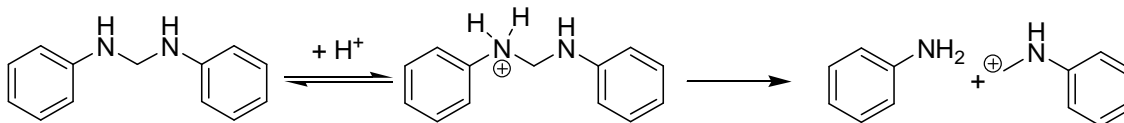


Figure 2.16: Cleavage of the aminal and formation of a carbenium ion.

This can be either an aromatic ring on *ortho* or *para* position or a nitrogen atom of an amino group. As there are a broad variety of nucleophiles available (aniline, the aminal itself, PABA, OABA) which all can be attacked at several positions, a broad variety of intermediates is formed from the aminal. In Figure 2.17 the nucleophilic attack of the carbenium ion on the *para* position of a PABA molecule is shown. This reaction yields an adduct of PABA and the protonated fragment of the aminal (pPABA), which should have a similar reactivity as PABA and can be formed once PABA is present in the reaction mixture.

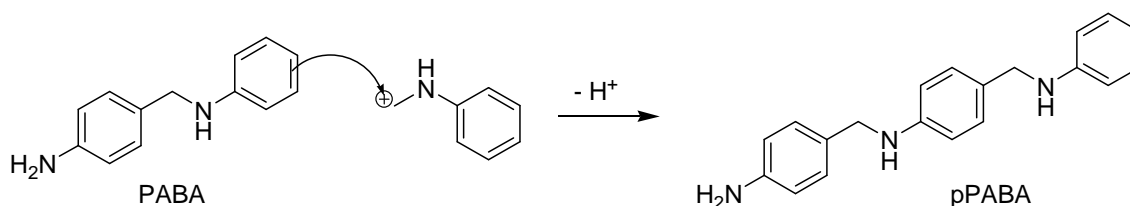


Figure 2.17: Reaction of the carbenium ion with PABA to form pPABA.

If the carbenium ion attacks another aminal on *ortho* or *para* positions of the phenyl ring a 3-ring aminal structure is formed which should retain its high reactivity, as it still contains the aminal function. This seems to be a logical explanation for the observation of the very short lived intermediates.

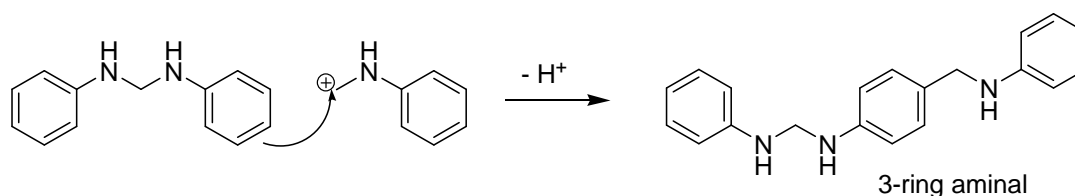


Figure 2.18: Reaction of the carbenium ion with aminal to form a highly reactive 3-ring aminal structure.

These primary products do all contain at least one secondary amino function, which is also not stable on contact with a Brønsted acid. The reaction of these *N*-alkylaniline derivatives with catalytic amounts of mineralic acids to (*para*-)alkylanilines is known in literature as Hofman-Martius rearrangement.¹²⁻¹⁴

The mechanism of this second reaction step is in literature also presumed to proceed *via* a free carbenium ion.² As it is well accepted that free carbenium ions are difficult to stabilize¹⁵, we suggest that the substrate undergoes an S_N2 -type nucleophilic substitution reaction. When the intermediate is adsorbed on a Brønsted acid site of the catalyst, the C-N bond will be weakened by the additional charge. The resulting positive partial charge on the C-atom makes it susceptible to a nucleophilic attack by the free electron pair of the amino function or the phenyl ring of aniline or one of the other reaction intermediates. A S_N2 -type reaction mechanism also explains the observed reaction order

of two for the rearrangement of PABA to 4,4'-MDA. A series of partially Na^+ cation exchanged dealuminated Y-type zeolites having concentration of SiOHAl groups inversely proportional to the exchange degree showed the same turnover frequency with all materials tested (see Table 2.1). This indicates that the strength and concentration of the acid sites does not play a major role. Thus, when pore diffusion limitations can be neglected, as it is the case for CBV 760, all Brønsted acid sites contribute equally to the overall reaction rate. This can be explained by the role of the acid site in the proposed reaction mechanism. The Brønsted acid site is only required for the activation of the intermediates by protonation and the resulting weakening of the C-N bond. The protonation of the secondary amine function is readily achieved also by weak acid sites, thus no influence of the strength of Brønsted acid sites is to be expected.

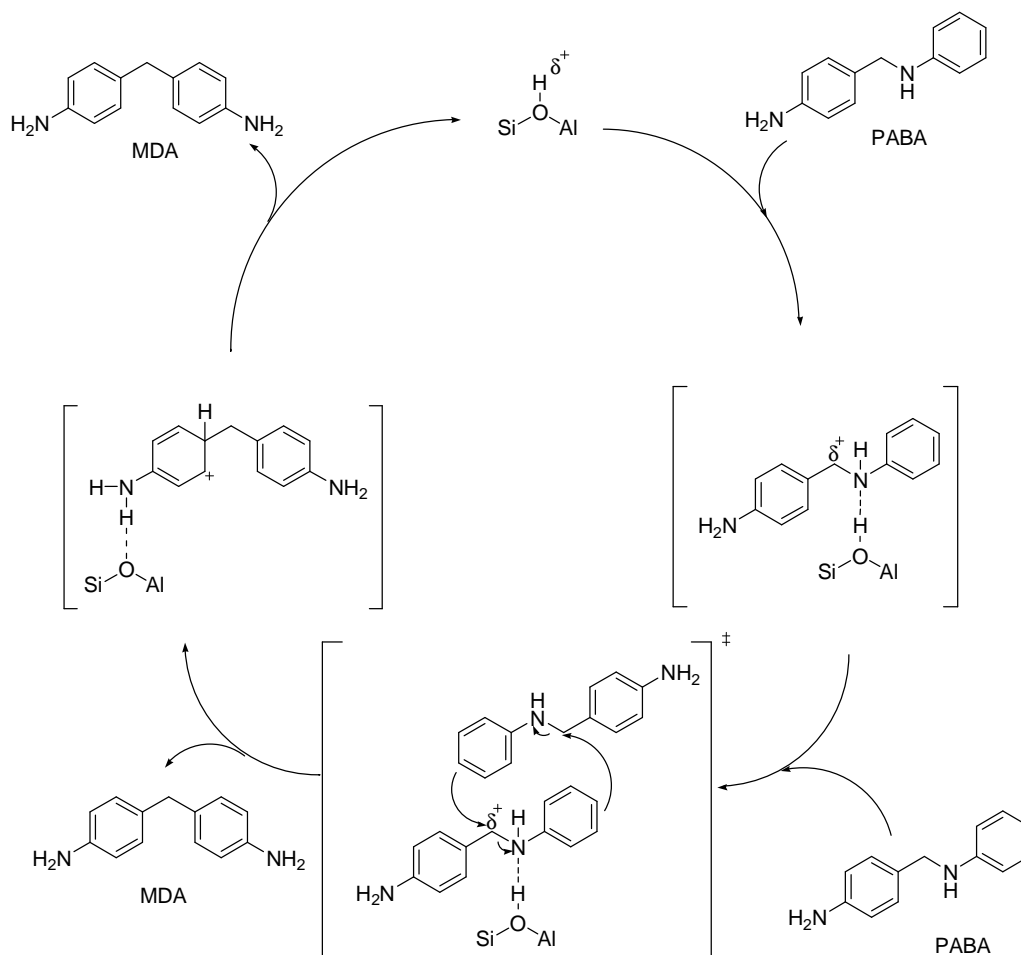


Figure 2.19: Proposed $\text{S}_{\text{N}}2$ type reaction mechanism on the example of 4,4'-MDA formation from PABA.

This reaction mechanism also provides an explanation for the formation of pMDA and MDA-PABA. pMDA is the product of a nucleophilic attack of a preformed 4,4'-MDA onto an “activated” PABA molecule, as illustrated in Scheme 2.20, and is a stable end product of the reaction. If the nucleophilic position for the attack is not the phenyl ring but the nitrogen itself, MDA-PABA is formed. It has been labeled MDA-PABA as it contains a methylene bridged biphenyl unit like MDA as well as the secondary amine motif from PABA. Because of this secondary amino function it is still reactive and can be further converted to MDA and/or PABA (see Scheme 2.21).

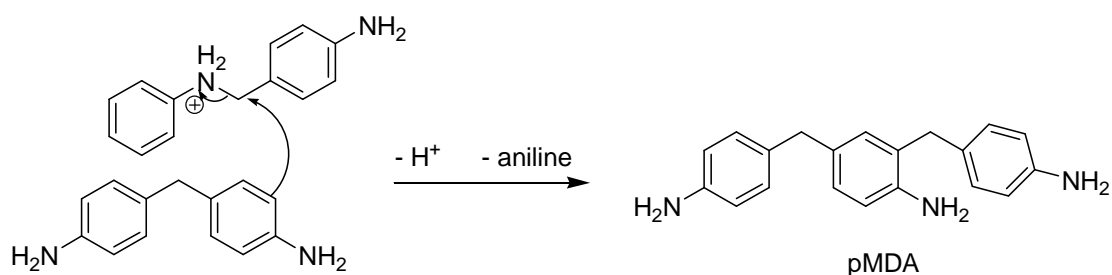


Figure 2.20: Formation of pMDA from 4,4'-MDA and PABA.

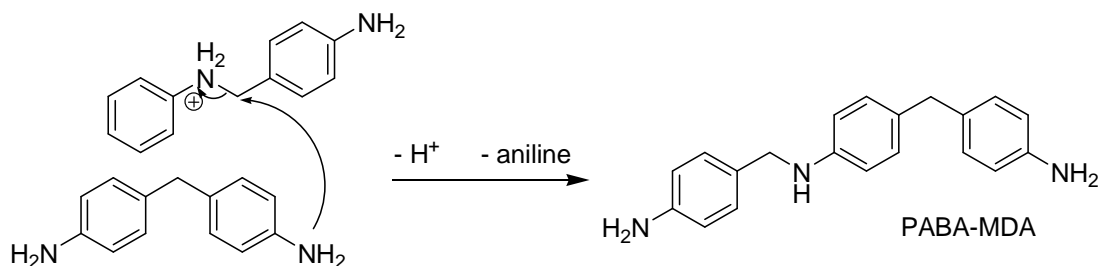


Figure 2.21: Formation of MDA-PABA from 4,4'-MDA and PABA.

The experiments with different aminal concentrations show that only the yields of 2,4'-MDA and OABA are affected significantly by the aniline concentration. This is in agreement with the proposed reaction mechanism, which does not point to reactions between the activated species and aniline. MDA is formed from PABA *via* a nucleophilic attack of PABA on a second (activated) PABA and is, therefore, second order in PABA. Aniline is a strong nucleophile and should, thus, be attacked by the active species. However, aniline is significantly smaller than PABA and can realign itself to attack the

electrophilic methylene-carbon with the free electron pair of the amino function, which is more nucleophilic than the phenyl ring system. Scheme 2.22 shows that the products of the reaction of PABA with aniline are again PABA and aniline and consequently no net reaction can be monitored.

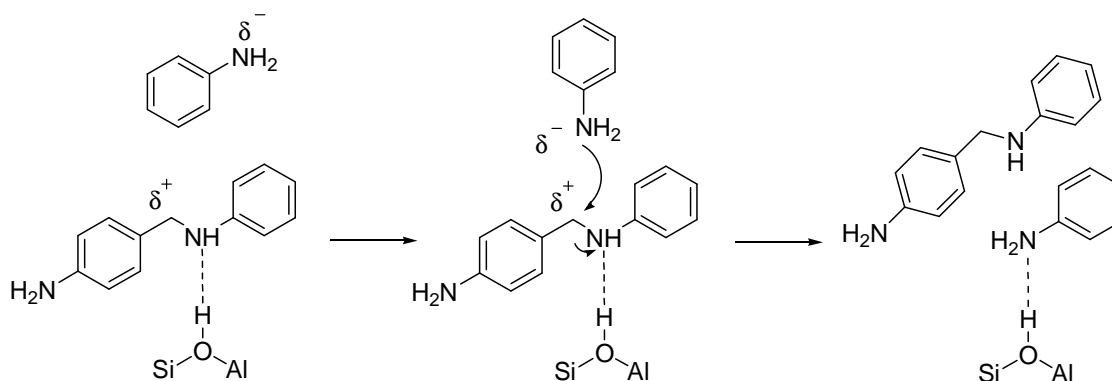


Figure 2.22: Reaction of PABA with aniline.

The decomposition of OABA is so slow at 100°C that the OABA is still present in the reaction mixture, when all other reactive intermediates have already reacted. Therefore, the only remaining reaction partners for OABA are other OABA molecules, which are only present at very low concentrations. Thus, the possibility of the mutual reaction of two OABA molecules is negligible. Aniline, which is present abundantly, may react, but the reaction products will yield OABA and aniline. Only in the few cases when OABA is reacting with a carbon atom of the phenyl ring of aniline, 2,4'-MDA and aniline are formed. This model explains why (a) the decomposition of OABA is very slow, (b) the reaction order of the OABA decomposition seems to follow first order kinetics in OABA instead of second and c) only the OABA and 2,4'-MDA yields are affected by the aniline concentration.

The activation energy for PABA decomposition (69 kJ/mol) and 4,4'-MDA formation (72 kJ/mol) are in good agreement and further demonstrate that 4,4'-MDA is generated from PABA. The relatively high apparent activation energy of about 70 kJ/mol and the reaction order of two found with H-CBV 760 indicate that this step of the reaction network is limited by microkinetics and not by mass transport. Over H-BEA 25, the

apparent activation energy for PABA decomposition was 37 kJ/mol and the reaction order was 1.5. The fact that only half the apparent activation energy and a reaction order of $(n+1)/2 = 1.5$ were found for H-BEA suggests that the reaction is limited by mass transport over the BEA zeolite (see also refs ^{3,5}). This hypothesis is further supported by the determined TOFs for H-BEA 25 and H-CBV 760. Note also, that the TOF for the dealuminated Y-type sample is more than 20 times higher than that for H-BEA 25 despite the variation in the ion exchange degree (which also varies the acid site strength).

The reason for the different behavior is attributed to the different pore structures of H-CBV 760 and H-BEA 25. Nitrogen physisorption showed that parent H-BEA 25 has next to none mesopore volume and, therefore, the active sites can only be reached through micropores. In contrast, H-CBV 760 has a significant mesopore volume ($0.18 \text{ cm}^3 \text{ g}^{-1}$). These mesopores provide better access to the near surface active acid sites minimizing the transport through the zeolite particles.

2.4.2 Simulation of the reaction network

The fact that the activated (bound on a Brønsted acid site) species will attack any available nucleophile results in a rather complex reaction network. In order to simplify this network for a simulation, only the eight major compounds of the reaction network are chosen for the calculation: the aminal (starting material), PABA, OABA, pPABA, MDA-PABA, 2,4'-MDA, 4,4'-MDA and pMDA. The 3-ring aminal species are not included in the model network because they are very short lived. Also 2,2'-MDA, *N*-methyl-MDA and a variety of structural motifs of pMDA, which can only be found in traces are neglected in modeling. Note, that the proposed reaction network is, however, capable to explain their formation.

The simplified reaction network with the eight included substances is shown in Scheme 2.23. The 15 separate reactions linking these eight substances can be described by a set of differential equations (Formulas 2 – 9) for the rates of formation/consumption of each of the involved substances. Nonlinear parameter fitting of the differential equations 2-9 to the experimental data (as shown in Fig. 2.8) was performed by using the CMA evolution strategy in Matlab.¹⁶ The root mean squared error normalized to the variance of the data (NRMS error) was used as the objective function to be minimized. To ensure that the

globally optimal parameter set was found, each optimization run was repeated three times with varying parameter sets of the evolution strategy.

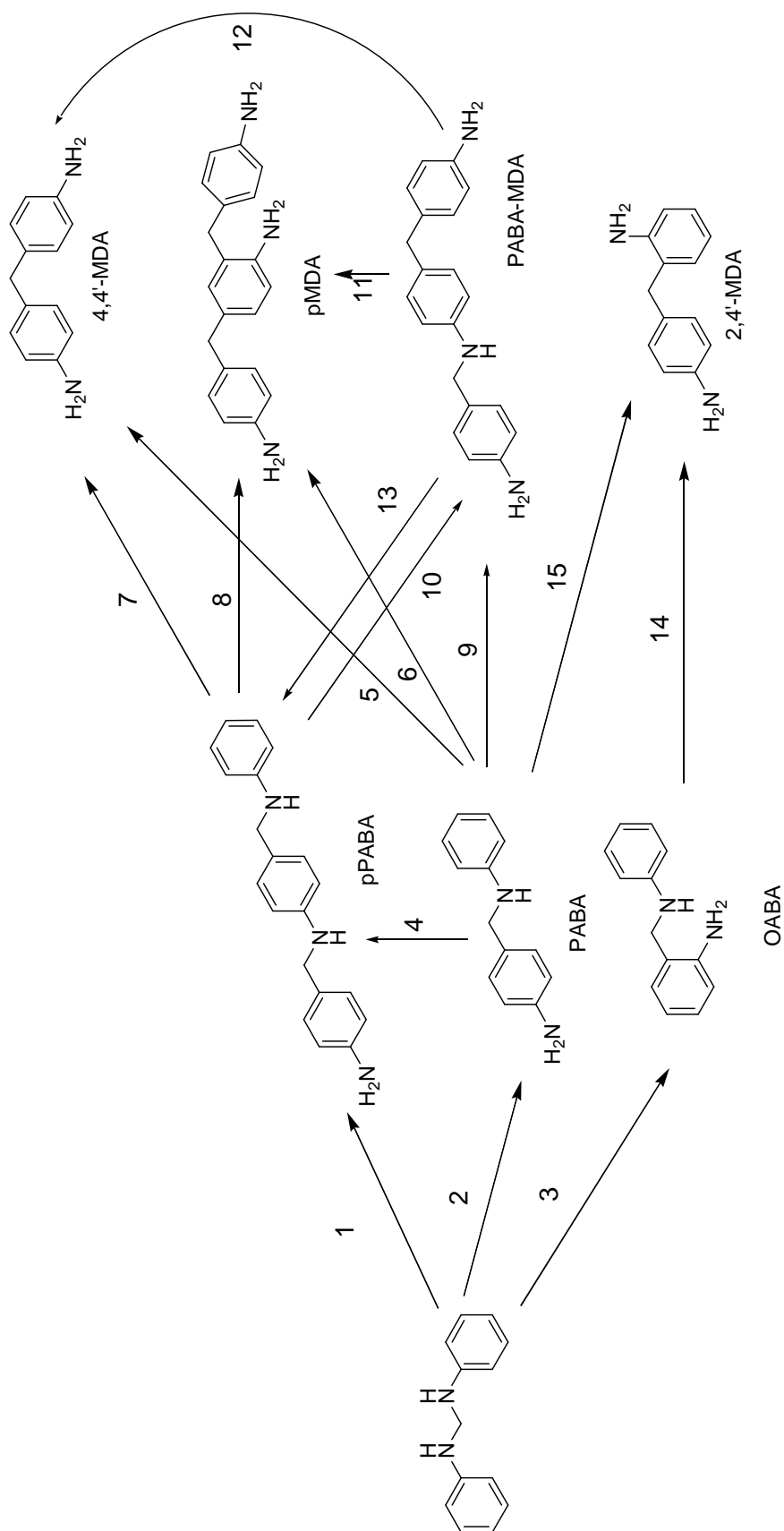


Figure 2.23: Simplified reaction network.

$$\frac{d(\text{aminal})}{dt} = -(k_1 + k_2 + k_3) \cdot [\text{aminal}] \quad (2)$$

$$\frac{d(\text{OABA})}{dt} = k_3 \cdot [\text{aminal}] - k_{14} \cdot [\text{OABA}] \quad (3)$$

$$\begin{aligned} \frac{d(\text{PABA})}{dt} &= k_2 \cdot [\text{aminal}] - k_4 \cdot [\text{PABA}]^2 - k_5 \cdot [\text{PABA}]^2 + k_8 \cdot [p\text{PABA}] \cdot [4,4'\text{MDA}] \\ &\quad - k_6 \cdot [\text{PABA}] \cdot [4,4'\text{MDA}] - k_9 \cdot [\text{PABA}] \cdot [4,4'\text{MDA}] \\ &\quad - k_{13} \cdot [\text{PABA}] \cdot [\text{MDA} - \text{PABA}] + k_7 \cdot [p\text{PABA}] \\ &\quad + k_{10} \cdot [p\text{PABA}] \cdot [4,4'\text{MDA}] - k_{15} \cdot [\text{PABA}]^2 \end{aligned} \quad (4)$$

$$\begin{aligned} \frac{d(p\text{PABA})}{dt} &= \frac{1}{2} \cdot k_2 \cdot [\text{aminal}] + \frac{1}{2} \cdot k_4 \cdot [\text{PABA}]^2 - k_7 \cdot [p\text{PABA}] \\ &\quad - k_8 \cdot [p\text{PABA}] \cdot [4,4'\text{MDA}] - k_{10} \cdot [p\text{PABA}] \cdot [4,4'\text{MDA}] \\ &\quad + k_{13} \cdot [\text{PABA}] \cdot [\text{MDA} - \text{PABA}] \end{aligned} \quad (5)$$

$$\begin{aligned} \frac{d(\text{MDA} - \text{PABA})}{dt} &= k_9 \cdot [\text{PABA}] \cdot [4,4'\text{MDA}] + k_{10} \cdot [p\text{PABA}] \cdot [4,4'\text{MDA}] \\ &\quad - k_{11} \cdot [\text{MDA} - \text{PABA}] - k_{12} \cdot [\text{MDA} - \text{PABA}] \\ &\quad - k_{13} \cdot [\text{MDA} - \text{PABA}] \cdot [\text{PABA}] \end{aligned} \quad (6)$$

$$\begin{aligned} \frac{d(4,4'\text{MDA})}{dt} &= k_5 \cdot [\text{PABA}]^2 + k_7 \cdot [p\text{PABA}] - k_6 \cdot [4,4'\text{MDA}] \cdot [\text{PABA}] \\ &\quad - k_8 \cdot [4,4'\text{MDA}] \cdot [p\text{PABA}] - k_9 \cdot [4,4'\text{MDA}] \cdot [\text{PABA}] \\ &\quad - k_{10} \cdot [4,4'\text{MDA}] \cdot [p\text{PABA}] + 2 \cdot k_{12} \cdot [\text{MDA} - \text{PABA}] \\ &\quad + k_{13} \cdot [\text{MDA} - \text{PABA}] \cdot [\text{PABA}] \end{aligned} \quad (7)$$

$$\frac{d(2,4'\text{MDA})}{dt} = k_{14} \cdot [\text{OABA}] + k_{15} \cdot [\text{PABA}]^2 \quad (8)$$

$$\begin{aligned} \frac{d(p\text{MDA})}{dt} &= k_6 \cdot [\text{PABA}] \cdot [4,4'\text{MDA}] + k_8 \cdot [p\text{PABA}] \cdot [4,4'\text{MDA}] \\ &\quad + k_{11} \cdot [\text{MDA} - \text{PABA}] \end{aligned} \quad (9)$$

The resulting time concentration profiles for PABA, OABA, pPABA, 4,4'-MDA, 2,4'-MDA, pMDA and MDA-PABA at 100°C, 60°C and 140°C are shown in Fig. 2.24-26. The simulated time concentration profiles are in very good agreement with the experimental data. Further evidence for the validity of the reaction network can be drawn from the fact, that it is possible to fit the experimental data also at significantly higher and lower temperatures (60°C and 140°C) by the same kinetic model. As the reaction at 60°C was carried out over night significant catalyst deactivation occurred during this significantly longer time frame. Therefore, the simulated profiles can not reproduce the composition of the reaction mixture measured the next morning, because the catalysts' activity has markedly decreased and higher intermediate and lower MDA concentrations are predicted. As the kinetic model does not include catalyst deactivation, it is of course unable to predict this behavior. Actually the observation that catalyst deactivation leads to a change in the time concentration profiles that can not be reproduced by the kinetic model provides evidence that the kinetic model is not actually too large. An over dimensioned kinetic network (to many parameters) would be able to reproduce any set of experimental data and would therefore contain no actual scientific information.

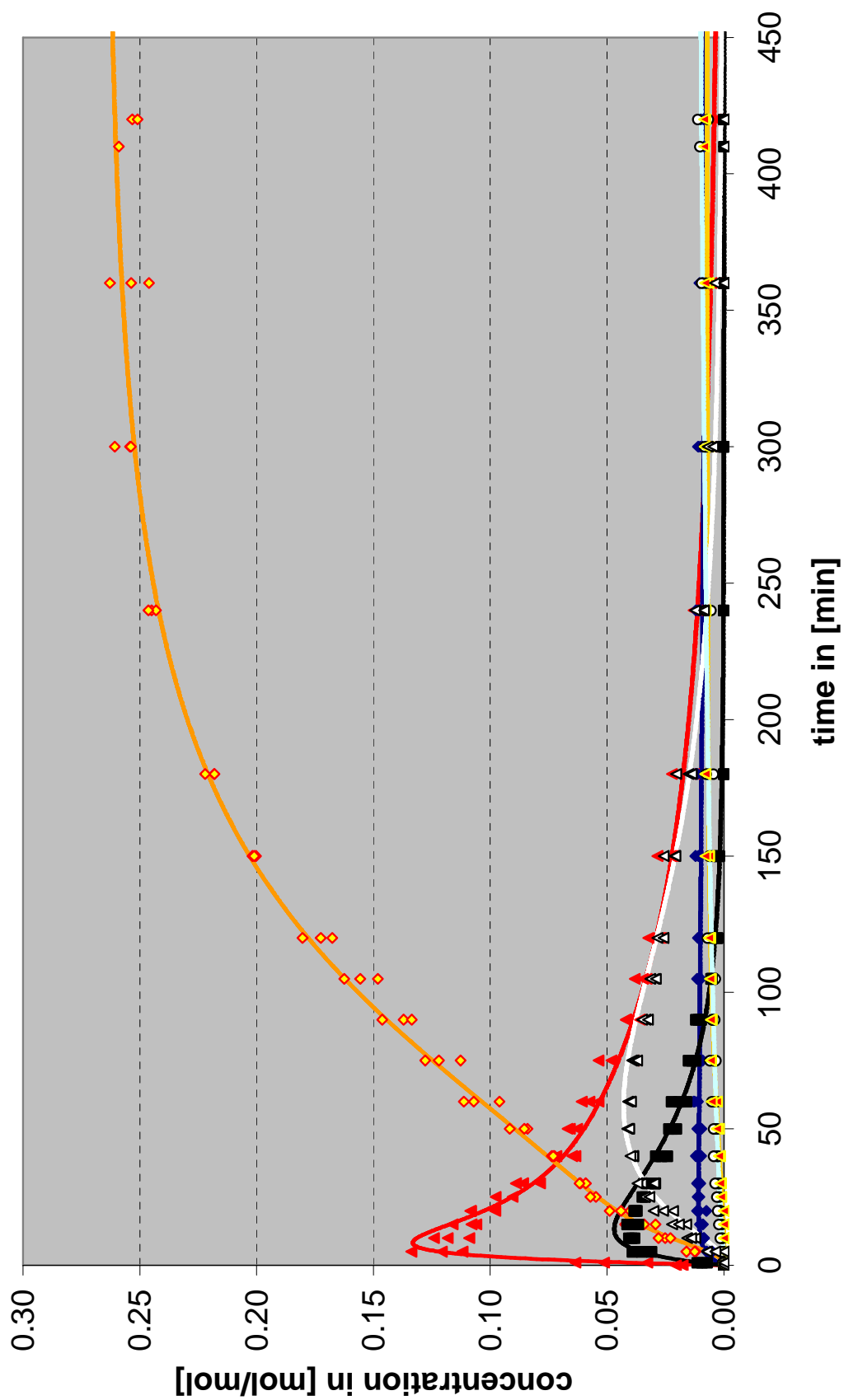


Figure 2.24: Simulated time concentration profile (full lines) of the synthesis of MDA from animal at 100°C over a dealuminated Y-type zeolite (CBV 760); \blacktriangleright PABA, \blacklozenge OABA, \blacklozenge 4,4'-MDA, \circ 2,4'-MDA, \blacksquare pPABA, \blacktriangledown MDA-PABA, \blacktriangleright pMDA.

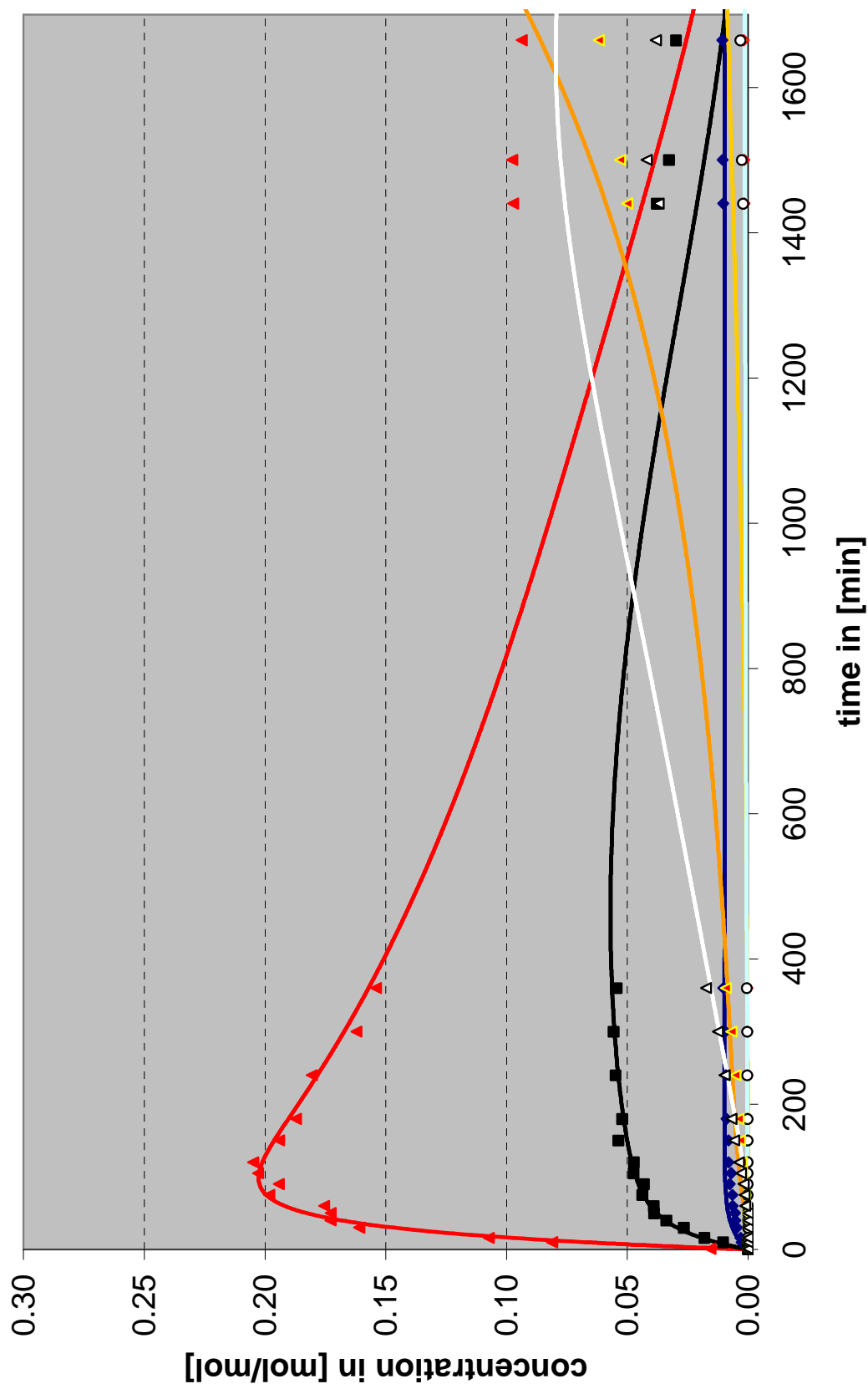


Figure 2.25: Simulated time concentration profile (full lines) of the synthesis of MDA from amination at 60°C over a dealuminated Y-type zeolite (CBV 760); \blacktriangle PABA, \blacklozenge OABA, \blacklozenge 4,4'-MDA, \circ 2,4'-MDA, \blacksquare pPABA, \blacktriangleright MDA-PABA, \blacktriangleright pMDA.

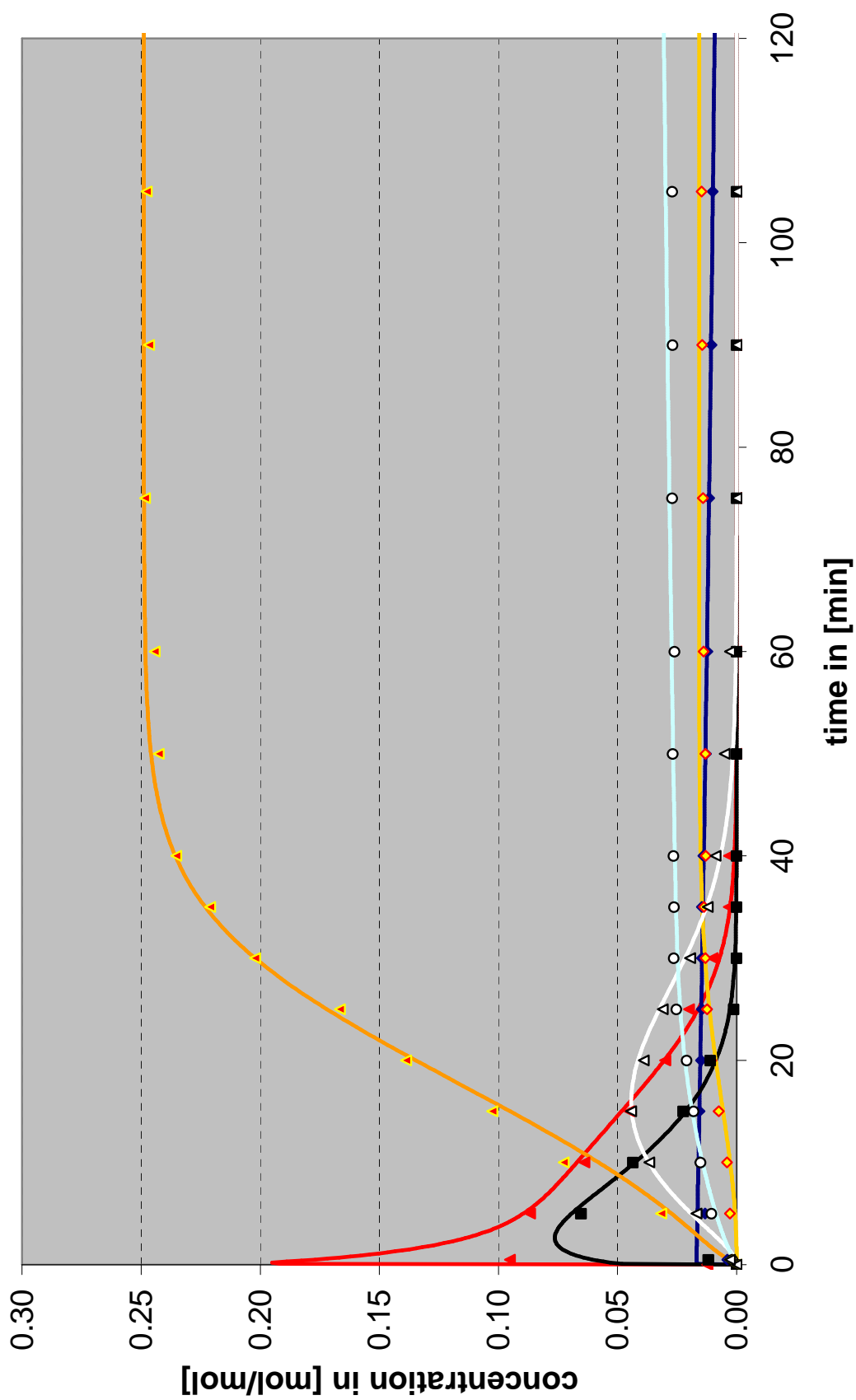


Figure 2.26: Simulated time concentration profile (full lines) of the synthesis of MDA from aminal at 140°C over a dealuminated Y-type zeolite (CBV 760); \blacktriangle PABA, \blacklozenge OABA, \circ 4,4'-MDA, \blacksquare pPABA, \blacktriangledown MDA-PABA, \blacktriangleright pMDA.

In the following the parity plots the correlation of the simulated profiles at 100°C and the measured data are shown. The accordance between theoretical and measured data is excellent in case of 4,4'-MDA, PABA and MDA-PABA and also very good for 2,4'-MDA, pMDA and pPABA. In case of OABA the parity plot is not significant, as its concentration rapidly reaches a constant level and therefore no data points at intermediate concentrations are available. The fit for the aminal concentration is the most difficult due to the problem of its experimental verification. Firstly the decomposition reaction of the aminal is very fast and therefore only very few data points are available and secondly the unstable aminal can not be detected directly but only from its decomposition products in the GC.

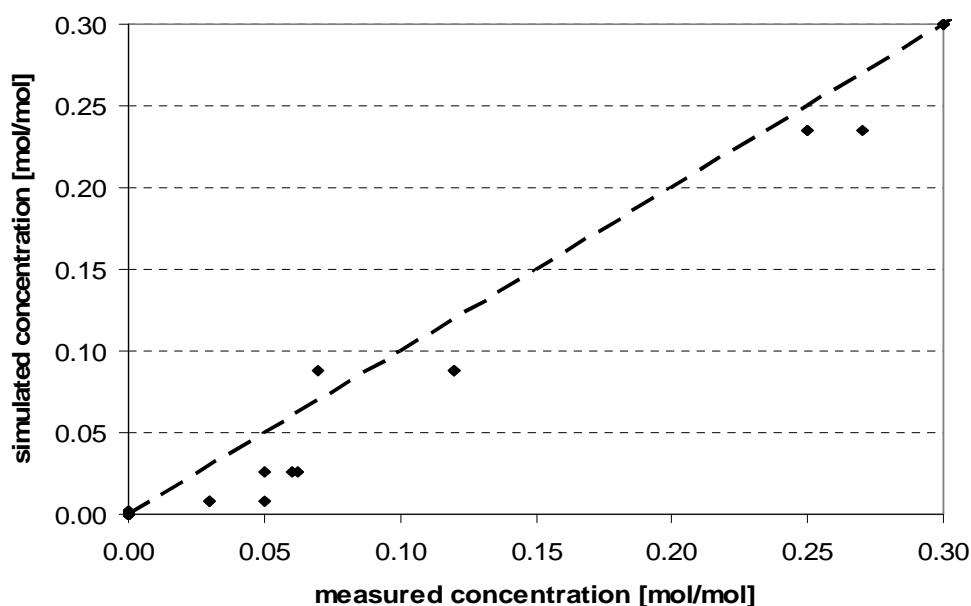


Figure 2.27: Parity plot for simulated and measured aminal concentration over H-CBV 760 at 100°C. Dashed line represents ideal match.

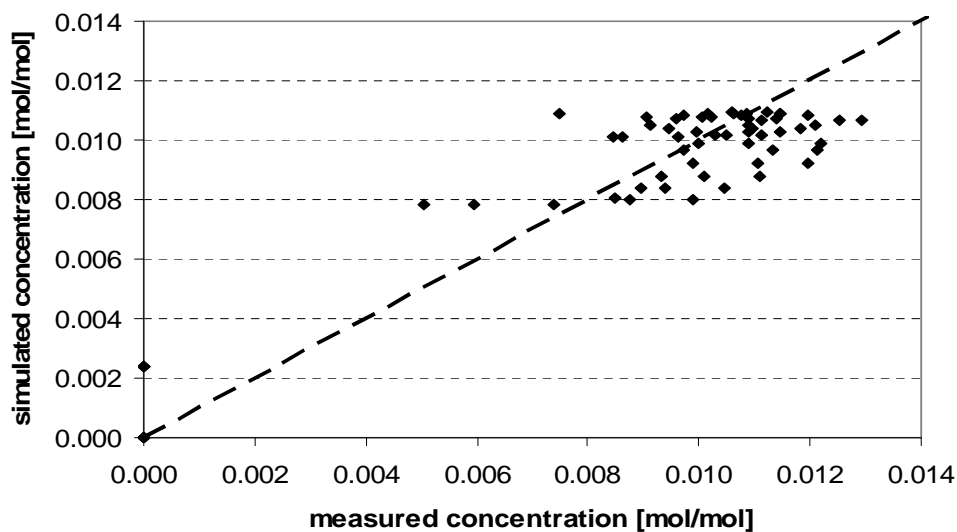


Figure 2.28: Parity plot for simulated and measured OABA concentration over H-CBV 760 at 100°C. Dashed line represents ideal match.

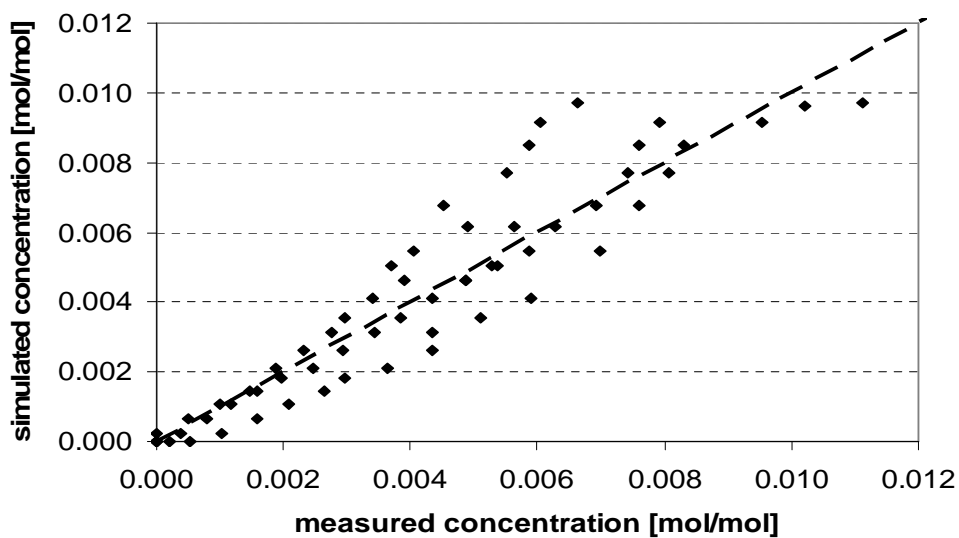


Figure 2.29: Parity plot for simulated and measured 2,4'-MDA concentration over H-CBV 760 at 100°C. Dashed line represents ideal match.

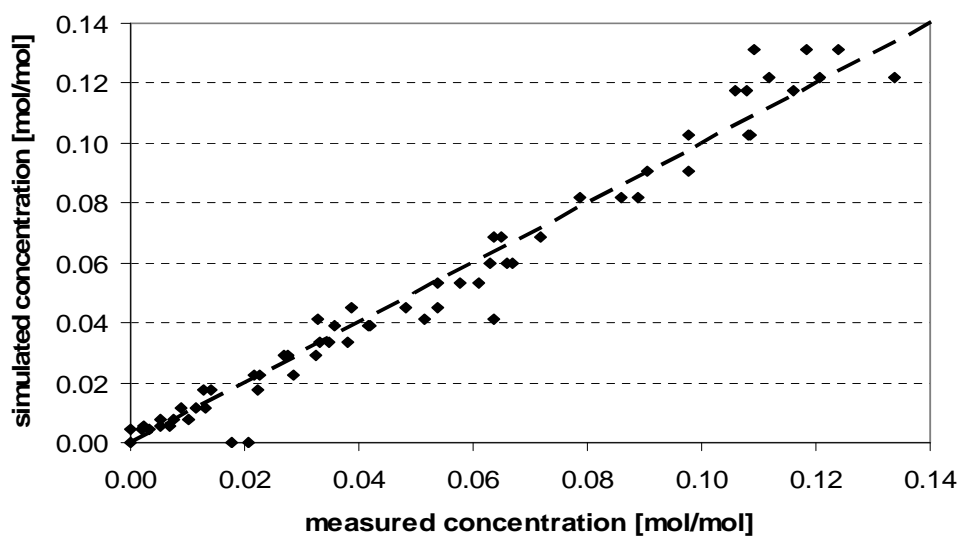


Figure 2.30: Parity plot for simulated and measured PABA concentration over H-CBV 760 at 100°C. Dashed line represents ideal match.

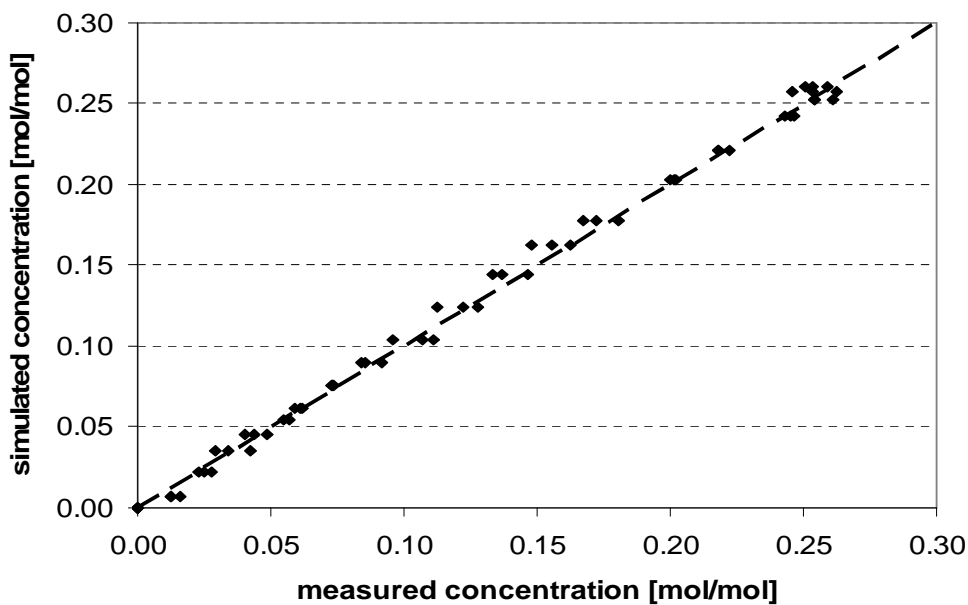


Figure 2.31: Parity plot for simulated and measured 4,4'-MDA concentration over H-CBV 760 at 100°C. Dashed line represents ideal match.

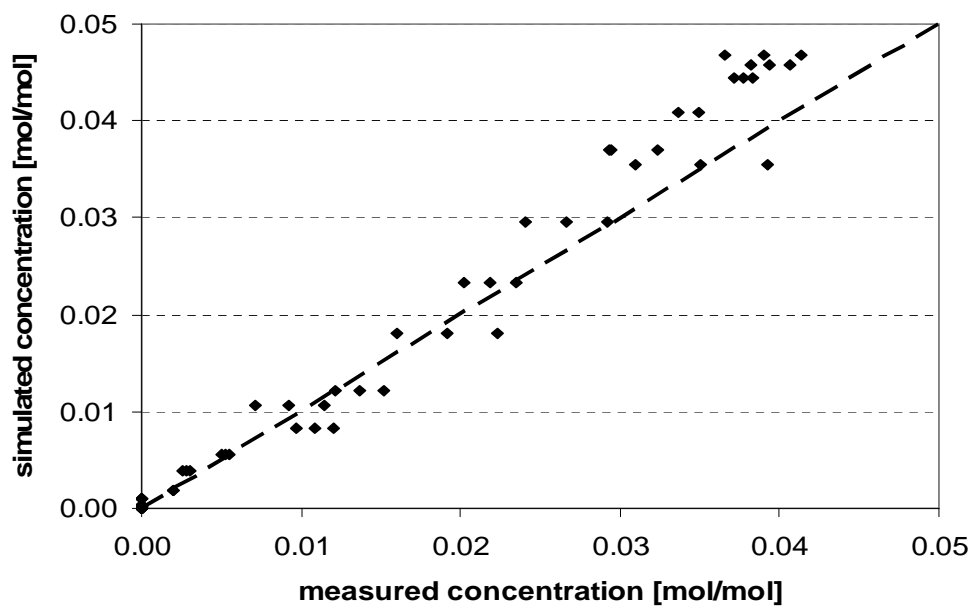


Figure 2.32: Parity plot for simulated and measured pPABA concentration over H-CBV 760 at 100°C. Dashed line represents ideal match.

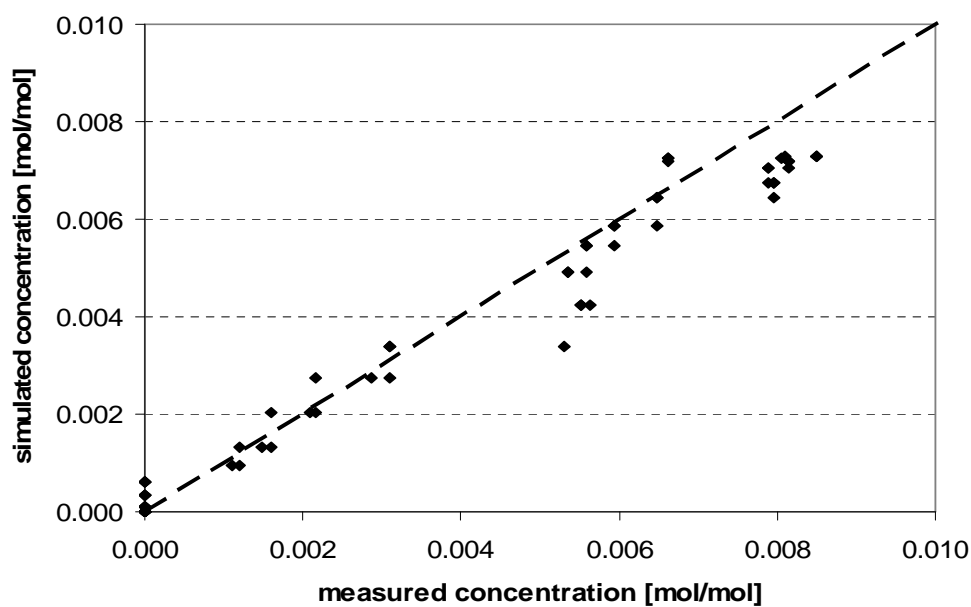


Figure 2.33: Parity plot for simulated and measured pMDA concentration over H-CBV 760 at 100°C. Dashed line represents ideal match.

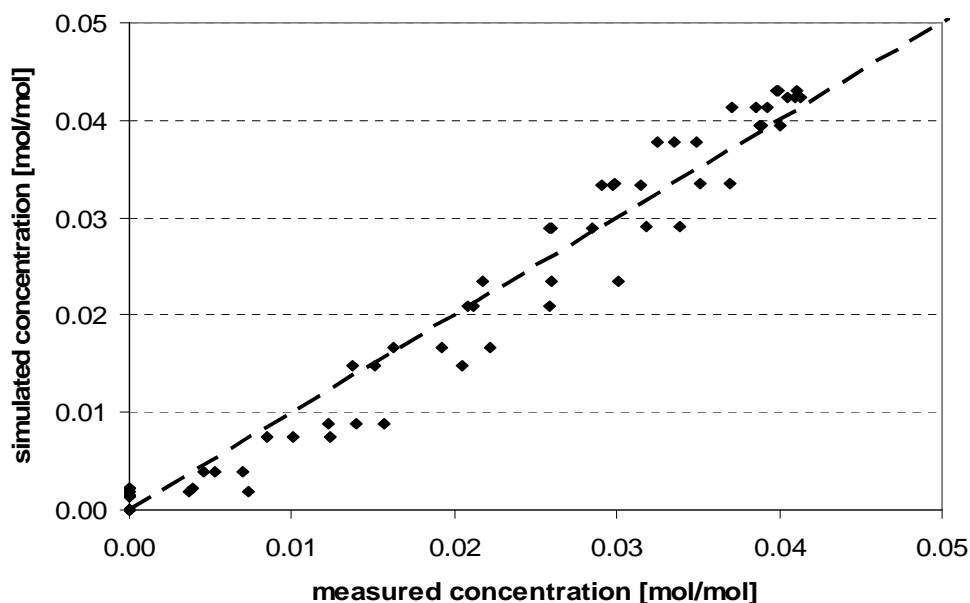


Figure 2.34: Parity plot for simulated and measured MDA-PABA concentration over H-CBV 760 at 100°C. Dashed line represents ideal match.

The parity plots show that the simulated profiles are in very good agreement with the measured data. The corresponding plots at 60 and 140°C are of similar quality but are not shown in detail. Although a further refinement of the reaction network, involving more reaction intermediates could provide even better fits, this course of action has not been pursued. The fact that the proposed reaction network is able to reproduce the measured time concentration profiles, as well as explain the observed reaction orders and activation energies, already provides solid evidence that the proposed reaction network and the reaction mechanism it is based upon are indeed valid for the synthesis of MDA over the applied dealuminated Y-type zeolite.

2.5 Conclusions

The aim of *Stage 1* of the project was the identification of the reaction network and mechanism involved in the formation of methylenedianiline over solid acid catalysts. We achieved this goal by using GC analysis to record detailed time concentration profiles of the synthesis of MDA from the condensation product of aniline and formaldehyde (aminal) over a dealuminated Y-type zeolite. From these profiles we were able to deduce the structure of several oligomer species, which were until now not distinguished in literature. We report that only some of these oligomers is really stable end products of the reaction (pMDA and constitution isomers thereof), while other oligomers are merely intermediates of the reaction (pPABA and MDA-PABA).

A detailed reaction network was developed based on a S_N2 type reaction mechanism, describing the reaction with high accuracy. Comparing zeolite catalysts without mesopores (BEA type zeolite) and those with mesopores (dealuminated Y-type zeolite H-CBV 760), we showed that the first step of the reaction network, the decomposition of the aminal, is limited by pore diffusion in both zeolite systems. The subsequent rearrangement of the *N*-alkylbenzylaniline intermediates, however, is limited by pore diffusion over zeolites that do not have mesopores (BEA), while it is not affected by mass transport limitation over the mesoporous dealuminated Y-type zeolite. Note that we are reporting here on H-BEA, because its small crystals lead to significantly higher catalytic performance compared to the larger crystals of a parent H-Y catalyst. The presence of mesopores, such as in the applied H-CBV 760, drastically improves catalytic activity by reducing mass transport limitation.

Detailed knowledge of the reaction network indicates that solid Brønsted acid catalysts with small crystal size and a pronounced mesoporosity offer ideal green catalytic routes for MDA synthesis. The solid acid helps avoid the use of HCl and the formation of stoichiometric amounts of NaCl in the process. A *systematic* study of the detailed role of the pore size, geometry and extend of mesoporosity is in progress and is the main topic of the next Chapter.¹⁷

ACKNOWLEDGMENTS

O.C. Gobin is gratefully acknowledged for performing the CMA evolution strategy calculations in Matlab. The authors are grateful to X. Hecht for BET measurements and M. Neukamm for SEM and AAS measurements. Financial and material support by the Dow Chemical Company are gratefully acknowledged. Furthermore the work at the Technische Universität München was funded by the DOW Chemical Company.

This chapter is based upon :

M. Salzinger, J.A. Lercher, *Green Chemistry*, paper submitted.

REFERENCES

- [1] TDI/MDI; Chem Systems Report 98/99 S8; Process Evaluation/Research Planning Program, *Chem Systems*, San Francisco, **1999**.
- [2] A. de Angelis, P. Ingallina, C. Perego, *Ind. Eng. Chem. Res.* **2004**, *43*, 1169.
- [3] A. Corma, P. Botella, C. Mitchell, *Chem. Comm.* **2004**, *17*, 2008.
- [4] T. Kugita, S. Hirose, S. Namba, *Catal. Today* **2006**, *111*, 275.
- [5] C. Perego, A. de Angelis, A. Carati, C. Flego, R. Villini, C. Rizzo, G. Bellussi, *Appl. Catal. A* **2006**, *307*, 128.
- [6] P. Botella Asuncion, J.K.P. Bosman, A. Corma, C.J. Mitchell, *US Patent 7,238,840 B2* **2007**.
- [7] Y. Kiso, T. Toshihiro, T. Hayashi, *EU Patent 0,329,367 A2* **1989**.
- [8] C. Perego, A. de Angelis, O. Farias, A. Bosetti, *EU Patent 1,055,663 A1* **2000**.
- [9] B.C. Lippens, B.G. Linsen, J.H. de Boer, *J. Catal.* 1964, *3*(1), 32.
- [10] G. Hasely, *J. Chem. Phys.* **1948**, *16*(10), 932.
- [11] E.P. Barret, L.G. Joiyner, P.P. Halenda, *J. Am. Chem. Soc.* **1953**, *73*, 373.
- [12] A.W. Hofman, C.A. Martius, *Ber.* **1871**, *4*, 742.
- [13] A.W. Hofman, *Ber.* **1872**, *5*, 704.
- [14] H. Hart, J.R. Kosak, *J. Org. Chem.* **1962**, *27*(1), 116.
- [15] W. Song, J.B. Nicholas, J.F. Haw, *J. Am. Chem. Soc.* 2001, *123*, 121-129.
- [16] Hansen, N., in: J. A. Lozano, P. Larranaga, I. Inza, E. Bengoetxea (Eds.), *The CMA evolution strategy: a comparing review, Towards a new evolutionary computation. Advances on estimation of distribution algorithms*, Springer **2006**, 75.
- [17] M. Salzinger, M.B. Fichtl, J.A. Lercher, *Appl. Catal. A*, paper submitted.

Chapter 3

On the influence of pore geometry and acidity on the activity of parent and modified zeolites in the synthesis of methylenedianiline

Methylenedianiline synthesis from formaldehyde and aniline is catalyzed by solid acid catalysts, such as zeolites, which offer strong acidity and high acid site density. Critical parameters for catalyst activity were explored using materials with MFI, BEA, MOR and FAU structure. While materials with MOR and MFI structure hardly show activity, BEA and FAU type zeolites are active and selective. The higher activity for the latter materials is related to their larger pore structure. Nevertheless, the reaction is limited by pore diffusion over parent BEA- and FAU-type zeolites. Mesoporous materials, such as dealuminated FAU, offer significantly higher activity as pore diffusion limitation can be overcome. Therefore, we synthesized and tested other mesoporous aluminosilicates such as desilicated BEA and the delaminated MWW materials ITQ-2 and MCM-36. It was shown that desilication increases the activity of parent BEA type zeolites for MDA formation, yet not to the same extent as dealumination in case of FAU. ITQ-2 shows promising results, but MCM-36 surpasses ITQ-2 in terms of activity by a factor of two displaying activities similar to the dealuminated FAU materials.

3. On the influence of pore geometry and acidity on the activity of parent and modified zeolites in the synthesis of methylenedianiline

3.1 Introduction

As already mentioned in the previous chapters it is the designated aim of this thesis to develop improved solid acid catalysts for the production of methylenedianiline (MDA) from aniline and formaldehyde. The first step toward the development of such an improved catalyst is to understand the reaction network that is involved in the formation of MDA and the reaction mechanism through which this reaction proceeds. This first step has been taken in *Stage 1* of the project and is reported in the previous chapter and in also in literature.¹ It was found that the reaction can be divided into two main steps: the decomposition of the preformed aminal (condensation product of aniline with formaldehyde) into intermediate species of benzyanilines and the rearrangement of these intermediates into stable MDA-isomers.

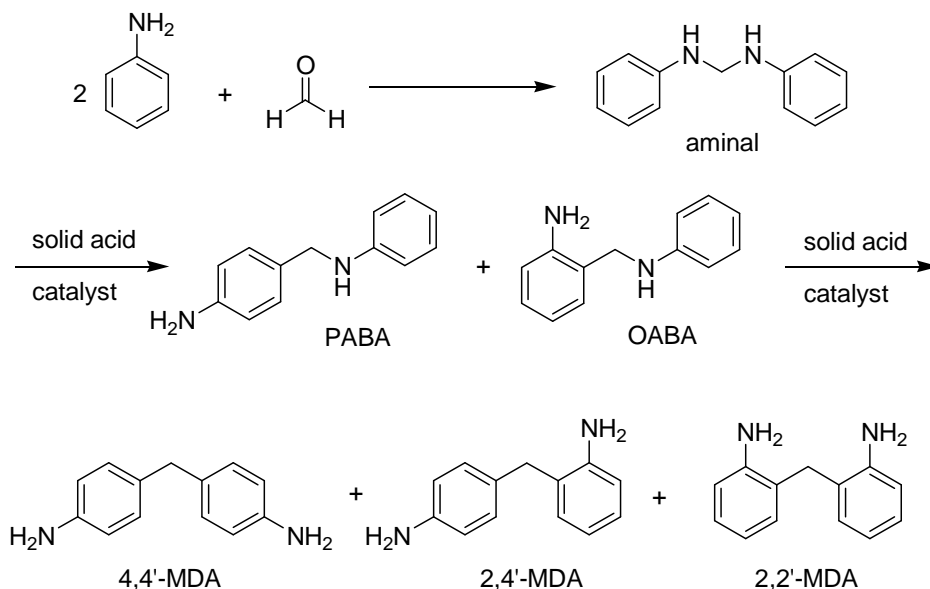


Figure 3.1: Simplified reaction sequence for the synthesis of MDA over zeolite catalysts.¹⁻³

By analysis of kinetic data we were able to suggest a more detailed reaction network and also a S_N2 -type reaction mechanism. Using this kinetic model it is possible to reproduce the measured concentration profiles in a simulation, such showing that the proposed model is valid. In contrast to previous publications^{4,5} we emanate from a S_N2 -type reaction of second order between an activated species, which is adsorbed on a Brønsted acid site and a second molecule. In the protonated molecule the C-N bond is weakened, resulting in a positive partial charge on the adjusting $-CH_2-$ carbon atom, rendering it susceptible for a nucleophilic attack by an electron rich function, such as the *para* or *ortho*-position of the phenyl ring of another molecule or also the amino function thereof. This is illustrated on the example of the formation of 4,4'-MDA from PABA in Fig. 3.2.

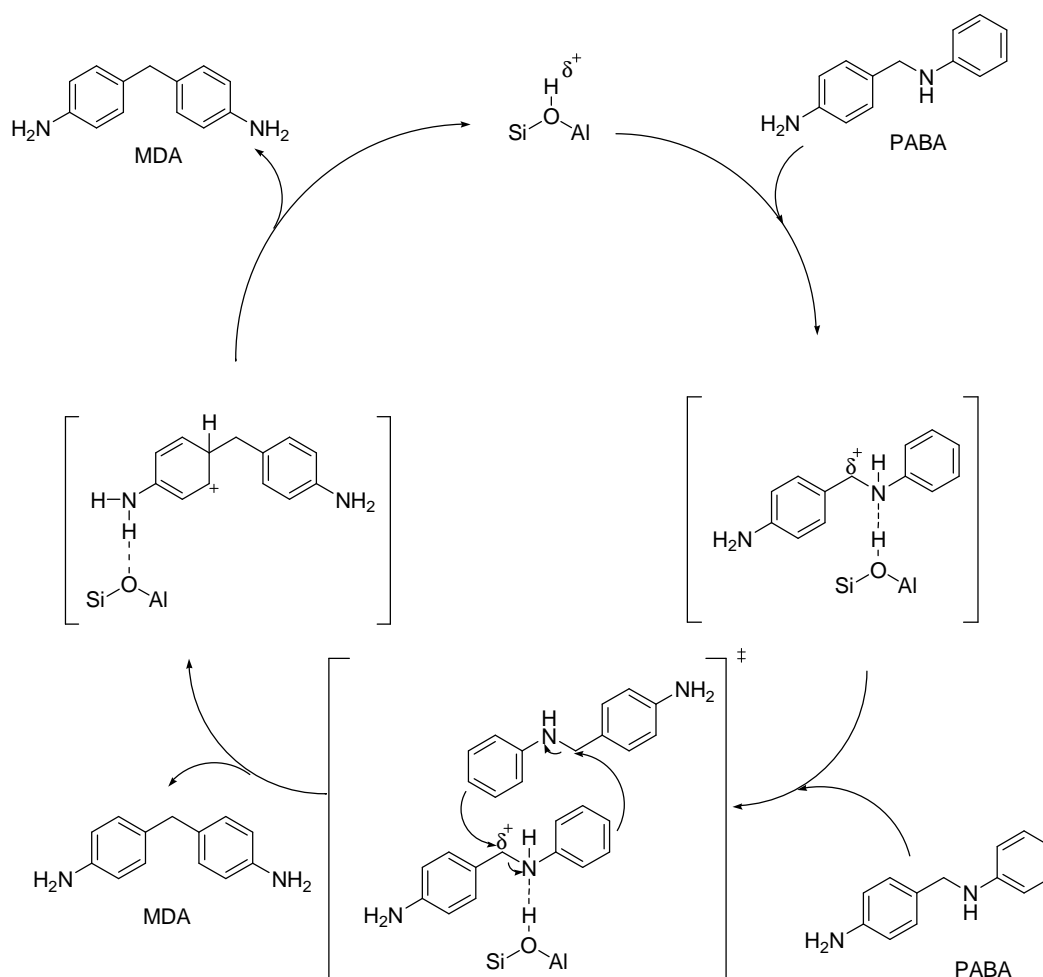


Figure 3.2: Proposed S_N2 -type reaction mechanism on the example of 4,4'-MDA formation from PABA.¹

The next towards the development of improved catalysts for MDA synthesis is to understand the influence of the choice of catalyst on the reaction in terms of activity and selectivity. Especially the impact of Brønsted acid site density and strength and pore size and geometry is of mutual interest.

Numerous studies and a great number of patents have been published on the use of zeolites in the production of MDA from aniline and formaldehyde.¹⁻⁸ As diffusion limitation of the bulky reactant species through the micropores is believed to be the limiting factor for the activity of parent zeolites several mesoporous and delaminated structures as well as nano-sized zeolite crystals were proposed as catalysts. Regrettably the conditions under which all these materials were tested are extremely incoherent as each group applies different reactor systems, reaction temperatures and/or concentrations.

In order to identify the physiochemical properties of a catalyst, which determine the activity, a series of zeolites has been explored and is described in the present study. Apart from parent MFI-, BEA-, FAU and MOR-type zeolites with varying Si/Al ratio, also delaminated materials, such as ITQ-2 and MCM-36, a series of dealuminated Y-types and a set of desilicated BEA-types were tested. All catalysts were characterized by elemental analysis, NH₃-TPD and nitrogen physisorption. Their activity in MDA synthesis and the turnover frequency of the strongly acidic protons of the zeolites for the formation of MDA was determined.

3.2 Methods

3.2.1 Materials

The amination solution used as starting material for all screening reactions, was prepared as follows. In a 1 L round bottom flask, 600 mL of aniline (6.58 mol, Sigma, purity \geq 99.5 %) were heated to 50°C under vigorous stirring. 100 mL of formalin (1.32 mol formaldehyde, Sigma, 37 wt. % of formaldehyde in water, stabilized with methanol) were added dropwise. After addition, stirring was continued for 1 h at 50°C. Water and methanol were removed by distillation in a Rotavapor. The concentration and purity of

the resulting solution of 1 equ. of amination in 3 equ. of aniline, which is ready for use in the test reactions, was verified by ^1H - and ^{13}C -NMR, as well as GC.

Three samples of ZSM-5 with different Si/Al ratio (H-MFI 90, H-MFI 240, H-MFI 400), three samples of BEA-type zeolite (H-Beta 25, H-Beta 35, H-Beta 150) and two samples of MOR-type zeolite (H-MOR 40, H-MOR 90) were provided by Südchemie. Parent (NH_4 -CBV 500) and dealuminated (H-CBV 720, H-CBV 740, H-CBV 760, H-CBV 780) Y-type zeolites were obtained from Zeolyst. The ammonium form of the parent Y-type sample had to be calcined at 450°C for 10 h in synthetic air prior to use. The resulting proton form was labeled H-CBV 500.

ITQ-2 and MCM-36 sample were prepared from the MCM-22 precursor (MCM-22(P)) according to literature.^{9,10}

The hydrothermal synthesis of the MCM-22(P) is carried out by using hexamethyleneimine (HMI, 99% Aldrich) as templating agent, SiO_2 (Aerosil 380, Degussa) as silica source, NaAlO_2 (Riedel-de Haën) as aluminum source, NaOH (Merck) for pH adjustment and water as solvent. In a typical synthesis, 0.18 g of NaAlO_2 and 0.65 g of NaOH are dissolved in 75 mL of H_2O . To this solution 5.08 g of HMI and 6.29 g of SiO_2 were added under vigorous stirring at room temperature. After stirring for 1 h at room temperature, the resulting homogenous gel is transferred into a PTFE-lined stainless steel autoclave for hydrothermal synthesis at 140°C for 9 days in an oven designated to rotate the autoclaves at 60 rpm. The solid product is recovered by filtration, washing and drying in air at 80°C .

MCM-22 is prepared from MCM-22(P) by calcination in synthetic air by heating 5 K min^{-1} to 120°C and holding for 1 h, followed by heating at 5 K min^{-1} to 450°C and holding for 10 h. The obtained white powder was identified as Na-MCM-22, by XRD and elemental analysis. In order to get the Brønsted acidic proton exchanged H-MCM-22 ion exchange is performed by suspending 3.80 g of Na-MCM-22 in 75 mL of 0.2 M NH_4Cl solution at 70°C over night followed by filtration and washing. To ensure complete removal of sodium the ion exchange is repeated three times. H-MCM-22 is obtained after calcination in synthetic air at 3 K min^{-1} to 120°C and holding for 1 h followed by heating at 3 K min^{-1} to 500°C and holding for 10 h. The resulting white powder is identified as H-MCM-22 by elemental analysis, XRD and TEM.

For the synthesis of ITQ-2, 8.60 g of MCM-22(P) are suspended in 101 g of H₂O, 105.5 g of tetrapropylammonium hydroxide solution (TPAOH, 20 wt% in H₂O, Aldrich) and 48.7 g of hexadecyltrimethylammonium bromide solution (CTMABr 25 wt% in H₂O, Fluka) at 80°C in a three necked round bottom flask equipped with magnetic stirring and a reflux condenser. After stirring for 16 h, the swollen material is treated for 1 h in an ultrasonic bath (100 W). After adjusting the pH to below 2 by addition of several drops of HCl conc., the solid is separated by centrifugation. Na-ITQ-2 is obtained by calcination in synthetic air by heating at 5 K min⁻¹ to 120°C and holding for 1 h, followed by heating at 5 K min⁻¹ to 450°C and holding for 10 h. In order to get the Brønsted acidic proton exchanged H-ITQ-2, ion exchange is performed by suspending 1.50 g of Na-ITQ-2 in 100 mL of 0.2 M NH₄Cl solution at 80°C over night followed by filtration and washing. The ion exchange is repeated three times to ensure complete removal of sodium. H-ITQ-2 is obtained by calcination in synthetic air at 3 K min⁻¹ to 120°C and holding for 1 h followed by heating at 3 K min⁻¹ to 500°C and holding for 10 h. The produced white powder is identified as H-ITQ-2 by elemental analysis, XRD and TEM.

For the synthesis of MCM-36, 3.44 g of MCM-22(P) are suspended in 10.3 g of H₂O, 55.0 g of tetrapropylammonium hydroxide solution (TPAOH, 20 wt% in H₂O, Aldrich) and 81.2 mL of hexadecyltrimethylammonium bromide solution (CTMABr 25 wt% in H₂O, Fluka) at 100°C in a three necked round bottom flask equipped with magnetic stirring and a reflux condenser. The pH is adjusted to 13.5 with NaOH. After stirring for 68 h at 100°C, a white solid is obtained by filtration, washing and drying in air at 80°C. 2.44 g of the dried product are mixed with 12.2 g of TEOS (99%, Aldrich) under N₂ atmosphere. After stirring at 90°C for 25 h, the mixture was hydrolyzed with 142 g of H₂O. Na-MCM-36 is obtained by filtration, washing and calcination in synthetic air by heating at 5 K min⁻¹ to 120°C and holding for 1 h, followed by heating at 5 K min⁻¹ to 450°C and holding for 10 h. In order to get the Brønsted acidic proton exchanged H-MCM-36 ion exchange is performed by suspending 2.00 g of Na-MCM-36 in 100 mL of 0.2 M NH₄Cl solution at 80°C over night followed by filtration and washing. The ion exchange is repeated three times to ensure complete removal of Sodium. H-MCM-36 is obtained by calcination in synthetic air at 3 K min⁻¹ to 120°C and holding for 1 h

followed by heating at 3 K min^{-1} to 500°C and holding for 10 h. The produced white powder is identified as H-MCM-36 by elemental analysis, XRD and TEM.

Desilication of zeolite BEA is performed by alkaline leaching.¹¹ For this, 6.64 g of zeolite BEA (H-Beta 35, Südchemie) are suspended in 200 mL of 0.2 M NaOH solution at 55°C under vigorous stirring for a given period of time. After centrifugation and washing, the isolated solid is suspended in 70 mL of 0.2 NH_4Cl over night at 70°C . Ion exchange is repeated three times to ensure complete removal of sodium. The proton form is obtained by calcination in synthetic air by heating at 5 K min^{-1} to 120°C , holding for 1 h, followed by heating at 5 K min^{-1} to 450°C and holding for 10 h. The samples are labeled H-BEA Xmin, with X representing the duration of the alkaline leaching treatment.

Al-MCM-41 was prepared according to literature¹² from sodium metasilicate (Na_2SiO_3 , Merck), Cetyltrimethylammoniumbromid (CTAB 25% in water, Aldrich), 10% aqueous tetramethylammonium hydroxide (TMAOH, Sigma) and sodium aluminate (NaAlO_2 , Riedel-de Haën). The aqueous solutions of CTAB (59.72 g) and TMAOH (3.58 g TMAOH solid in 32.3 mL water) were added to solution of 14.0 g sodium metasilicate solution in 60 mL of water under vigorous agitation at room temperature. Then the sodium aluminate solution (1.03 g NaAlO_2 in 25.0 mL water) was added dropwise under vigorous stirring at room temperature. H_2SO_4 was added to the gel mixture to adjust the pH to approximately 11 before heating. The resulting gel mixture had a molar composition of $\text{SiO}_2 : 0.25 \text{ CTAB} : 0.24 \text{ TMAOH} : 0.033 \text{ Al}_2\text{O}_3 : 60 \text{ H}_2\text{O}$, and was stirred for 16 h at room temperature. Hydrothermal treatment was performed at 100°C for six days. The product was filtered, washed, dried in air and calcined in synthetic air at 550°C for 12 h. The obtained Na/Al-MCM-41 sample was ion exchanged with 0.2 M NH_4Cl solution at 368 K three times, and then washed, dried and calcined at 773 K for 12 h to prepare H/Al-MCM-41.

SBA-15 and Al-SBA-15 (X) with various Si/Al ratios were synthesized following published procedures.¹³⁻¹⁶ The incorporation of Al into the SBA-15 mesostructure was carried out by a direct synthesis method using Al-alkoxides as Al source. In a typical synthesis, 40 g of tetra ethyl ortho silicate (TEOS) and an amount of aluminum *tert*-butoxide calculated to obtain Si/Al ratios equal to 10, 20, 30, 40 are added to 336 ml of

deionized water containing 10.3 mL of HCl conc. After stirring the mixture of Pluronic P123, HCl and water over night, a clear solution was obtained. Then TEOS and the respective amounts of $\text{Al}(t\text{BuO})_3$ were added and the resulting solution was slowly stirred for an additional 24 h at room temperature. The final gel was aged for 48 h at 100°C under static conditions. Finally, the product was filtered, dried in air and calcined at 550°C for 12 h in synthetic air to remove the organic template (heating rate of 1 K/min; synthetic air flow 200 mL/min).

3.2.2 Characterization

Nitrogen physisorption isotherms were measured using a PMI automated sorptometer at liquid nitrogen temperature (77 K), after outgassing under vacuum at 623 K for 4 h. The apparent surface area was calculated by applying the Brunauer–Emmett–Teller (BET) theory to the adsorption isotherms over a relative pressure range from 0.01 to 0.09. The micropore volumes were evaluated using the t-plot method¹⁷ according to Hasely.¹⁸ The mesopore volumes were determined by the cumulative pore volume of pores with diameters ranging from 2 – 50 nm according to the BJH method.¹⁹ Because of the limitations of the PMI instrument, the isotherms were measured at relative partial pressures higher than $10^{-5} p/p^0$.

For TPD experiments, approximately 50 mg of sample were activated for 1 h at 723 K in a six port parallel vacuum system (0.8 Pa). After activation, the samples were contacted with 1 mbar of NH_3 at 373K for 1 h, followed by degassing for 2 h at 373 K. For desorption, the samples were heated up to 1043 K with an increment of 10 K min^{-1} . Ammonia desorption was monitored by mass spectrometry (Pfeiffer QMS 200 Prisma). The amount of desorbed ammonia was determined by integration of the MS signal and calibration to a standard material (MFI 90; 360 $\mu\text{mol g}^{-1}$).

The elemental composition of the applied catalysts was determined by atomic adsorption spectroscopy in a Unicam M Series Flame-AAS equipped with an FS 95 autosampler and a GF 95 graphite furnace. The crystallinity of the synthesized and modified materials was analyzed by powder X-ray diffraction using a Philips X'Pert Pro System (Cu- $\text{K}\alpha_1$ radiation, 0.154056 nm) at 45 kV / 40 mA in step scan of 0.017° min^{-1} from 5° to 70° 2 θ . Transmission electron microscopy (TEM) was measured on a JEOL-

2011 electron microscope operating at 200 kV. Prior to the measurements, the powdered samples were suspended in ethanol and dried on a copper-carbon-grid.

3.2.3 Catalytic reaction

A ChemSpeed Accelerator SLT synthesis robot with eight parallel reactors was used for catalytic test reactions. For the test reaction, 15 mL of the aminal solution were placed in a 27 mL double jacket glass reactor prefilled with 0.79 g of catalyst. The reactors are heated to 100°C, dispersion of the catalyst is ensured by a vibration-plate operating at 1400 rpm. After defined time intervals 100 μ L of sample were taken from the reaction mixture and diluted with 0.9 mL of acetonitrile (Sigma, purity $\geq 99.5\%$), containing 1 mL of diphenylmethane (Fluka, purity $\geq 99\%$) per 100 mL of acetonitrile as internal standard. After removal of the catalyst by filtration through a syringe filter (Minisart SRC; 0.20 μ m, d = 4 mm), the sample was analyzed by GC.

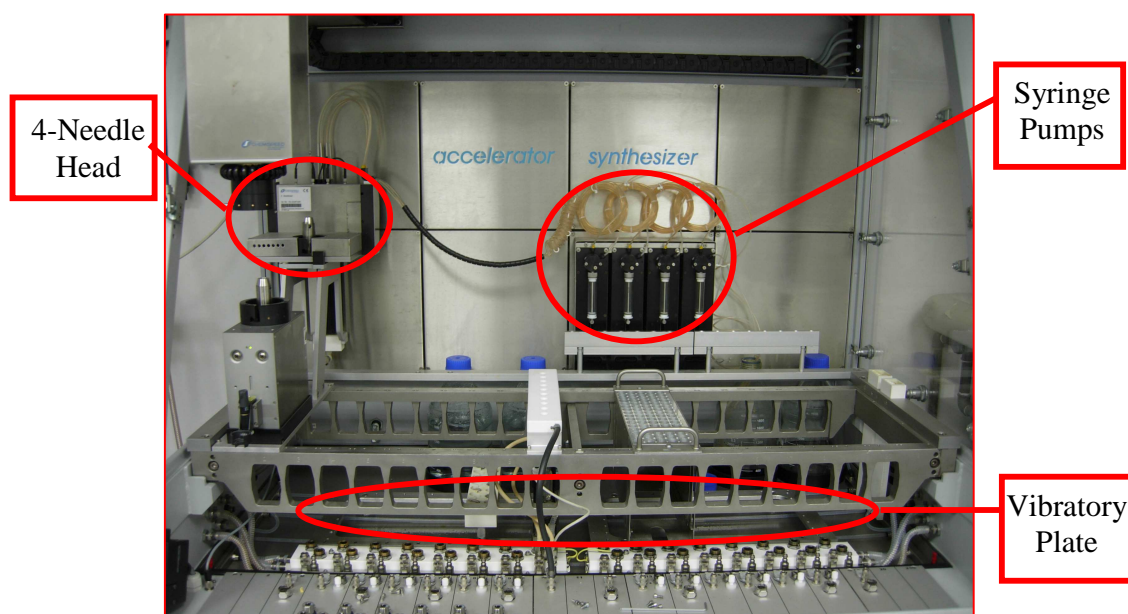


Figure 3.3: ChemSpeed Accelerator SLT 106.

For GC analysis a Shimadzu GC 2010, equipped with an Optima 35 MS column (length = 30 m, ID = 0.32 mm, film thickness 0.25 μ m), a FID detector and an autosampler was used. A temperature profile beginning at 60°C, hold for 5 min, heating

with an increment of 15 K min⁻¹ to 170°C, holding for 40 min, heating with 25 K min⁻¹ up to 300°C, holding for 15 min and heating with 25 K min⁻¹ up to 350°C and holding this temperature for 2 min was applied. The injection volume was set to 1 µL with the injection port heated to 280°C and a split ratio of 50. The instrument was calibrated to 4,4'-MDA, 2,4'-MDA, PABA, OABA and aminal, the response factors for heavier products were assumed to be identical in first approximation and were estimated by closing the mass balance of the reaction.

The TOFs of the applied catalysts were determined by normalizing the initial rate of 4,4'-MDA formation to the amount of applied catalyst and its concentration of Brønsted acid sites according to equation 1. As our previous work has shown that all Brønsted acid sites contribute equally to the overall acidity, distinguishing between strong and weak Brønsted acid sites is not necessary.¹

$$TOF[\text{min}^{-1}] = \frac{\text{rate of 4,4'-MDA formation } [\text{mol}_{4,4'\text{-MDA}} / (\text{mol}_{\text{aniline}} \cdot \text{min} \cdot \text{g}_{\text{cat}})]}{\text{acidity } [\text{mol}/\text{g}_{\text{cat}}] \cdot n_{\text{aniline}} [\text{mol}]} \quad (1)$$

3.2.4. Modeling

Atom positions in the discussed zeolite framework types were obtained from the corresponding crystallographic information files (CIF) offered by the Database of Zeolite Structures.²⁰ The initial structure of PABA was optimized in MPQC²¹ using B3LYP DFT and a 6-31+G(d,p) basis set. The molecule is fitted into to zeolite pore system using the potential energy derived by Lennard-Jones parameters²² as a figure of merit. The refined parameters are the position of the molecule in the zeolite channel as well as a rotation of rigid molecule parts around the benzene-NH-, benzene-CH₂- and -CH₂-NH- bond in PABA. The final images were created using Diamond²³, radii of the ions are the suggested values of 0.4 Å for Si⁴⁺ and 1.35 Å for O²⁻.²⁴

3.3. Results

3.3.1 Catalyst characterization

The elemental composition of the applied catalysts as determined by AAS, their micro- and mesopore volumes and their acidity, measured by NH₃-TPD, are shown in table 3.1. XRD analysis verified the crystallinity of all commercial samples.

Table 3.1: Elemental composition, pore volumes and acidity of commercial zeolite samples.

Material	Si/Al ratio	Acidity [$\mu\text{mol/g}$]	V_{micro} [cm^3/g]	V_{meso} [cm^3/g]	TOF [min^{-1}]
H-MFI 90	45	351	0.12	0.03	0
H-MFI 240	123	124	0.15	0.01	0
H-MFI 400	205	76	0.14	<0.01	0
H-MOR 40	19	760	0.18	0.02	0
H-MOR 90	44	410	0.18	0.03	0
H-BEA 25	13	530	0.16	<0.01	24
H-BEA 35	18	538	0.21	<0.01	30
H-BEA 150	79	229	0.23	0.02	15
H-CBV 500	2.7	1240	0.27	0.06	14
H-CBV 720	14	474	0.31	0.19	431
H-CBV 740	22	292	0.29	0.21	409
H-CBV 760	30	391	0.28	0.18	390
H-CBV 780	42	143	0.32	0.18	415

The applied commercial catalysts have Si/Al ratios ranging from 2.7 for parent Y-type zeolite H-CBV 500 to over 200 for the ZSM-5 sample H-MFI-400. Accordingly, the acidity of the sample ranges from 1240 $\mu\text{mol/g}$ for H-CBV 500 to very low values of merely 76 $\mu\text{mol/g}$ for the low Al H-MFI-400 sample. The samples of parent MFI, BEA, MOR and FAU show next to none mesoporosity, which can be attributed to interparticular mesopores.²⁵ Only the dealuminated FAU samples H-CBV 720, H-CBV 740, H-CBV 760 and H-CBV 780 display significant mesopore volumes of about 0.19 cm^3/g .

The elemental composition as determined by AAS, micro- and mesopore volumes and Brønsted acidity, measured by NH₃-TPD, for catalysts prepared or modified in this study are shown in Table 3.2. Alkaline leaching of parent BEA-type zeolite H-BEA 25 results in a significant gain in acidity from 530 μmol/g for the parent material to about 900 μmol/g in the desilicated samples. After 30 min of alkaline treatment, the acidity did not further change.

Nitrogen physisorption experiments showed that the mesoporosity of the material gradually increases with increasing treatment time. While the parent material does not contain mesopores, a mesopore volume of 0.21 cm³/g was found in the 15 min leached sample, 0.24 cm³/g after 30 min and 0.28 – 0.33 cm³/g in the samples with longer treatment times.

Table 3.2: *Elemental composition, pore volumes and acidity of synthesized zeolite samples.*

Material	Si/Al ratio	acidity [μmol/g]	V _{micro} [cm ³ /g]	V _{meso} [cm ³ /g]	TOF [min ⁻¹]
H-BEA 15 min	13	836	0.09	0.21	56
H-BEA 30 min	12	895	0.10	0.24	55
H-BEA 45 min	11	899	0.08	0.28	59
H-BEA 60 min	12	874	0.11	0.32	62
H-BEA 90 min	10	809	0.13	0.31	62
H-BEA 135min	9.4	868	0.13	0.32	68
H-BEA 240 min	8.3	826	0.09	0.32	66
H-MCM-22	38	327	0.13	0.07	0
H-MCM-36	37	209	<0.01	0.25	375
H-ITQ-2	40	364	<0.01	0.24	165
H/Al-MCM-41	14	203	<0.01	0.19	477
SBA-15 (∞)	pure SiO ₂	<25	0.11	1.11	0
SBA-15 (33)	1470	<25	0.09	1.19	0
SBA-15 (100)	163	<25			n.n.
SBA-15 (50)	199	40	0.10	1.21	(1000)
SBA-15 (33)-2	113	99	0.11	0.87	555
SBA-15 (20)	40	140			409
SBA-15 (10)	13	373	0	0.02	206

XRD analysis further supports the theory that most of the damage to the BEA framework is done in the first 15 – 30 min of the alkaline leaching. Compared with the XRD diffraction pattern of the parent H-BEA 25 sample, the desilicated samples show a pronounced loss of crystallinity (Fig. 3.4). However, XRD does not show any evidence for further significant changes in the BEA framework with increasing treatment time.

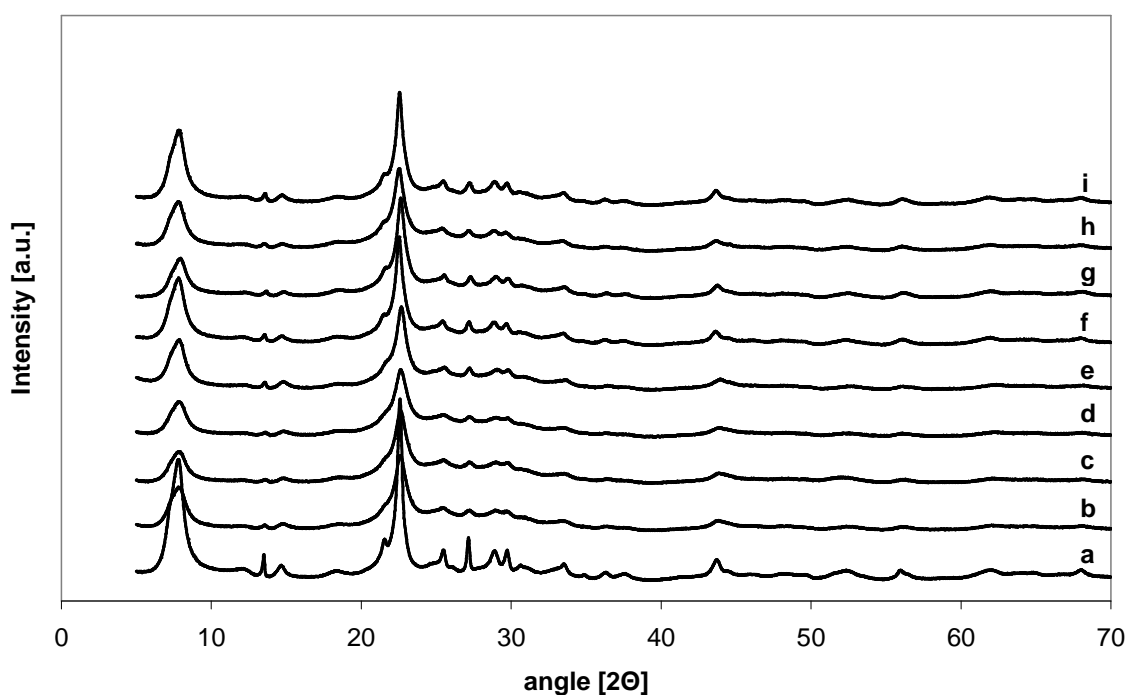


Fig. 3.4: XRD diffraction patterns of a) parent H-BEA 25, b) H-BEA 15 min, c) H-BEA 30 min, d) H-BEA 45 min, e) H-BEA 60 min, f) H-BEA 90 min, g) H-BEA 135 min, h) H-BEA 240 min, i) H-BEA 1020 min.

In order to verify that the synthesis was successful samples of H-MCM-22, H-ITQ-2 and H-MCM-36 were analyzed by XRD. TEM images of the three samples are shown in Fig. 3.6a-c. H-MCM-22 displays the honeycomb pattern of 0.5 nm pores. The images of H-ITQ-2 and H-MCM-36 show that the layers of MCM-22 are almost completely delaminated and, in the case of H-ITQ-2, randomly oriented. In Figure 3.6c the cup-shaped cavities on both sides of the MWW-sheets of MCM-36 are clearly discernible.

The X-ray diffraction patterns of the uncalcined MCM-22(P), calcined H-MCM-22, H-ITQ-2 and H-MCM-36 are shown in Fig. 3.5. As was to be expected, the broad signals in the precursor get significantly sharper after calcination to H-MCM-22 as the MWW-layers are merging during calcination, thus, forming the MCM-22 zeolite framework. The signals in the delaminated materials are much broader or have completely disappeared compared to MCM-22(P). The Si/Al ratio of the synthesis gel of the MCM-22 precursor synthesis was about 45. The final calcined materials have a slightly higher Al content, resulting in Si/Al ratios of about 38. Upon delamination, the acidity of the material slightly increased from 327 $\mu\text{mol/g}$ of the H-MCM-22 material to 364 $\mu\text{mol/g}$ in H-ITQ-2. Pillaring of the swollen MCM-22(P) led to a significant loss in acidity to 209 $\mu\text{mol/g}$ in H-MCM-36.

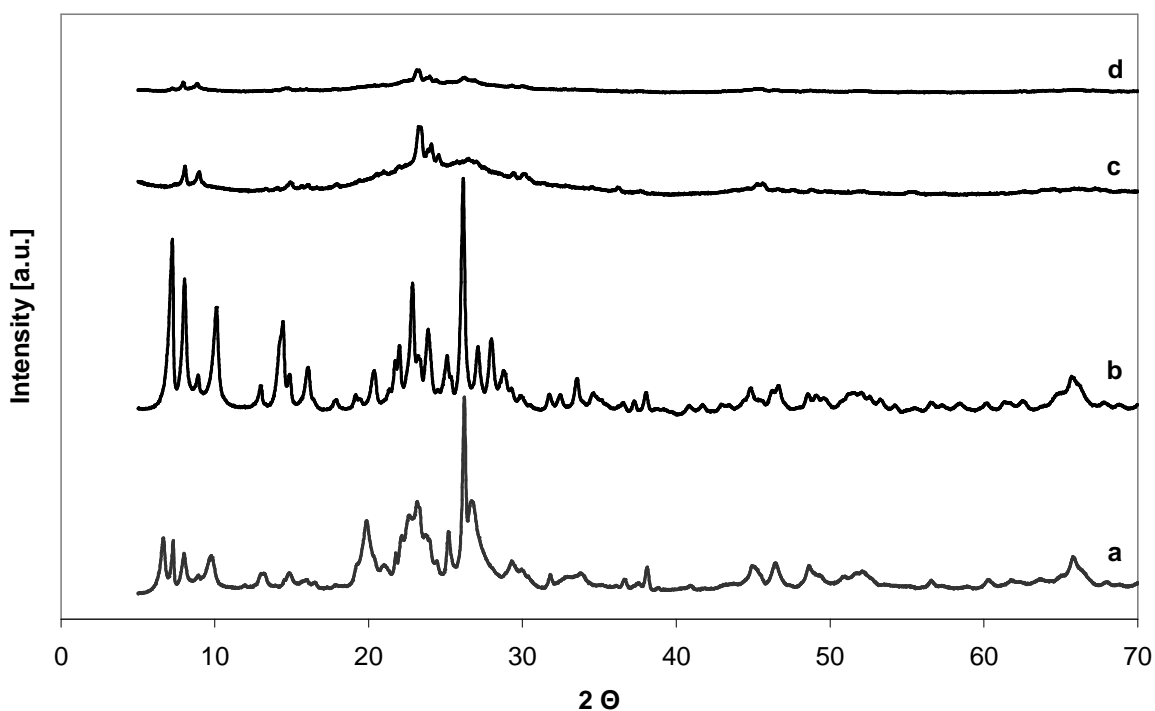


Fig. 3.5: Powder X-ray diffraction patterns of a) MCM-22(P), b) H-MCM-22, c) H-ITQ-2 and d) H-MCM-36.

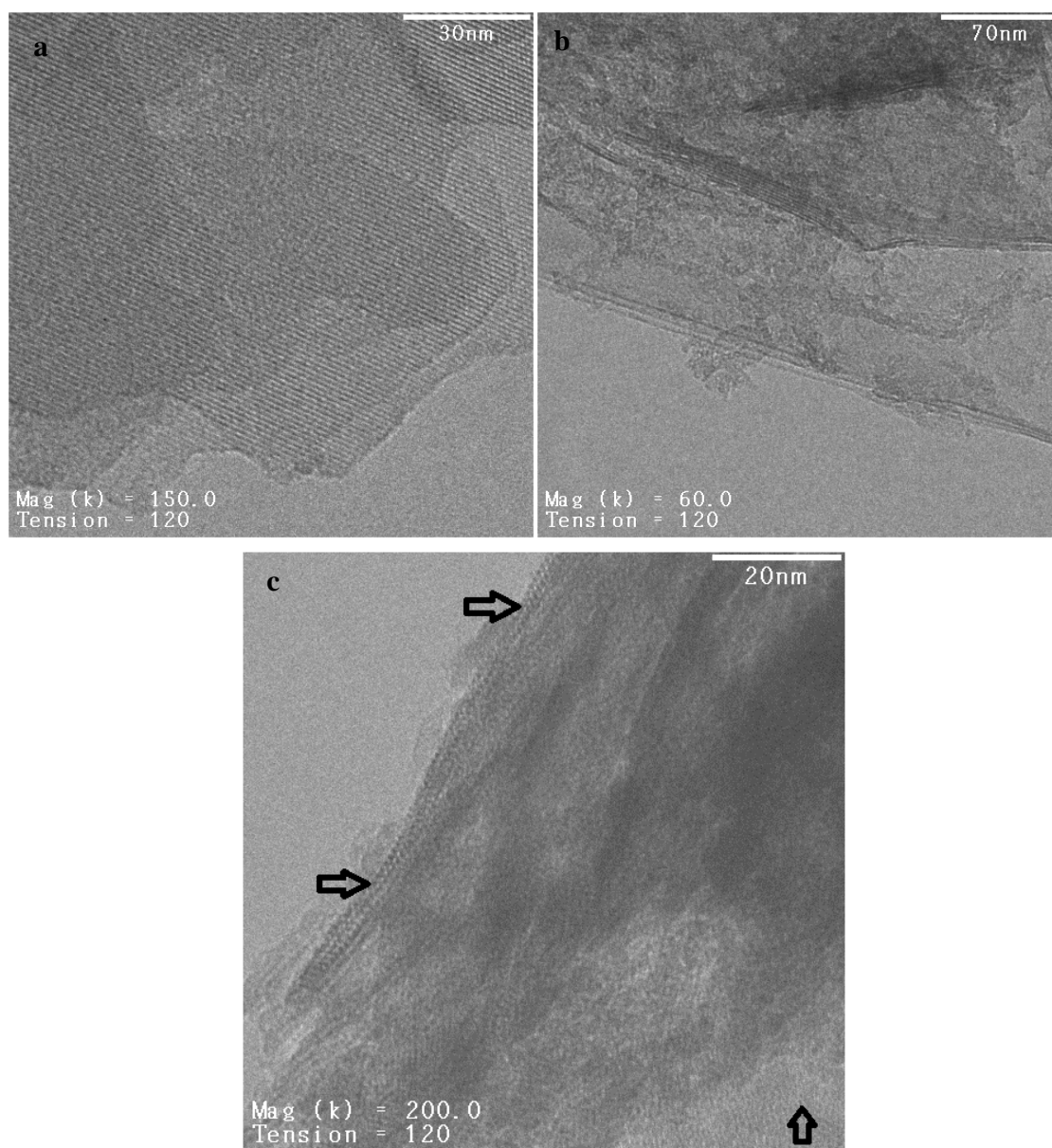


Fig. 3.6: TEM images of a) H-MCM-22, b) H-ITQ-2 and c) H-MCM-36.

The Si/Al ratio in the prepared MCM-41 sample was 14, hence notably higher than in the synthesis gel where a Si/Al ratio of 9 was chosen. Nitrogen physisorption indicated that no micropores are present in the synthesized materials as was expected for MCM-41. The mesopore volume of $0.19 \text{ cm}^3/\text{g}$, however, is significantly lower than comparable values published for Al-MCM-41 (about $0.70 \text{ cm}^3/\text{g}$).¹³ X-ray diffraction shows one dominating peak at about $0.8^\circ 2\theta$ and three smaller signals at 2.5° , 4.5° and $5.0^\circ 2\theta$. Transmission

electron microscopy verifies the presence of ordered mesopores of roughly 35 Å diameter in a hexagonal structure.

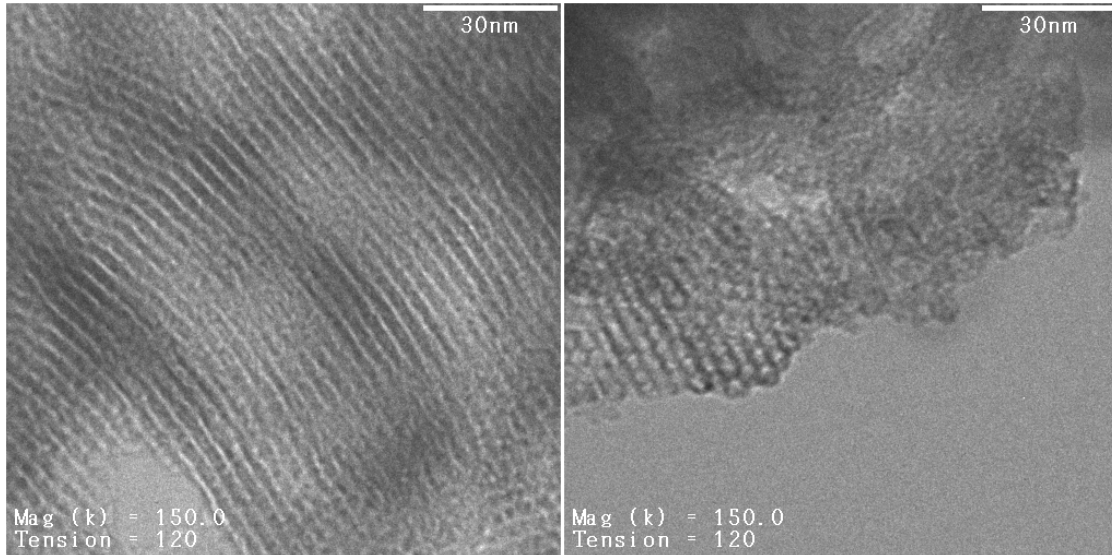


Fig. 3.7: TEM images of H/Al-MCM-41

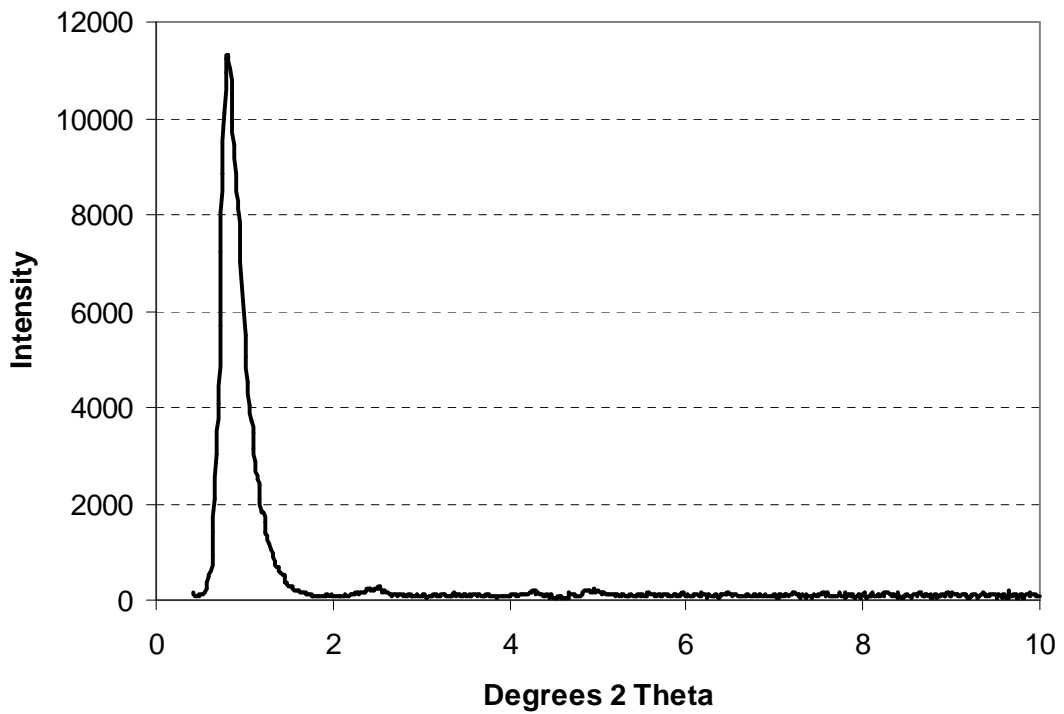


Fig. 3.8: X-ray diffraction pattern of H/Al-MCM-41.

Elemental analysis of the SBA-15 (X) samples revealed, that only a fraction of the Al precursor in the synthesis gel is incorporated into the final sample. Only when higher Al contents (Si/Al ratio < 20 in the gel) are applied, notable amounts of Al are incorporated into the final product. Surprisingly the first synthesis of SBA-15 (33) yielded a material in almost pure SiO₂ form (Si/Al 1470). Upon repeating this experiment a material (SBA-15 (33)-2) with Si/Al ratio of 113 was obtained, which fits into the observed trend for the other materials. NH₃-TPD measurements verified the low Al content, as very poor acidities were found. In case of SBA-15 (100) the acidity was below detection limit. The pure SiO₂ reference sample SBA-15 (∞) and the SBA-15 (33) showed no determinable Brønsted acidity as well. Only the samples with higher Al content SBA-15 (20) and (10) show significant acidity of 140 and 373 μmol/g, respectively. X-ray diffraction patterns only show the characteristic low angle reflex at about 1° 2Θ for the samples with low Al content. While the pure SiO₂ samples of SBA-15 (∞) and SBA-15 (33) show very similar and intense signals, the intensity of the signal drastically decreases with increasing Al content of the sample. The peak is already very faint for SBA-15 (50) and has completely vanished in case of SBA-15 (20) and (10).

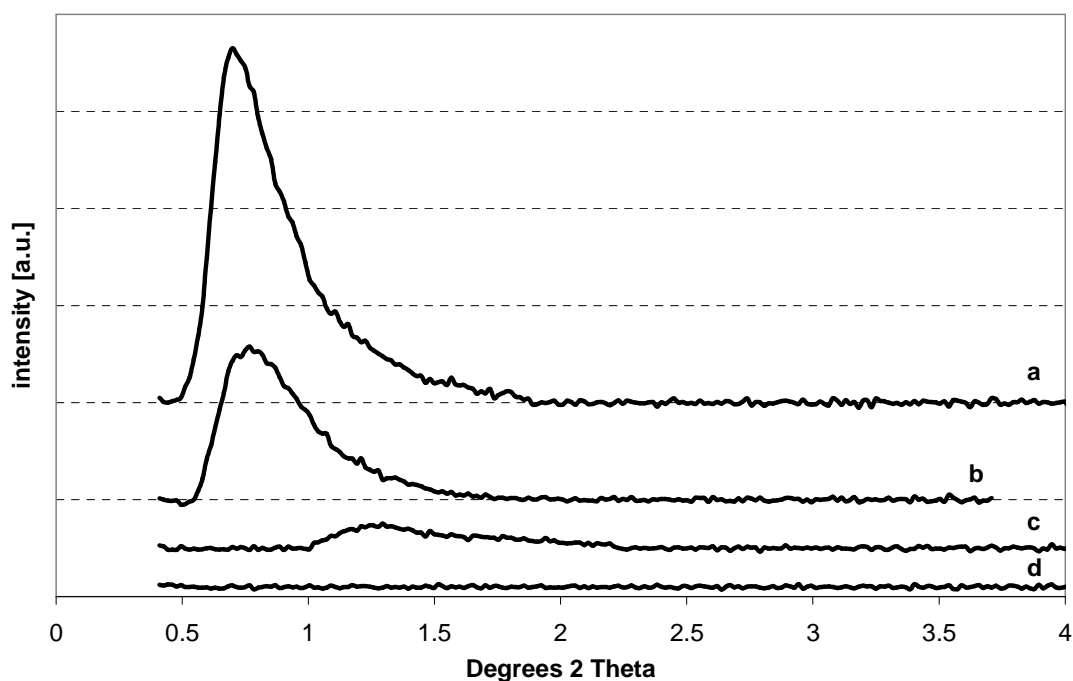


Figure 3.9: X-ray diffraction patterns of a) SBA-15 (33)-2, b) SBA-15 (100), c) SBA-15 (50) and d) SBA-15 (20).

Nitrogen physisorption experiments yielded almost identical results for the pure SiO_2 sample SBA-15 (∞) and the other Al-free SBA-15 (33) sample. Both display the parallel hysteresis loop typical for materials with regular mesopores, such as SBA-15. Also the calculated mesopore volumes of 1.11 and 1.19 cm^3/g are in the expected range for SBA-15 materials. As more Al is incorporated into the framework the BET surface and mesopore volume of the materials decrease, e.g. SBA-15 (33)-2 has a mesopore volume of 0.87 cm^3/g . At even higher Al concentrations in the synthesis gel and in the final material the mesopore volume almost vanishes. SBA-15 (10) for example only displays a mesopore volume of 0.02 cm^3/g .

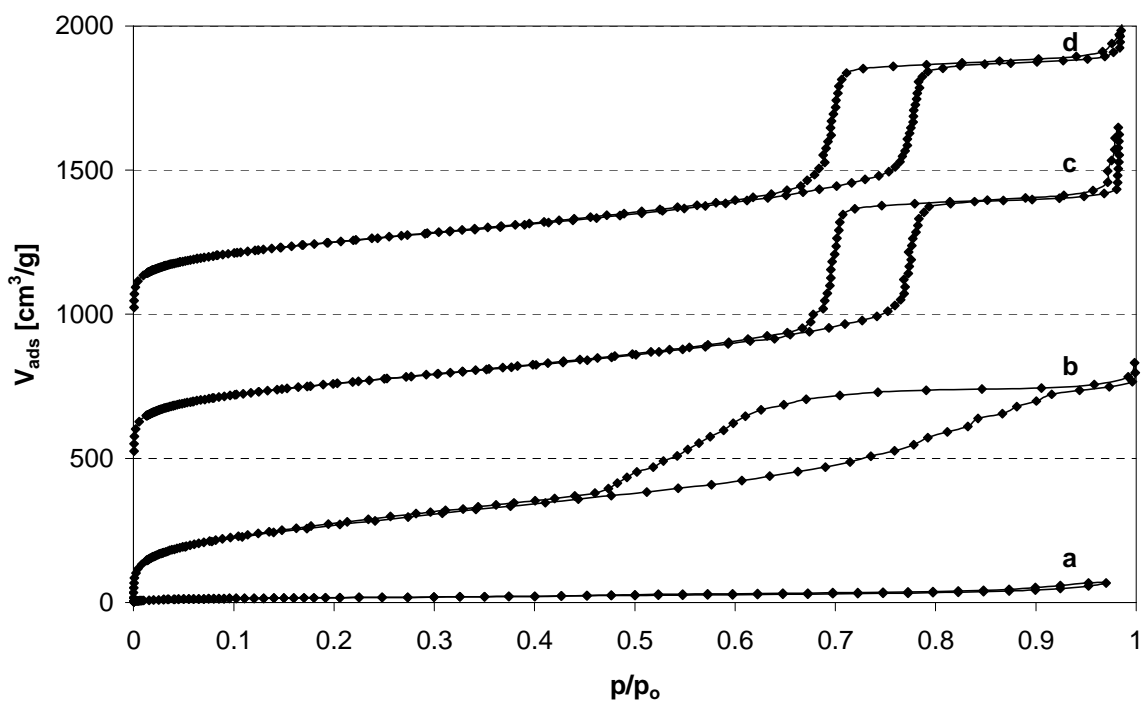


Figure 3.10: Adsorption isotherms of nitrogen on a) SBA-15 (10), b) SBA-15 (33)-2, c) SBA-15 (33) and d) SBA-15 (∞).

Transmission electron microscopy also indicates that the pure SiO₂ samples SBA-15 (∞) and SBA-15 (33) exhibit a regular structure with uniform mesopores of about 50 Å diameter. As higher Al contents are applied more and more amorphous domains are found in the samples. Eventually no ordered domains could be found in the SBA-15 (20) and (10) samples, which appear to be completely amorphous, as was already shown in XRD.

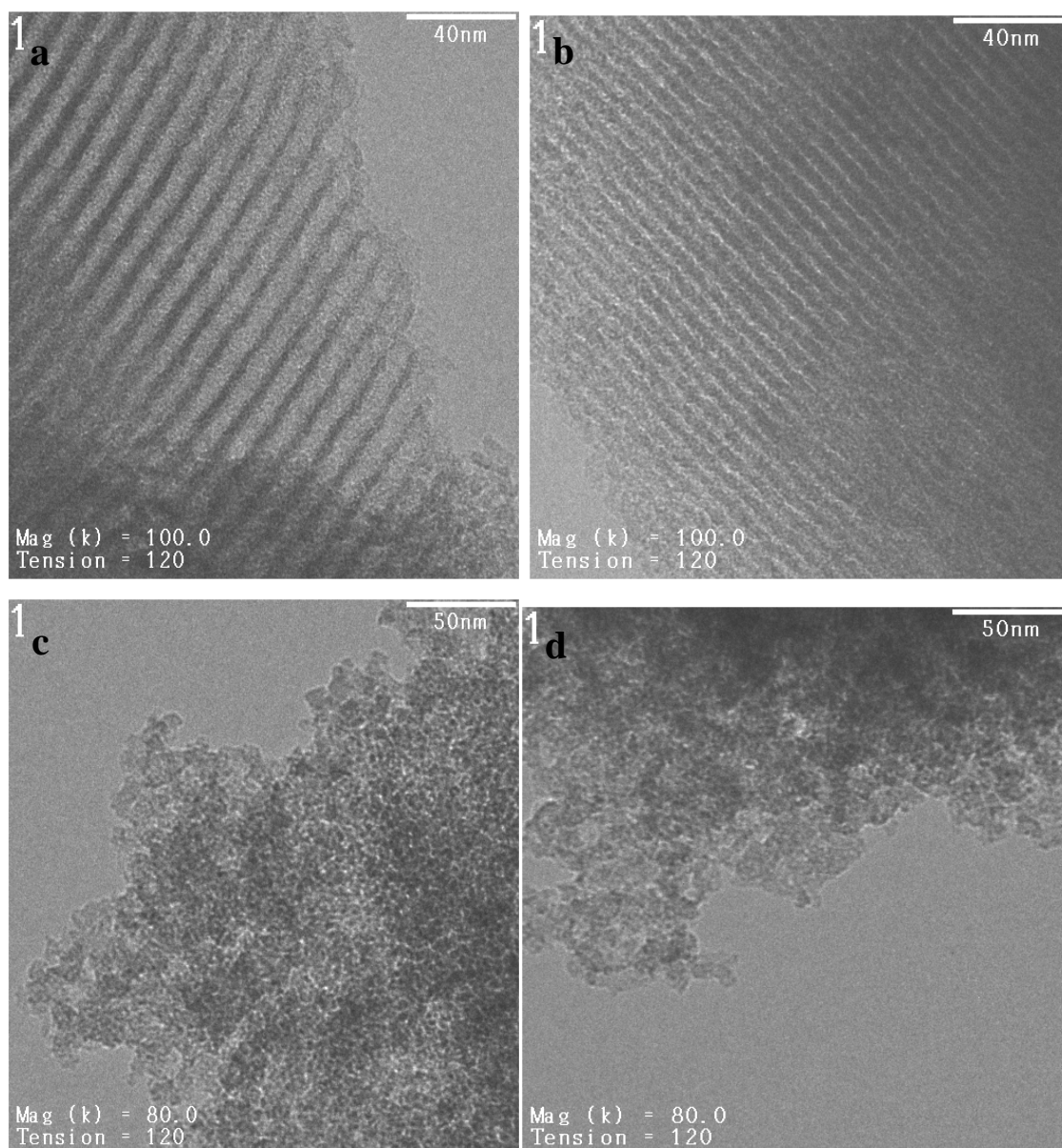


Figure 3.11: Transmission electron micrographs of a), b) SBA-15 (33)-2 and c), d) SBA-15 (20).

3.3.2 Catalytic reaction

The activity of the commercial and synthesized zeolite samples was determined in a test reaction. All materials are evaluated by their initial rate of 4,4'-MDA formation, which is normalized to each materials' acidity for better comparison. The obtained TOFs are included in Tab. 1 and 2. The parent zeolite samples of MFI and MOR structure type display no detectable activity, as no 4,4'-MDA was formed during the test reaction. H-MCM-22 also shows no detectable activity. The parent zeolite samples of FAU and BEA structure type show only poor activity for MDA formation. The TOFs reach values between 14 and 30 min⁻¹. The highest relative activities were found for the dealuminated Y-type zeolites of the H-CBV 720 - 780 series, reaching TOFs of around 400 min⁻¹. Therefore, H-CBV 720, which has the highest acid site density of these materials, is the most active catalyst tested so far. Upon alkaline leaching, the activity of H-BEA 25 increases significantly. The TOFs more than double from 24 min⁻¹ for the parent zeolite to 55 – 68 min⁻¹ for the desilicated material. Both delaminated materials display improved activity of 165 min⁻¹ for H-ITQ-2 and 375 min⁻¹ for H-MCM-36. The H/Al-MCM-41 displays an even higher TOF of 477 min⁻¹. Both SBA-15 samples which contain no Al (SBA-15 (∞) and SBA-15 (33)-2) formed no 4,4'-MDA during the test reaction. Over the SBA-15 (100) some 4,4'-MDA could be detected, however to its acidity, which is below detection limit no TOF could be obtained. A similar problem is encountered in case of SBA-15 (50). As its acidity is close to the detection limit, the calculated TOF of about 1000 min⁻¹ is potentially error prone and may actually be significantly lower. The activity of the SBA-15 (33)-2, SBA-15 (20) and SBA-15 (10) samples decreases notably with increasing Al content from 555 min⁻¹ to 409 min⁻¹ and finally 206 min⁻¹, respectively.

3.4 Discussion

The very poor activity of MFI-type zeolites can easily be explained by comparing the size of the reactants with the size of the pore openings in ZSM-5. Fig. 4 shows a reactant molecule (PABA) inside a ZSM-5 pore. Due to the non-linear $-\text{CH}_2-\text{NH}-$ fragment in PABA, the molecule does not fit into 10-membered pore system ($\sim 5.5 \text{ \AA}$). Therefore, only acid sites at the pore entrances and on the outer surface are accessible for the reactant molecules. However, such sites are at best one third of the acid sites in an MFI material.²⁶ It appears that the concentration of these sites in the parent material is even lower than this. The fact that only a small fraction of its acid sites can take part in the reaction explains the very poor activity of MFI-type catalysts.

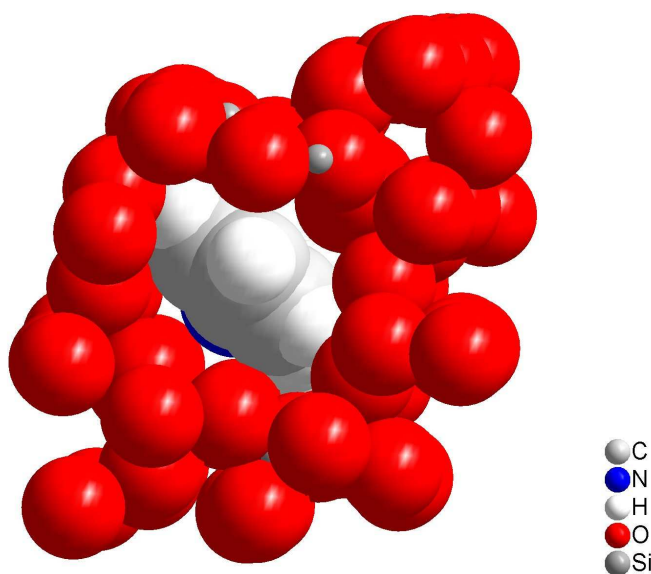


Fig. 3.12: Model of PABA molecule in a ZSM-5 pore.

Parent BEA-type catalysts display TOFs of about 25 min^{-1} , indicating the slow formation of small amounts of 4,4'-MDA during the test reaction. The reason for the activity of BEA-type zeolites, while ZSM-5 proved to be almost inactive, is located in its pore structure. While the 5.5 \AA pores in MFI are too small for the reactants to enter, the pores in zeolite BEA, which are about 7 \AA large, are just large enough for the reactants to pass. Furthermore, a $\text{S}_{\text{N}}2$ -type reaction between two reactant molecules, as postulated in

our previous work,¹ can take place in the pore intersections in zeolite BEA as shown in Fig. 5. However, due to the very tight fit of the reactants in the 12-membered pores, strong mass transport limitation due to pore diffusion is to be expected. The influence of pore diffusion on the synthesis of MDA in parent zeolite frameworks has already been discussed in detail in literature.^{1,2,6}

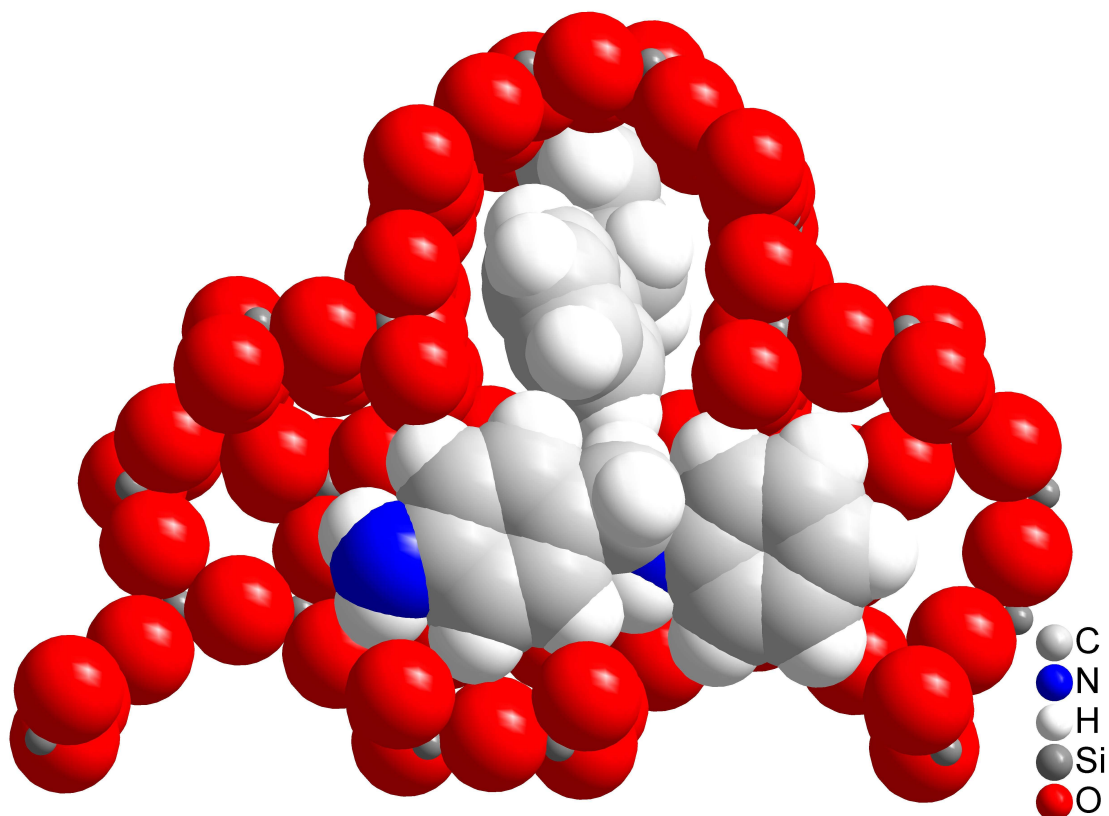


Fig. 3.13: Model of two PABA molecules in a BEA pore intersection.

The same observation holds true for parent FAU-type zeolite H-CBV 500. Just as the BEA zeolites, it displays some, but poor activity for MDA formation. An S_N2 -like reaction can take place in the supercages of zeolite Y, with one reactant placed in the supercage and a second molecule attacking it through the entrance of the supercage, as shown in Fig. 3.14.

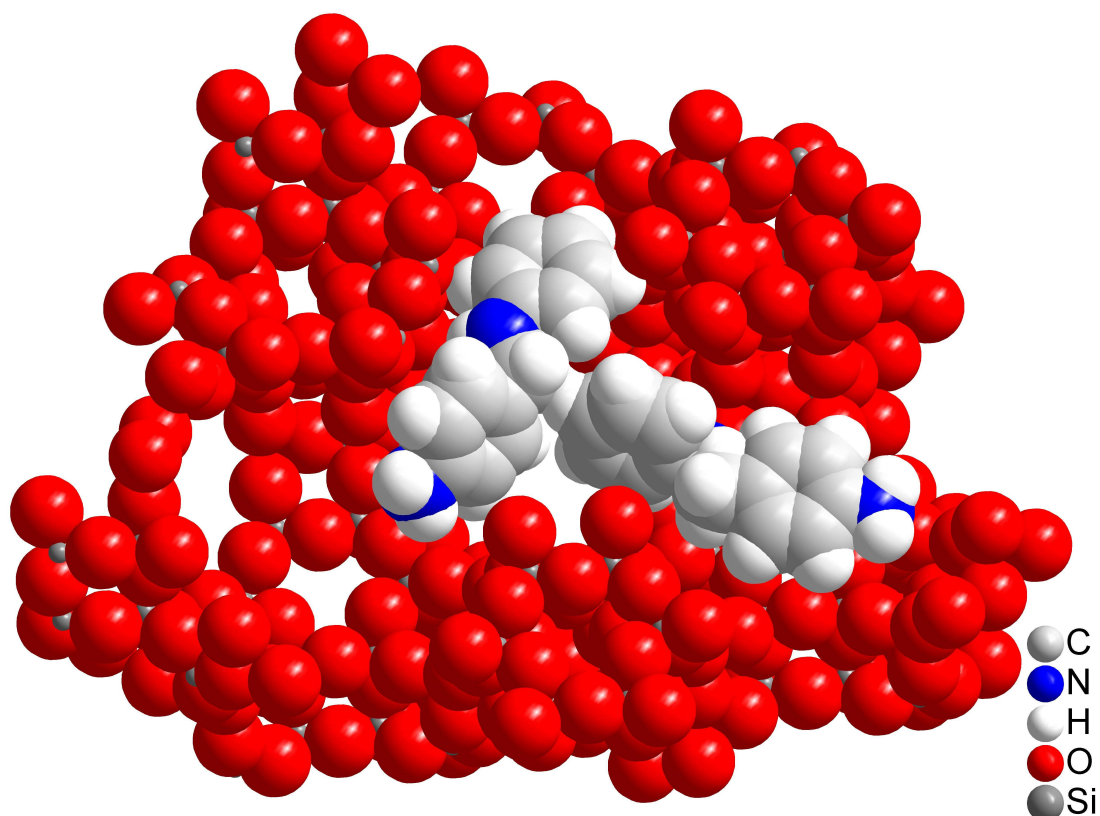


Fig. 3.14: Model of two PABA molecules in a FAU supercage.

The very poor activity of MOR-type zeolites seems surprising at first, as the reactants should be able to enter the slit-shaped 12-membered pore openings as shown in Fig. 3.15. However, there are no pore intersections (of 12-membered pores) or supercages in the MOR structure where a reaction between two reactants is possible. When a reactant, such as PABA, is located within such a pore, there is no possibility to attack it at its methylene-unit by a second molecule, as it is completely shielded by the pore walls. Therefore, the reaction can only take place at the outer surface and the pore entrances as in case of MFI-type zeolites, which likewise display very poor activity.

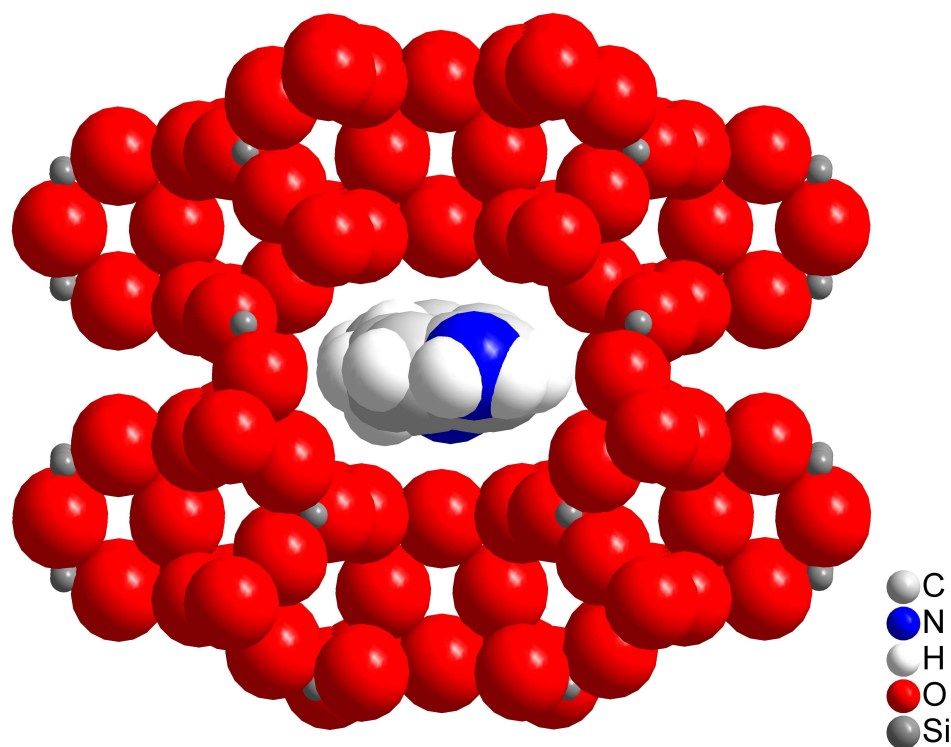


Fig. 3.15: Model of a PABA molecule in a MOR pore.

By far the highest activities were found for the series of dealuminated faujasites H-CBV 720 – 780. The reason for the high activity of these materials is related to their mesoporosity. The mesopores in the dealuminated materials provide better access to the Brønsted acid sites, thus, minimizing mass transport limitations.¹

Thus, dealumination was proven to increase the activity of a parent zeolite for MDA formation markedly by introducing mesoporosity. However, dealumination does inevitably decrease the acid site concentration as removing aluminum from the zeolite framework also eliminates the associated bridging SiOHAl group.

A variant approach to introduce mesoporosity without decreasing the zeolites acid site concentration is to remove the Si from the framework. This can be achieved by leaching the zeolite in basic medium, i.e., treating the zeolite with alkaline solution, which causes desilication and so the formation of mesopores.

As starting material for alkaline leaching H-BEA 25 was chosen, as it is among the most active parent zeolites. H-CBV 500 was deliberately not used for desilication experiments as it already has a very high Si/Al ratio and therefore, the removal of Si is

believed to cause too much damage to the zeolite framework, leading eventually to a collapse of the whole structure. In order to study the influence of the treatment time on the structure and acidity of H-BEA 25, samples were desilicated for different time intervals between 15 min and over 1000 min.

XRD analysis of the parent and the desilicated samples show that already after 15 min of alkaline leaching, the BEA framework is severely damaged. However, no further change in the samples crystallinity was found with increasing treatment time. NH_3 -TPD showed a significant increase in acidity from 530 $\mu\text{mol/g}$ for the parent H-BEA 25 samples to about 900 $\mu\text{mol/g}$ for the leached samples. The increase in acidity was expected as the removal of Si leads to a loss of weight in the sample, while the number of acid sites (defined by tetrahedral Al^{3+}) remains constant.

Elemental analysis by AAS shows an ongoing removal of Si from the framework with increasing treatment time and the Si/Al ratio in the sample is constantly but slowly decreasing. However, AAS also shows that the most dramatic changes in composition occur in the first 15 – 30 min of leaching time. In line with AAS analysis, the (meso-)pore volumes derived from N_2 -physisorption experiments indicate a fast formation of mesopore volume (0 – 0.24 cm^3/g) in the first 30 min of leaching time and a slow increase in mesopore volume from 0.28 to 0.33 cm^3/g with increasing treatment time.

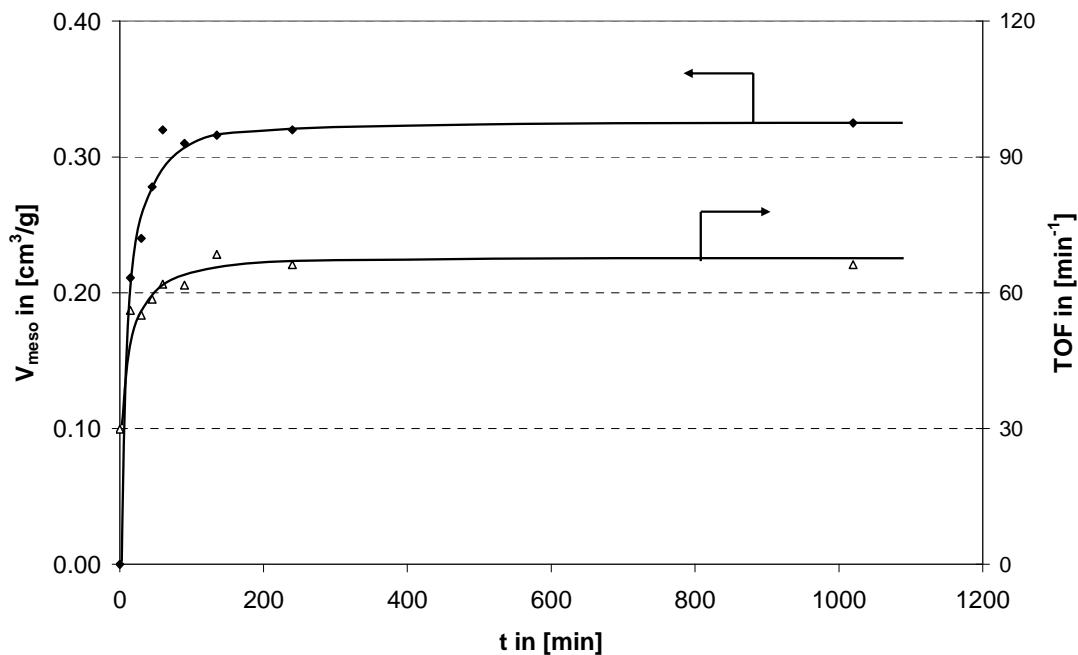


Fig. 3.16: Influence of leaching time on mesopore volume and activity.

The influence of leaching time on the mesopore volume and catalytic activity of H-BEA is graphically illustrated in Figure 3.16. The TOFs of the desilicated material doubles compared to parent H-BEA 25. Compared to the parent material, the actual activity of the material does in fact quadruple, as the acid site concentration itself increases. The TOFs slightly increase with further increasing treatment time. This observation is line with the slightly increasing mesopore volume over time. However, the actual TOFs are still lower compared with those of dealuminated Y-type zeolites. These relatively low TOFs and the fact that the TOFs are still increasing with increasing mesopore volume suggest that the reaction is still limited by pore diffusion or that the transition state itself is restricted.

To overcome this to a more drastic degree H-MCM-36 and H-ITQ-2 were both synthesized from a common MCM-22(P). The Si/Al ratios of the final materials were hardly affected by the delamination and were stable at about 38 and, so, slightly lower than the Si/Al ratio in the synthesis gel, which was 45. TEM and XRD analysis showed that the layers of MCM-22(P) were successfully delaminated. The XRD patterns of H-ITQ-2 and H-MCM-36 indicate that the MWW-layers in H-MCM-36 are reduced in size

also with respect to their intact sheet portion, as the signals in the XRD pattern of H-MCM-36 are significantly broader compared to H-ITQ-2.

N₂-physisorption experiments showed that hardly any micropores were left after delamination and similar mesopore volumes of about 0.25 cm³/g are created in both materials. The acidity of the materials did change significantly during the delamination process. While the acidity of H-MCM-36 dropped from 327 μmol/g in H-MCM-22 to 209 μmol/g, the acidity of H-ITQ-2 increased slightly to 364 μmol/g. The reason for the loss of apparent acid site concentration in case of H-MCM-36 is most likely caused by the increase in weight of the sample by the pillaring with TEOS. The reason for the increased acid site density in H-ITQ-2 is the high basicity in the delamination process, which may cause desilication, as already discussed for the alkaline leaching of H-BEA 25. However, this loss of Si was not substantiated by elemental analysis.

Parent H-MCM-22 displays no determinable activity for MDA formation. This is not surprising, as its pores are of similar size as those of ZSM-5, showing also extremely poor activity (see Fig 3.12). The mesopores in H-MCM-36 and H-ITQ-2, however, provide easy access to the acid sites and therefore, both materials display good activity for MDA formation. The TOF of H-MCM-36 is with 375 min⁻¹ similar to the delaminated faujasites and more than twice as high as the TOF of H-ITQ-2 (165 min⁻¹). The reason for the higher activity of H-MCM-36, although it displays similar mesopore volume and size, is defects in the MCM-22 lattice layers. These defects are formed during the delamination process and provide even better access to the acid sites. As the delamination conditions are more severe for MCM-36 (68 h @ 100°C) than for ITQ-2 (16 h @ 80°C) it is plausible that the MWW-layers in MCM-36 are damaged to a larger extent, resulting in a more open structure and therefore higher activity.

The H/Al-MCM-41 sample was found to have a very low Si/Al ratio of 14 but only a Brønsted acidity of 203 μmol/g. A possible explanation for this is the presence of large amounts of extraframework Al or even an amorphous Al-oxide phase. The formation of a (defective) MCM-41 structure alongside another amorphous Al-oxide phase would explain the surprisingly low mesopore volume of 0.19 cm³/g and the unexpected presence of large, unordered macropores. It furthermore provides an explanation for the poor quality of the XRD data. Also the TEM images indicate the presence of an amorphous

phase besides the ordered MCM-41 structure. However, the TOF of the material was determined as 477 min^{-1} , which surpasses even the dealuminated Y-type zeolites. It seems, that the presence of ordered mesopores is beneficial for a catalysts' activity. The reason for the poor quality of the material might be the extremely high Al concentration in synthesis mixture. Materials with lower Al content might yield MCM-41 samples with higher crystallinity, higher Brønsted acidity and therefore even higher activity.

In the synthesis of SBA-15 it could clearly be observed, that the presence of low Al concentrations in the synthesis mixture (below 3% respective to Si+Al total) results in the formation of a well ordered SBA-15 structure, in which only small amounts of Al are incorporated. Actually, in case of SBA-15 (33) next to none of the Al was incorporated into the structure (Si/Al almost 1500) and a well ordered SBA-15 structure was obtained. With increasing Al content an increasingly "defect" SBA-15 structure is obtained, which manifests by decreasing mesopore volumes and decreasing intensity of the (100) signal in the X-ray diffraction patterns. Finally, at Al contents above 5% the crystallization is disturbed to such an extent that a purely amorphous aluminosilicate with no regular pores, but with high Al content is formed. The activity measurements above these materials revealed that the higher the crystallinity of the materials is, the higher are their TOFs. This reinforces the conclusion drawn from the MCM-41 sample that the presence of regular mesopores is beneficial for the activity of a catalyst. Naturally the pure Si samples, which provide the best crystallinity but no acidity, showed no activity at all.

3.5 Conclusion

It was shown that the activity of an aluminosilicate catalyst for MDA formation is influenced by both the materials acid site density and pore structure. As long as materials with similar structures (zeolite framework types) are compared, the actual activity is a direct function of the total number of Brønsted acid sites in the reactor, as the TOFs are constant within a series, if pore diffusion can be neglected. As this is not the case for the parent zeolites and desilicated BEA samples their TOFs are affected by the degree of mass transport limitation. The pore structure of the applied catalysts has a pronounced influence on activity. Whereas MFI- and MWW-type zeolites are almost inactive because the reactants are too large to enter their pores and reaction can therefore only take place on the outer surface, parent FAU and BEA type materials show a certain activity as the S_N2 -type reaction can take place in the supercages (FAU) or pore intersections (BEA). However, kinetic data suggests that the reaction is heavily limited by pore diffusion in these materials. Mass transport limitation can be overcome by creating mesopores in the zeolite framework, as was shown for the dealuminated FAU catalysts.

It was verified that dealumination causes a dramatic increase in catalyst activity by creating mesopores, while on the other hand also decreasing the catalysts acid site density. Desilication by alkaline leaching seems to be a promising pathway for catalyst development as it does likewise create mesopores in a zeolite framework, but does not actually increase the materials' acid site density. It was shown, however, that while indeed mesopores were created by alkaline leaching, only a moderate gain in actual activity was achieved. Also at treatment times of up to 17 hours, the mesopores created by desilication are not sufficient to overcome mass transport limitation in the process.

The use of designed mesoporous aluminosilicates, such as the delaminated materials MCM-36 and ITQ-2 is an interesting and potentially powerful strategy. While ITQ-2 reaches about half the TOF of the dealuminated FAUs, MCM-36 displays significantly higher activity, comparable to the dealuminated catalysts. The higher activity of MCM-36 compared to the closely related ITQ-2 is attributed to defects in the MWW-layers of which both materials are composed. In MCM-36, more of these lattice defects are formed due to the more severe swelling conditions, thus leading to higher activity.

Ordered mesopores aluminosilicates such as MCM-41 and SBA-15 also show very promising results. In case of SBA-15 one is facing the problem that the one step synthesis of Al-SBA-15 by adding an Al-precursor to the synthesis mixture fails. Either Al is not incorporated to the structure and well ordered, but non-acidic SBA-15 is formed, or an Al-rich but amorphous aluminosilicate is yielded. One way around this problem would be the two step synthesis of Al-SBA-15 by forming a well ordered pure silica material according to established techniques and then add the Al by impregnation with aluminumnitrate and ongoing calcination, as proposed by Hensen *et al.*²⁷

The incorporation of Al into the MCM-41 structure is easier, but still challenging at high Al concentrations. The synthesis described herein aims at a Si/Al ratio of 9 and yields an at least partially amorphous defective MCM-41 structure. Optimization of synthesis conditions and a slightly lower Al content should provide pathways to MCM-41 materials with better crystallinity and even higher activity.

ACKNOWLEDGMENTS

The authors are grateful to X. Hecht for BET measurements, M. Neukamm for AAS measurements and S. Scholz and S. Wyrzgol for TEM images. Financial and material support of the Dow Chemical Company are gratefully acknowledged. Furthermore the work at the Technische Universität München was funded by the DOW Chemical Company.

This chapter is based upon :

M. Salzinger, M.B. Fichtl, J.A. Lercher, *Appl. Catal. A*, paper submitted.

REFERENCES

- [1] M. Salzinger, J.A. Lercher, *Green Chemistry*, paper submitted.
- [2] T. Kugita, S. Hirose, S. Namba, *Catal. Today* **2006**, *111*, 275.
- [3] P. Botella Asuncion, J.K.P. Bosman, A. Corma, C.J. Mitchell, *US Patent 7,238,840 B2* **2007**.
- [4] A. de Angelis, P. Ingallina, C. Perego, *Ind. Eng. Chem. Res.* **2004**, *43*, 1169.
- [5] C. Perego, A. de Angelis, A. Carati, C. Flego, R. Villini, C. Rizzo, G. Bellussi, *Appl. Catal. A* **2006**, *307*, 128.
- [6] A. Corma, P. Botella, C. Mitchell, *Chem. Comm.* **2004**, *17*, 2008.
- [7] Y. Kiso, T. Toshihiro, T. Hayashi, *EU Patent 0,329,367 A2* **1989**.
- [8] C. Perego, A. de Angelis, O. Farias, A. Bosetti, *EU Patent 1,055,663 A1* **2000**.
- [9] A. Corma, V. Fornes, S.B. Pergher, Th.L.M. Maesen, J.G. Buglass, *Nature* **1998**, *396*, 353.
- [10] Y.J. He, G.S. Nivarthi, F. Eder, K. Seshan, J.A. Lercher, *Microporous Mesoporous Mat.* **1998**, *25*, 207.
- [11] I. Melián-Cabrera, S. Espinosa, J.C. Groen, B. v/d Linden, F. Kapteijn, J.A. Moulijn, *J. Catal.* **2006**, *238*, 250.
- [12] G.M. Kumaran, S. Garg, K. Soni, M. Kumar, J.K. Gupta, L.D. Sharma, K.S. Rama Rao, G. Murali Dhar, *Microporous Mesoporous Mat.* **2008**, *114*, 103.
- [13] Y. Sun, Y. Yue, Z. Gao, *Appl. Catal. A* **1997**, *161*, 121.
- [14] D. Zhao, J. Feng, Q. Huo, N. Melosh, G.H. Fredrickson, B.F. Chmelka, G.D. Stucky, *Science* **1998**, *279*, 548.
- [15] Y.-H. Yue, A. Gedeon, J.-L. Bonardet, J.B. d'Espinose, N. Melosh, J. Fraissard, *Chem. Commun.* **1999**, *19*, 1967.
- [16] Y.-H. Yue, A. Gedeon, J.-L. Bonardet, J.B. d'Espinose, N. Melosh, J. Fraissard, *Stud. Surf. Sci. Catal.* **2000**, *129*, 209.
- [17] B.C. Lippens, B.G. Linsen, J.H. de Boer, *J. Catal.* **1964**, *3(1)*, 32.

-
- [18] G. Hasely, *J. Chem. Phys.* **1948**, 16(10), 932.
- [19] E.P. Barret, L.G. Joiyner, P.P. Halenda, *J. Am. Chem. Soc.* **1953**, 73,373.
- [20] C. Baerlocher, L.B. McCusker, *Database of Zeolite Structures*, <http://www.iza-structure.org/databases/> **2009**
- [21] C.L. Janssen, I.B. Nielsen, M.L. Leininger, E.F. Valeev, J.P. Kenny, E.T. Seidl, *The Massively Parallel Quantum Chemistry Program (MPQC), Version 2.3.1(MPICH)*, Sandia National Laboratories, Livermore, CA, USA, **2008**.
- [22] D. Duddeldam, S. Calero, T.J.H. Vlugt, R. Krishna, T.L.M. Maesen, B. Smit, *J. Phys. Chem B* **2007**, 108, 12301.
- [23] K. Brandenburg, M. Bernt, *Diamond Version 3.1e*, Crystal Impact GbR, Bonn, **2007**.
- [24] C. Baerlocher, L. B. McCusker, D. H. Olson, *Atlas of Zeolite Framework Types*, 6. edition, **2007**, 9.
- [25] L. Teyssier, M. Thomas, C. Bouchy, J.A. Martens, E. Guillon, *Microporous Mesoporous Mat.* **2006**, 100, 6.
- [26] S. Zheng, H. Heydenrych, A. Jentys, J.A. Lercher, *J. Phys. Chem. B* **2002**, 106, 9552.
- [27] E.J.M. Hensen, D.G. Poduval, P.C.M.M. Magusin, A.E. Coumans, J.A.R. van Veen, *J. Catal.* **2010**, 269, 201.

Chapter 4

Investigations on the deactivation of aluminosilicate catalysts during methylenedianiline synthesis

The production of methylenedianiline from formaldehyde and aniline can be catalyzed by solid acid catalysts, such as zeolites, amorphous aluminosilicates and clays. It was shown previously that the application of mesoporous aluminosilicates, such as steamed FAU, MCM-41 or MCM-36, greatly enhances the rate of MDA formation by avoiding mass transport limitation. However, deactivation of the catalytic material is still a major problem and prohibits an industrial application. In this study we propose a deactivation mechanism based on the previously described reaction network and mechanism. The assumption that catalyst deactivation proceeds via the growth of an oligomeric MDA species inside the pore system was verified by isolation of this species from a deactivated catalyst. As this process is an intrinsic part of the catalytic reaction itself, the formation of such an oligomer can not be prevented totally. We propose, however, that large ordered mesopores and lower acid site density should have a positive impact on catalyst lifetime. We therefore synthesized samples of MCM-36 and MCM-41 with different Al-content and studied the impact of the materials' Brønsted acidity and their mesoporosity on lifetime compared to commercial steamed FAU samples.

4. Investigations on the deactivation of aluminosilicate catalysts during methylenedianiline production

4.1 Introduction

As we have shown in previous work, it is possible to produce methylenedianiline (MDA), which is an important raw material for the synthesis of polyurethanes, in high yields from formaldehyde and aniline by solid acid catalysis.¹ As the reaction is heavily limited by pore diffusion over (exclusively microporous) parent zeolites, the application of mesoporous aluminosilicates is vital in order to avoid mass transport limitation and achieve high activity.²⁻⁷ Among the mesoporous materials proposed as catalysts for the process hierarchically structured materials such as MCM-41, MCM-36 and SBA-15 have shown very promising results in terms of activity.¹ Comparable results can also be obtained using steamed Y-type catalysts of the CBV 720 – 780 series.

All catalysts proposed and tested so far for the production of methylenedianiline were suffering from rapid deactivation. The reason for their deactivation is not understood so far. For an industrial realization of the solid acid catalyzed production of MDA it is necessary to find ways to avoid these deactivation processes. Whether and how this can be achieved by the choice of reaction conditions, catalyst design and/or regular regeneration cycles has yet to be determined.

It is the aim of this work to determine and understand the processes leading to catalyst deactivation and to propose ways to avoid or slow down these processes. In earlier work we already proposed a reaction network and mechanism for the formation of methylenedianiline from the condensation product of aniline and formaldehyde (aminal).² The reaction mechanism as shown in Fig. 4.1 emanates from a protonation of the secondary amino group of an intermediate species. By this protonation the adjoining C-N bond is weakened, resulting in a partial positive charge on the carbon atom. This position is thus activated for a nucleophilic attack by any nucleophile in the reaction mixture. In Fig. 4.1 this is the *para* position of another *para*-aminobenzylaniline (PABA) molecule.

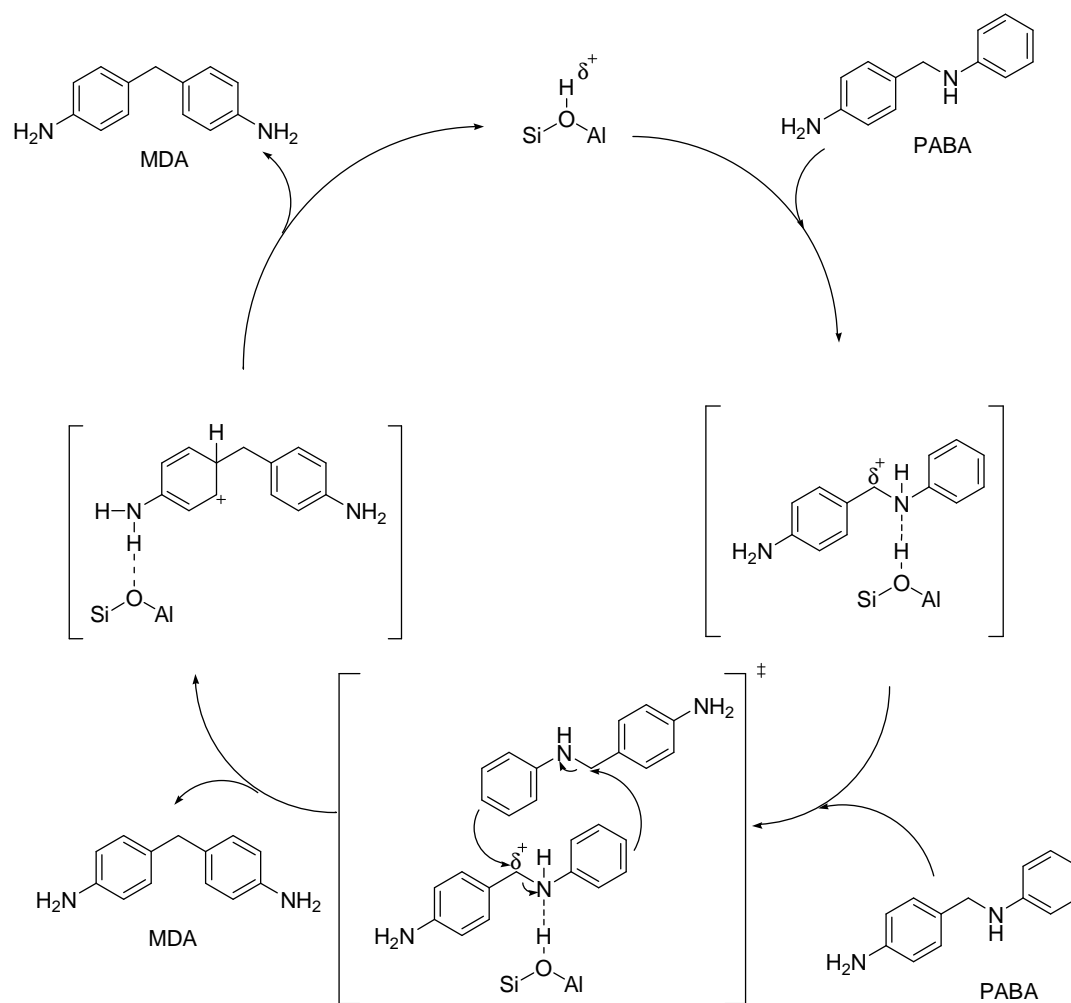


Figure 4.1: Reaction mechanism of the formation of MDA from PABA.²

As the *para* and *ortho* positions of the phenylring systems, as well as the primary amino functions of all involved molecules are strong nucleophiles as well, a broad variety of intermediates and products is formed during the reaction. As long as these intermediates still contain at least one secondary amino function, they can still be activated and attacked by other nucleophiles.

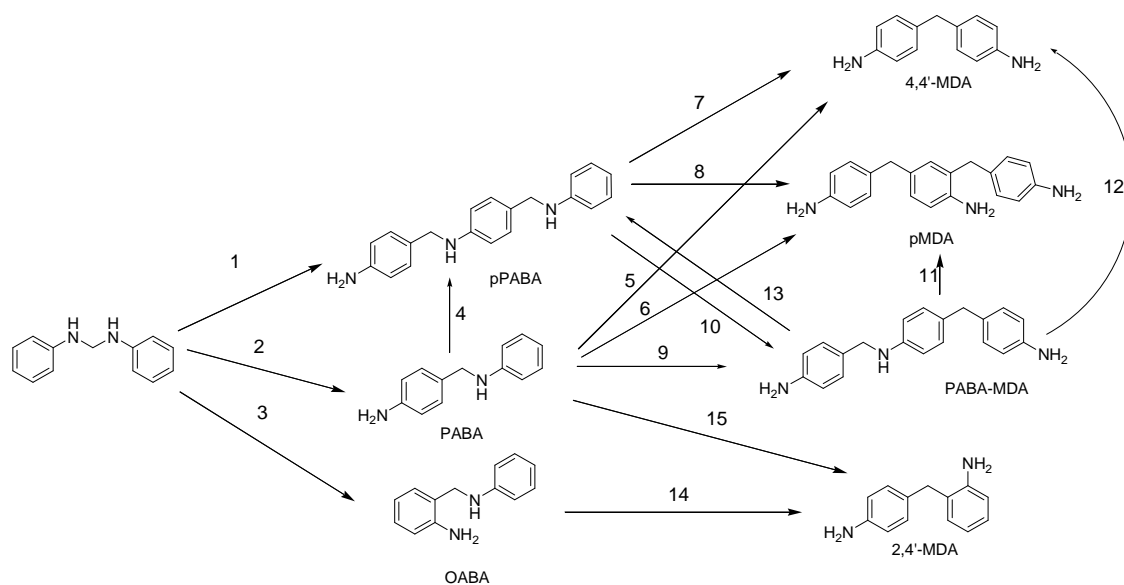


Figure 4.2: Simplified reaction network of the formation of MDA from animal.²

As the electron rich ring system of MDA is also a valid nucleophile, the attack of an activated intermediate onto an MDA molecule yields a stable 3-ring MDA structure (pMDA). Obviously this pMDA structure is again a valid nucleophile that can be subject to further reactions with activated intermediate species, leading to the growth of oligomeric MDA species on the catalyst.

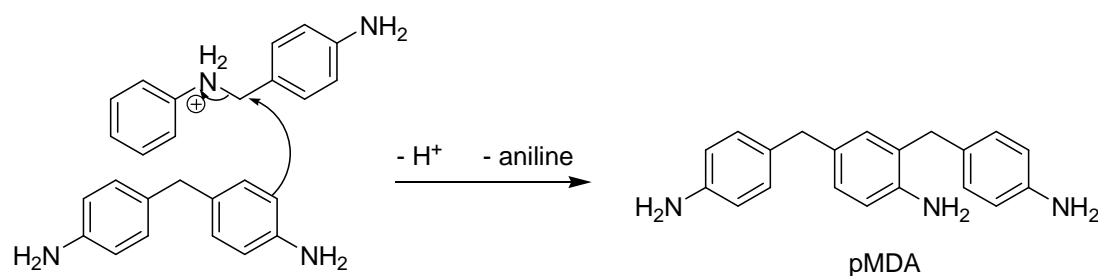


Figure 4.3: Formation of pMDA from 4,4'-MDA and PABA.²

The presence of a 3-ring pMDA structure in the reaction mixture was already proven by GC/MS analysis in previous work.² First aim of this work is to prove the presence of heavier pMDA species on the catalyst surface, as we believe these molecules to be the source of catalyst deactivation. Due to their large molecular weight and numerous amino functions, which can interact strongly with the Brønsted acid sites of the catalyst, these

heavy pMDA species adsorb very strongly on the catalyst surface and are virtually impossible to desorb, such blocking the active sites. For this same reason, heavy pMDA species can not be detected in the reaction mixture, e.g. by HPLC. It is necessary to dissolve the catalyst framework of a deactivated catalyst and analyze the organic residue in order to verify the existence of these species in a deactivated catalyst.

We propose two hypothetical pathways to prolong catalyst lifetime:

- a) A decrease in acid site density would reduce the binding sites for pMDA species and thus weaken its bonding to the surface, making it easier to desorb. Furthermore, a lower acid site density should decrease the probability of chain growth, thus slowing down the formation of heavy pMDA species.
- b) The use of (ordered) mesoporous aluminosilicates should make desorption of pMDA species easier, as physisorption in mesopores is weaker than in micropores, which envelop the whole pMDA molecule tightly. Furthermore, ordered mesoporous materials, such as MCM-41 and MCM-36, have been shown to be more effective catalysts as steamed faujasites or amorphous aluminosilicates (which feature randomly sized mesopores).

In order to test these hypotheses we will determine the lifetime behavior of a series of parent BEA type zeolites and dealuminated Y-type zeolites of the CBV series and compare it to the behavior of synthesized MCM-36 and MCM-41 samples of similar acidity.

4.2 Methods

4.2.1 Materials

The aminimal solution, which was used as starting material for all screening reactions, was prepared as follows. In a 1 L round bottom flask 600 mL of aniline (6.58 mol, Sigma, purity $\geq 99.5\%$) were heated to 50°C under vigorous stirring. 100 mL of formalin (1.32 mol formaldehyde, Sigma, 37% wt of formaldehyde in water, stabilized with methanol) were added drop wise. After addition stirring was continued at 50°C for 1 h. Water and methanol were removed by distillation in a rotavapor. Concentration and purity of the resulting solution of 1 equ. of aminimal in 3 equ. of aniline, which is ready for use in the test reactions, was verified by ^1H - and ^{13}C -NMR, as well as GC.

The dealuminated Y-type zeolites (H-CBV 720, H-CBV 740, H-CBV 760, H-CBV 780) for lifetime testing were purchased from Zeolyst. Three samples of BEA-type zeolite (H-Beta 25, H-Beta 35, H-Beta 150) were provided by Südchemie.

MCM-36 (X) samples with Si/Al ratios of X=10, 20, 30 and 50 were prepared from the respective MCM-22(P) materials according to literature.^{8,9}

Hydrothermal synthesis of MCM-22(P) is carried out by using hexamethyleneimine (HMI, 99% Aldrich) as templating agent, SiO_2 (Aerosil 380, Degussa) as silica source, NaAlO_2 (Riedel-de Haën) as aluminum source, NaOH (Merck) for pH adjustment and water as solvent. The gel compositions were the following:

$\text{SiO}_2 : x \text{ NaAlO}_2 : 0.18 \text{ NaOH} : 0.5 \text{ HMI} : 45 \text{ H}_2\text{O}$ with $x = 0.1, 0.05, 0.03$ or 0.02 .

In a typical synthesis the respective amount of NaAlO_2 and 0.76 g of NaOH are dissolved in 85 mL of H_2O . To this solution 5.21 g of HMI and 6.29 g of SiO_2 are added under vigorous stirring at room temperature. After stirring for 1 h at room temperature the resulting homogenous gel is transferred into a PTFE-lined stainless steel autoclave for hydrothermal synthesis at 140°C for 9 days in an oven designated to rotate the autoclaves at 40 rpm for 9 days. The solid product is recovered by filtration, washing and drying in air at 80°C.

For the synthesis of H-MCM-36 (X) the respective MCM-22(P) is suspended in a threefold excess (by mass) of H_2O , a 16 fold excess of tetrapropylammonium hydroxide solution (TPAOH, 20 wt% in H_2O , Aldrich) and a 23 fold excess of

hexadecyltrimethylammonium bromide solution (CTMABr 25 wt% in H₂O, Fluka) at 100°C in a three necked round bottom flask equipped with magnetic stirring and a reflux condenser. The pH is adjusted to 13.5 with NaOH. After stirring for 68 h at 100°C a white solid is obtained by filtration, washing and drying in air at 80°C. The dried product is mixed with a five fold excess of TEOS (99%, Aldrich) under N₂ atmosphere. After stirring at 90°C for 25 h the mixture was hydrolyzed with a tenfold excess of H₂O for 6 h at 40°C. Na-MCM-36 is obtained by filtration, washing and calcination in synthetic air by heating at 5 K min⁻¹ to 120°C and holding for 1 h, followed by heating at 3 K min⁻¹ to 550°C and holding for 12 h. In order to obtain the Brønsted acidic proton exchanged H-MCM-36 ion exchange is performed by suspending 2.00 g of Na-MCM-36 (X) in 100 mL of 0.2 M NH₄Cl solution at 80°C over night, followed by filtration and washing. The ion exchange is repeated three times to ensure complete removal of Sodium. H-MCM-36 is obtained by calcination in synthetic air at 3 K min⁻¹ to 120°C and holding for 1 h, followed by heating at 3 K min⁻¹ to 550°C and holding for 10 h.

H-MCM-41 (X) samples were prepared according to literature¹⁰ with Si/Al ratios of X = 10, 20, 30 and 50 from sodium metasilicate (Na₂SiO₃, Merck), cetyltrimethylammoniumbromid (Aldrich), 10% aqueous tetramethylammonium hydroxide (TMAOH, Sigma) and sodium aluminate (NaAlO₂, Riedel-de Haën). The aqueous solutions of CTMABr (10.52 g in 60 mL of water) and TMAOH (10.13 g) were added to a solution of 24.50 g sodium metasilicate in 80 mL of water under vigorous agitation at room temperature. Then the sodium aluminate solution (0.943 g; 0.471 g; 0.314 g and 0.189 g, NaAlO₂, respectively, in 60 mL water) was added dropwise under vigorous stirring at room temperature. H₂SO₄ was added to the gel mixture to adjust the pH to approximately 11 before heating. Hydrothermal treatment was performed at 100°C for six days in teflon lined stainless steel autoclaves. The product was filtered, washed, dried in air and calcined in synthetic air at 550°C for 12 h. The obtained Na-MCM-41 (X) samples were ion exchanged with 0.2 M NH₄Cl solution at 80°C five times and then washed, dried and calcined at 550°C for 12 h to prepare H-MCM-41 (X).

4.2.2 Characterization

Nitrogen physisorption isotherms were measured using a PMI automated sorptometer at liquid nitrogen temperature (77 K), after outgassing under vacuum at 623 K for 4 h. The apparent surface area was calculated by applying the Brunauer–Emmett–Teller (BET) theory to the adsorption isotherms over a relative pressure range from 0.01 to 0.09. The micropore volumes were evaluated using the t-plot method¹¹ according to Hasely.¹² The mesopore volumes were determined by the cumulative pore volume of pores with diameters ranging from 2 – 50 nm according to the BJH method.¹³ Because of the limitations of the PMI instrument, the isotherms were measured at relative partial pressures higher than $10^{-5} p/p^0$.

For TPD experiments approximately 50 mg of sample were activated for 1 h at 723 K in a six port parallel vacuum system (0.8 Pa). After activation the samples were contacted with 1 mbar of NH_3 at 373 K for 1 h, followed by degassing for 2 h at 373 K. For desorption the samples were heated up to 1043 K with an increment of 10 K min^{-1} . Ammonia desorption was monitored by mass spectrometry (Pfeiffer QMS 200 Prisma). The amount of desorbed ammonia was determined by integration of the MS signal and calibration to a standard material (MFI 90; $360 \mu\text{mol g}^{-1}$).

The elemental composition of the applied catalysts was determined by atomic adsorption spectroscopy in a Unicam M Series Flame-AAS equipped with an FS 95 autosampler and a GF 95 graphite furnace. The crystallinity of the synthesized and modified materials was analyzed by powder X-ray diffraction using a Philips X'Pert Pro System (Cu- $\text{K}\alpha_1$ radiation, 0.154056 nm) at 45 kV / 40 mA in step scan of $0.017^\circ \text{ min}^{-1}$ from 5° to $70^\circ 2\theta$. Transmission electron microscopy (TEM) was measured on a JEOL-2011 electron microscope operating at 200 kV. Prior to the measurements, the powdered samples were suspended in ethanol solution and dried on a copper-carbon-grid.

MALDI-TOF/TOF measurements were performed in substance without matrix on an ultraflex TOF/TOF by Bruker.

4.2.3 Chemical pulping of deactivated zeolite

For identification of the proposed heavy pMDA species inside a deactivated zeolite 1.0 g of zeolite H-BEA 25 were added to 20 g of the aminal mixture and heated to 140°C

for three days. Complete deactivation of the catalytic material was verified by GC analysis as the addition of fresh aminal resulted in no further 4,4'-MDA formation. The catalyst was separated from the reaction mixture by filtration and washed with hot aniline. The resulting residue was dissolved in a platinum crucible by repeated dropwise addition of 20% HF and continuous evaporation by heating with a quartz iodine lamp. The residue was taken up in water and extracted with toluene three times. The combined organic layers were dried over Na₂SO₄, toluene was removed under reduced pressure. The obtained highly viscous black oil was analyzed by elementary analysis, NMR and MALDI-TOF/TOF.

4.2.4 Catalytic reaction

A ChemSpeed Accelerator SLT 106 synthesis robot with eight parallel reactors was used for catalytic test reactions. For the test reaction 15 mL of the aminal solution were placed in a 27 mL double jacket glass reactor that was prefilled with 0.20 g of catalyst. The reactors were heated to 100°C and dispersion of the catalyst is ensured by a vibration-plate operating at 1400 rpm. 100 µL of sample were taken from the reaction mixture after defined time intervals and diluted with 0.9 mL of acetonitrile (Sigma, purity ≥99.5%), containing 1 mL of diphenylmethane (Fluka, purity ≥99%) per 100 mL of acetonitrile as internal standard. After removal of the catalyst by filtration through a syringe filter (Minisart SRC; 0.20 µm, d = 4 mm) the sample was analyzed by GC.

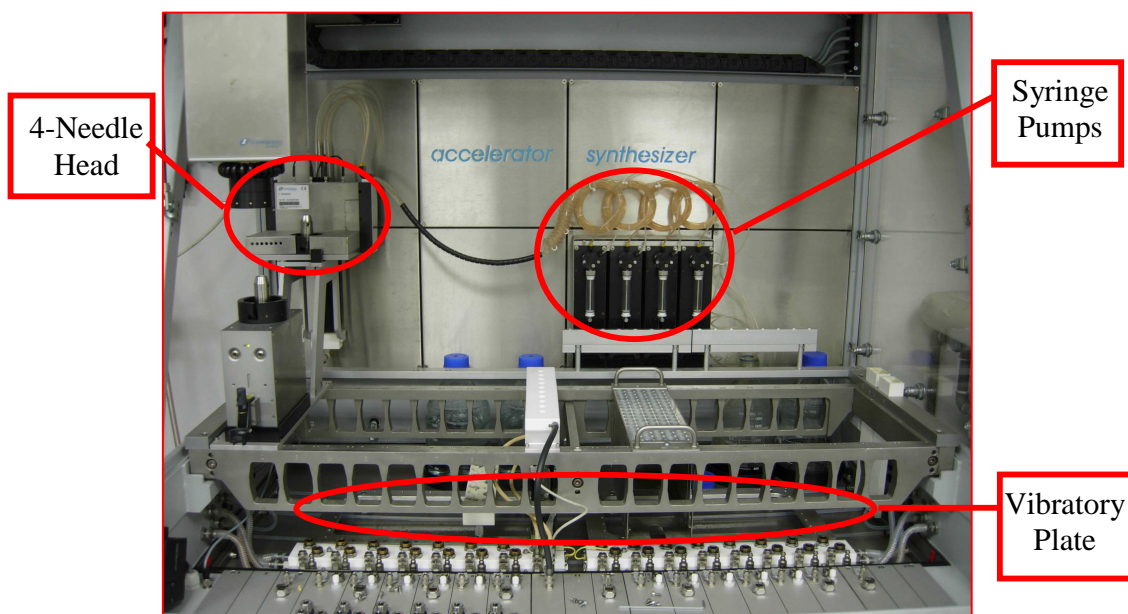


Figure 4.4: ChemSpeed Accelerator SLT 106.

For GC analysis a Shimadzu GC 2010, equipped with an Optima 35 MS column (length = 30 m, ID = 0.32 mm, film thickness 0.25 μm), an FID detector and an autosampler was available. A temperature profile beginning at 60°C, hold for 5 min, heating with an increment of 15 K min^{-1} to 170°C, holding for 40 min, heating with 25 K min^{-1} up to 300°C, holding for 15 min and heating with 25 K min^{-1} up to 350°C and holding this temperature for 2 min was applied. The injection volume was set to 1 μL with the injection port heated to 280°C and a split ratio of 50. The instrument was calibrated to 4,4'-MDA, 2,4'-MDA, PABA, OABA and aminal, the response factors for heavier products were assumed to be identical in first approximation and were estimated by closing the mass balance of the reaction.

The TOFs of the applied catalysts were determined by normalizing the initial rate of 4,4'-MDA formation to the amount of applied catalyst and its acidity according to equation 1:

$$TOF[\text{min}^{-1}] = \frac{\text{rate of 4,4'-MDA formation } [\text{mol}_{4,4'\text{-MDA}} / (\text{mol}_{\text{aniline}} \cdot \text{min} \cdot \text{g}_{\text{cat}})]}{\text{acidity } [\text{mol}/\text{g}_{\text{cat}}] \cdot n_{\text{aniline}} [\text{mol}]} \quad (1)$$

4.2.5 Continuous lifetime testing

For continuous lifetime testing an upflow tubular reactor was commissioned. It consists of a double jacket glass reactor, equipped with a frit at the bottom for fixation of the catalyst/inert filling material bed and an overflow hose at the top end for collecting samples. As starting material the aminal/aniline mixture, prepared as described above, was dosed *via* a HPLC pump Abimed Gilson Type 307. For heating the setup is equipped with a thermostat T 500 by Tamson. The reactor has an inner diameter of about 2.0 cm and a height (frit to frit) of 5.1 cm, resulting in an empty tube volume of 16 mL. The reactor is filled with 3 mm glass pearls as inert material and 0.50 g of catalyst sieved to 0.18 – 0.28 mm. The flow rate was set to 0.05 mL/min resulting in a residence time of about 3 h. Previously recorded residence time profiles verified that the reactor can be modeled as a series of 2 - 3 CSTR under these conditions, thus ensuring homogenous deactivation of the catalyst through the whole reaction volume. The reaction temperature was set to 100°C. In order to prevent evaporation of volatile compounds in the reaction mixture, the reactor is equipped with a reflux condenser. The catalyst's activity was determined by collecting samples at defined time intervals and analyzing these by GC with the method described for the catalytic test reaction. The yield of 4,4'-MDA was chosen as benchmark for activity.

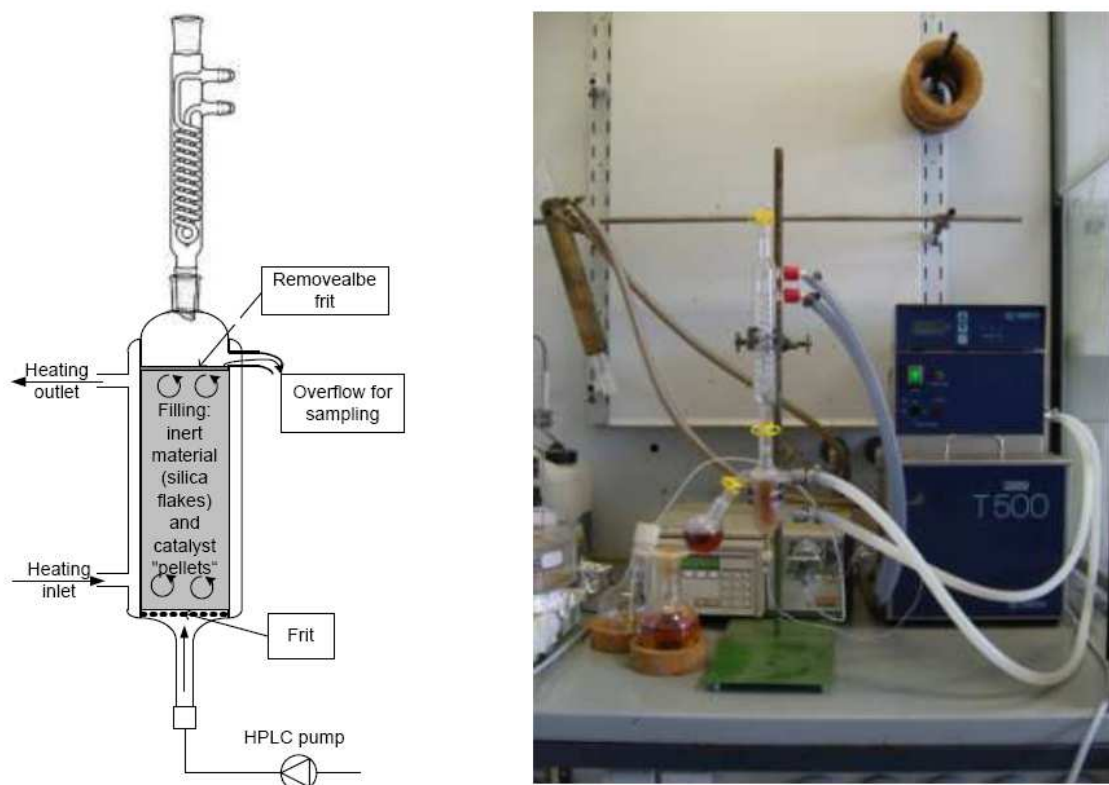


Figure 4.5: left: schematic design of the continuous upflow reactor for lifetime testing; right: photograph of the actual setup.

4.3 Results

4.3.1 Catalyst characterization

The elemental composition of the applied catalysts as determined by AAS, their micro- and mesopore volumes and their acidity, measured by NH₃-TPD, are shown in table 4.1. X-ray diffraction patterns were used to access the crystallinity of the synthesized MCM-36 and MCM-41 samples.

Table 4.1: Elemental composition, pore volumes and acidity of the applied catalysts.

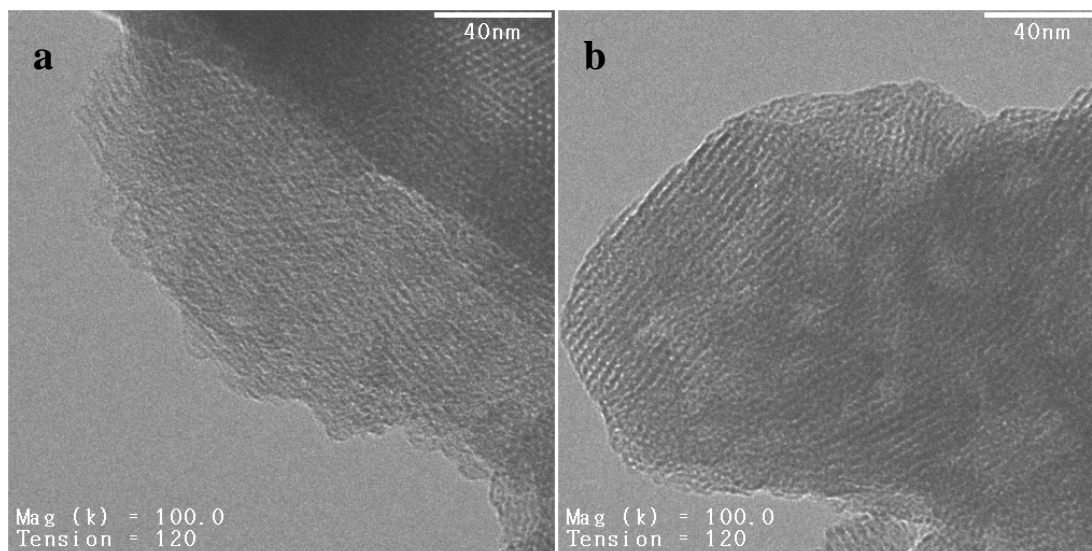
Material	Si/Al ratio	acidity [$\mu\text{mol/g}$]	V_{micro} [cm^3/g]	V_{meso} [cm^3/g]	TOF [min^{-1}]
H-BEA 25	13	530	0.16	<0.01	24
H-BEA 35	18	538	0.21	<0.01	30
H-BEA 150	79	229	0.23	0.02 ^a	15
H-CBV 720	14	474	0.31	0.19	431
H-CBV 740	22	292	0.29	0.21	409
H-CBV 760	30	391	0.28	0.18	390
H-CBV 780	42	143	0.32	0.18	415
H-MCM-36 (10)	16	416	0.04	0.15	126
H-MCM-36 (20)	21	359	0.01	0.17	304
H-MCM-36 (30)	31	249	<0.01	0.30	205
H-MCM-36 (50)	58	149	0.04	0.17	0
H-MCM-41 (10)	5.1	501	<0.01	0.26	164
H-MCM-41 (20)	12	201	<0.01	0.41	409
H-MCM-41 (30)	65	90	<0.01	0.63	519
H-MCM-41 (50)	81	52	<0.01	0.46	553

a) attributed to interparticular mesopores¹⁴

The applied commercial catalysts have Si/Al ratios ranging from 13 to 79 in case of the BEA type series and 14 to 72 for the CBV series of dealuminated faujasites. In line with their Al-contents, the acid site density of the materials increase with increasing Al-content. While the acidity of the BEA type materials lies between 538 and 229 $\mu\text{mol/g}$, the CBV materials show lower acidity at similar Si/Al ratios. This can be attributed to the formation of extraframework Al during the dealumination process by steaming.^{15,16} While the samples of parent BEA type zeolite show next to none mesoporosity, the

dealuminated FAU samples H-CBV 720, H-CBV 740, H-CBV 760 and H-CBV 780 display significant mesopore volumes of about $0.19 \text{ cm}^3/\text{g}$.

The prepared MCM-41 (X) samples were found to have Si/Al ratios, which differ significantly from the ratios in the respective synthesis gels. While samples with high Al-content (Si/Al 10 and 20) tend to incorporate more Al, samples with lower Al-content tend to incorporate only part of the Al in the synthesis gel. The acidity of the MCM-41 samples ranges from $501 \mu\text{mol/g}$ to $52 \mu\text{mol/g}$ and decreases sharply with decreasing Al-content. Nitrogen physisorption shows that no micropores are present in any of the MCM-41 samples. The calculated mesopore volumes increase with decreasing Si/Al from $0.26 \text{ cm}^3/\text{g}$ in MCM-41 (10) to $0.63 \text{ cm}^3/\text{g}$ in MCM-41 (30). The MCM-41 (50) sample, however, has a mesopore volume of $0.46 \text{ cm}^3/\text{g}$. X-ray diffraction analysis of the MCM-41 (X) samples showed, that the crystallinity of the material decreases with increasing Al content. The same trend could be observed by transmission electron microscopy. Fig. 4.6a-d show images taken from the MCM-41 (X) series, which exhibit the typical hexagonal pore structure of MCM-41 materials. While TEM images of all prepared samples indicated the formation of an MCM-41 phase, increasing amounts of an amorphous phase and defect sites are present in the samples with increasing Al-content.



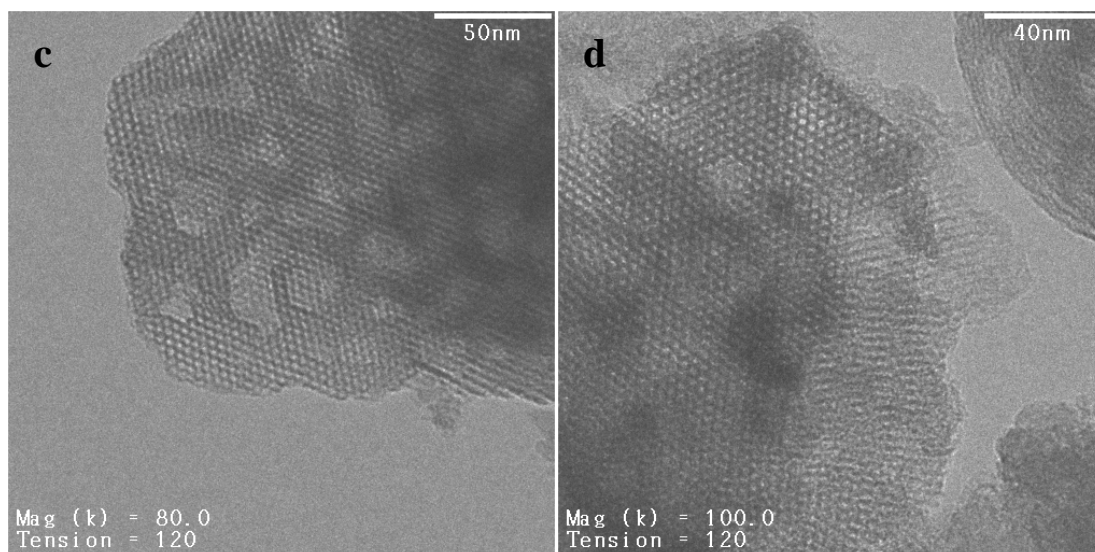


Figure 4.6a-d: Transmission electron microscopy of a) MCM-41 (10), b) MCM-41 (20), c) MCM-41 (30), d) MCM-41 (50),

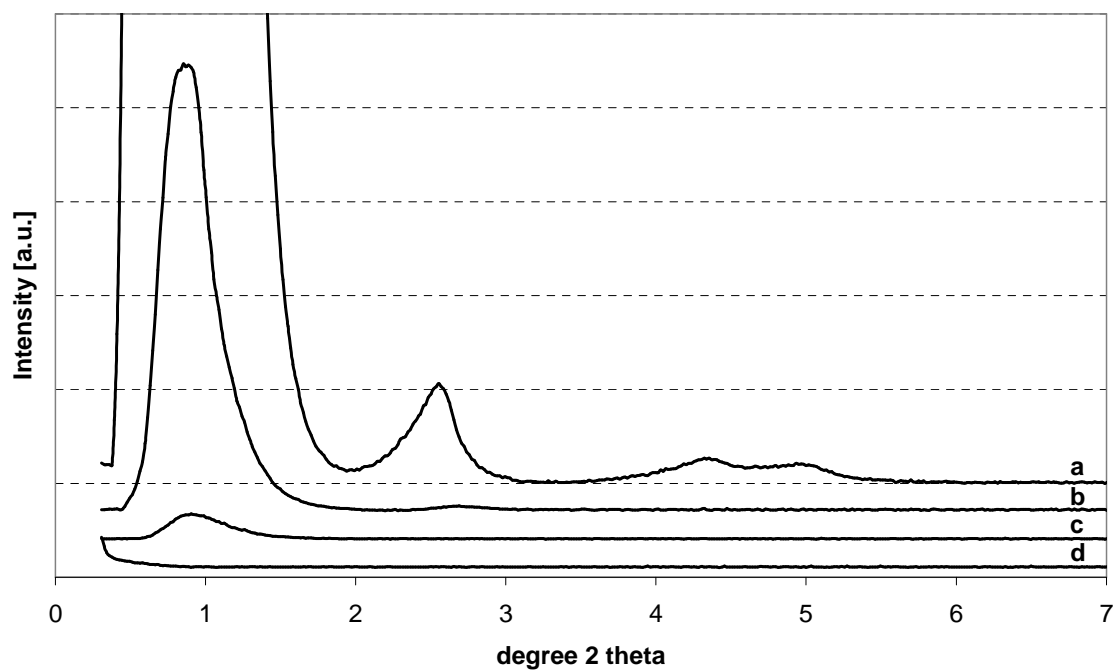


Figure 4.7: X-ray diffraction patterns of a) MCM-41 (50), b) MCM-41 (30), c) MCM-41 (20) and MCM-41 (10)

The synthesized MCM-36 samples display a slightly higher Si/Al ratio as was applied in the synthesis gels, due to the post-synthetic pillaring with TEOS. The acidity of the samples decreases from 416 $\mu\text{mol/g}$ to 149 $\mu\text{mol/g}$ with decreasing Al-content. Nitrogen physisorption indicated some unexpected microporosity and a rather low mesopore volume of 0.15 cm^3/g for the MCM-36 (10) sample with the highest Al-content. MCM-36 (20) and (30) show no microporosity and increasing mesopore volume with decreasing Al-content. MCM-36 (50) yet again displays some micropore volume and a decreased mesopore volume. X-ray diffraction patterns of MCM-36 (20) and (30) are almost identical and exhibit the typical broad signals due to delamination and damaging of the MWW layers of MCM-22(P) during the swelling procedure. The XRD of MCM-36 (10) displays significantly sharper signals, thus indicating less severe damage of the MWW layers in the final material. The MCM-36 (50) pattern, however, looks completely different. It could be identified as a slightly damaged ZSM-12 material. Transmission electron microscopy of MCM-36 (30) showed the typical arrangement of “cups” (see arrows in Fig. 4.9) in the delaminated MWW layers of a MCM-36 material.

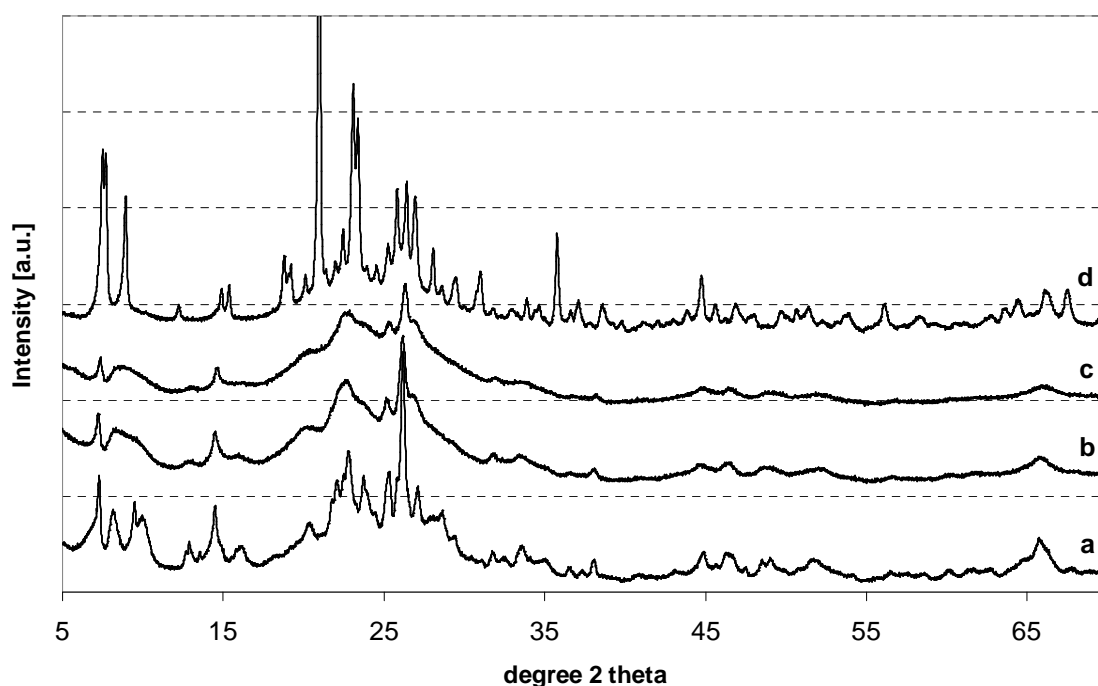


Figure 4.8: X-ray diffraction patterns of a) MCM-36 (10), b) MCM-36 (20), c) MCM-36 (30) and MCM-36 (50).

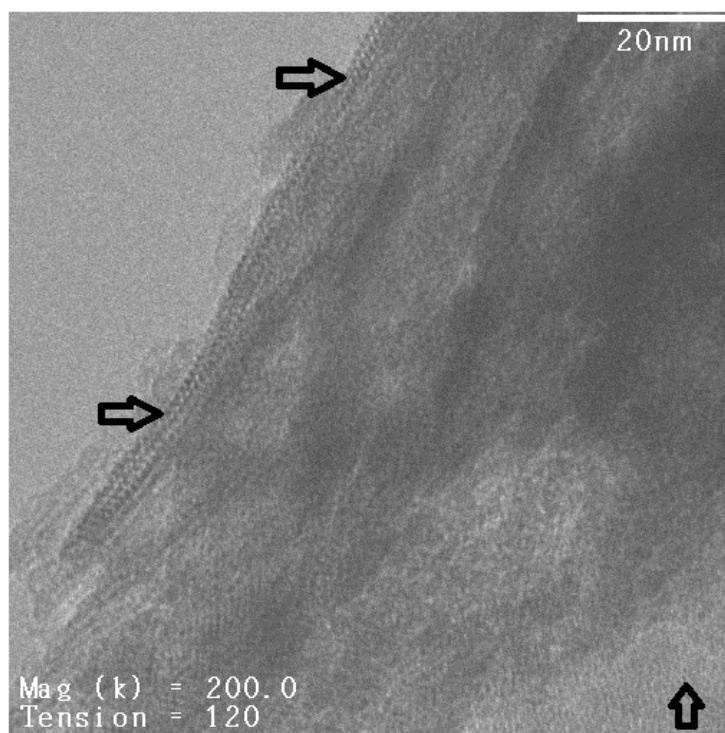


Figure 4.9: Transmission electron microscopy of MCM-36 (30).

4.3.2 Chemical pulping of deactivated zeolite

The highly viscous dark brown oil that was extracted from the deactivated zeolite was analyzed by elementary analysis and MALDI-TOF/TOF and $^1\text{H-NMR}$. The elementary composition of the material was determined as follows C: 77.2%, H: 6.7% and N: 13.1%. $^1\text{H-NMR}$ (not shown) showed a broad multiplet signal in the region of 6–7 ppm associated to aromatic protons, a diffuse signal at ~ 4.8 ppm originating from the protons on an aromatic amino-function and several “spikes” at ~ 3.5 ppm, which can be attributed to $-\text{CH}_2-$ bridges between aromatic rings. MALDI-TOF/TOF shows groups of signals which are separated by 108 m/z. Each of the signals can be subdivided into several signals divided by 15 m/z. The most dominant signal is at 284 m/z, signals with higher m/z decrease in intensity (with the exception of a signal at 764 m/z). Individual signals can be resolved until $m/z \approx 1500$.

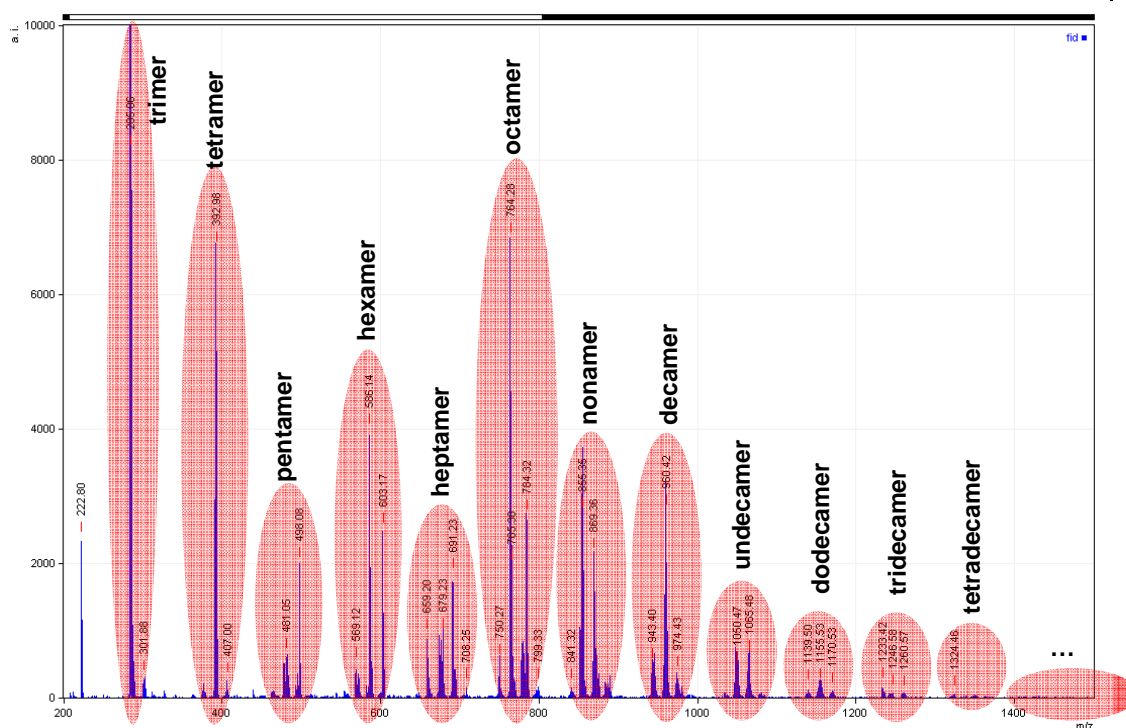


Figure 4.10: Result of MALDI-TOF analysis of the extracted material.

4.3.3 Catalytic reaction

The determined TOFs of all materials are shown in table 4.1. The parent BEA type materials display very poor activity as indicated by their TOFs of about 25 min^{-1} . The dealuminated Y-types show uniform TOFs of about 400 min^{-1} . Among the MCM-36 materials, the sample with the lowest Al-content produced no 4,4'-MDA during the test reaction and its TOF was therefore 0 min^{-1} . For MCM-36 (10), (20) and (30) TOFs of $126 \mu\text{mol/g}$, $304 \mu\text{mol/g}$ and $205 \mu\text{mol/g}$, respectively, were found. The TOFs of the MCM-41 samples increase from $164 \mu\text{mol/g}$ to $553 \mu\text{mol/g}$ with decreasing Al-content.

4.3.4 Continuous lifetime testing

Preliminary experiments showed no stable operation point could be reached, because catalyst deactivation is too fast over the applied catalysts. As the decrease in catalyst activity seems to be a linear function of time, the slope of the deactivation branch of the 4,4'-MDA yield *versus* time plots was used as indicator for catalyst deactivation.

Within the series of dealuminated Y-types the slopes of the deactivation profiles are almost identical at about $0.046\% \text{ min}^{-1}$. The maximum yields of 4,4'-MDA are increasing with increasing acidity as expected.

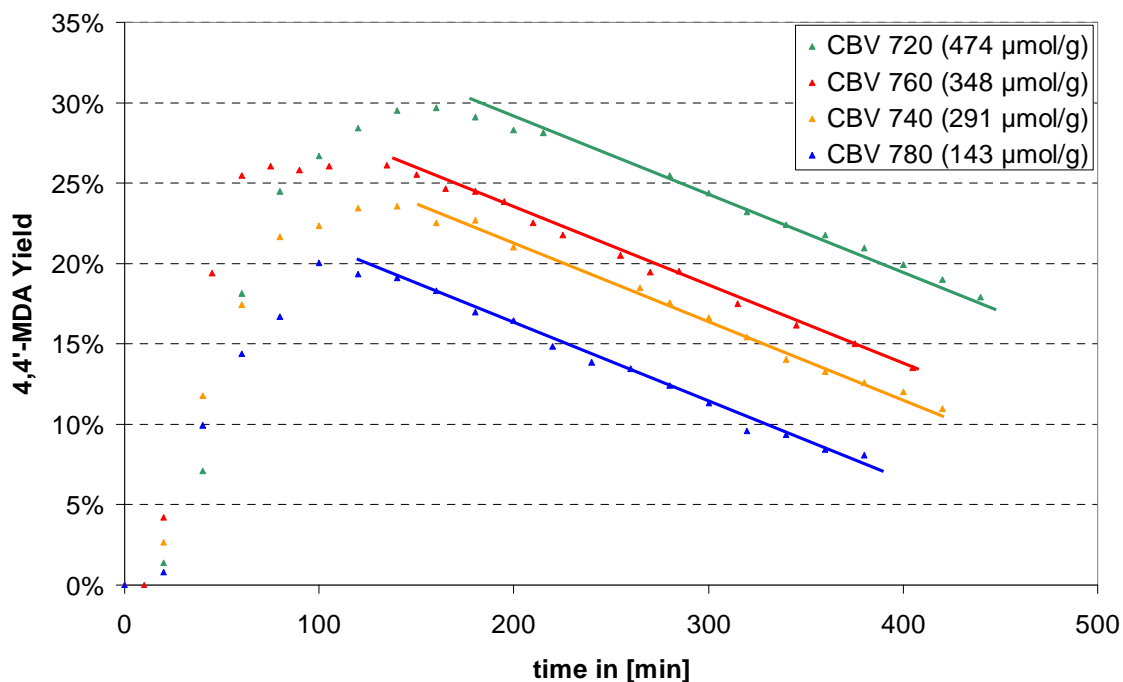


Figure 4.11: Deactivation behavior of dealuminated Y-type zeolites.

As the activity of parent zeolite BEA is significantly smaller compared to the dealuminated Y-types (as can be seen in the determined TOFs), the amount of catalyst was increased from 0.50 g to 1.50 g in order to achieve comparable yields. The determined deactivation rates are decreasing from $0.021\% \text{ min}^{-1}$ for BEA 25, to $0.012\% \text{ min}^{-1}$ over BEA 35 and $0.006\% \text{ min}^{-1}$ over BEA 150.

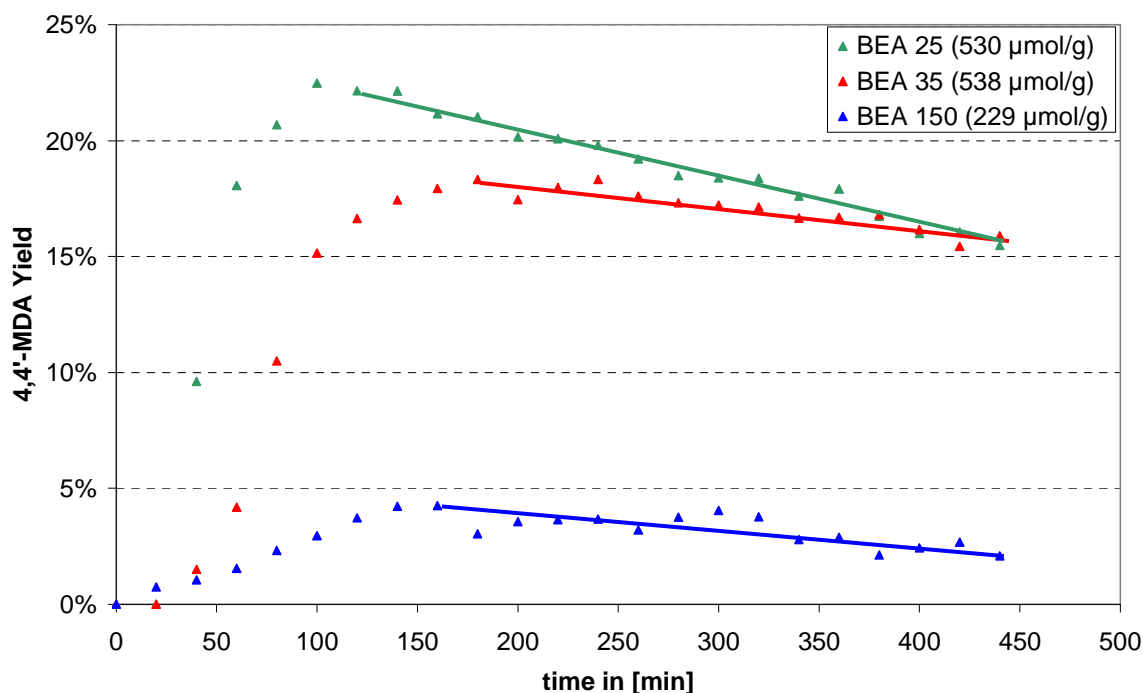


Figure 4.12: Deactivation behavior of parent BEA-type zeolites.

Deactivation of the MCM-41 materials is about 10 times slower compared to the BEA and FAU samples. It is therefore necessary to measure overnight in order to obtain reliable deactivation rates. Due to an instrument malfunction MCM-41 (10) and (20) could not be measured over night and no deactivation rates could be calculated. Their start-up behavior however is in line with the MCM-41 (30) and (50) samples and their deactivation rates should therefore be similar and close to $0.0025 \text{ \% min}^{-1}$. The determined maximum yields are in agreement with the previously determined activities.

Under identical reaction conditions MCM-36 reaches similar 4,4'-MDA yield as MCM-41. The deactivation rates over MCM-36, however, are slightly larger ($0.0035 \text{ \% min}^{-1}$). As MCM-36 (50) displayed next to none catalytic activity in the test reaction it was not tested in the continuous lifetime experiments.

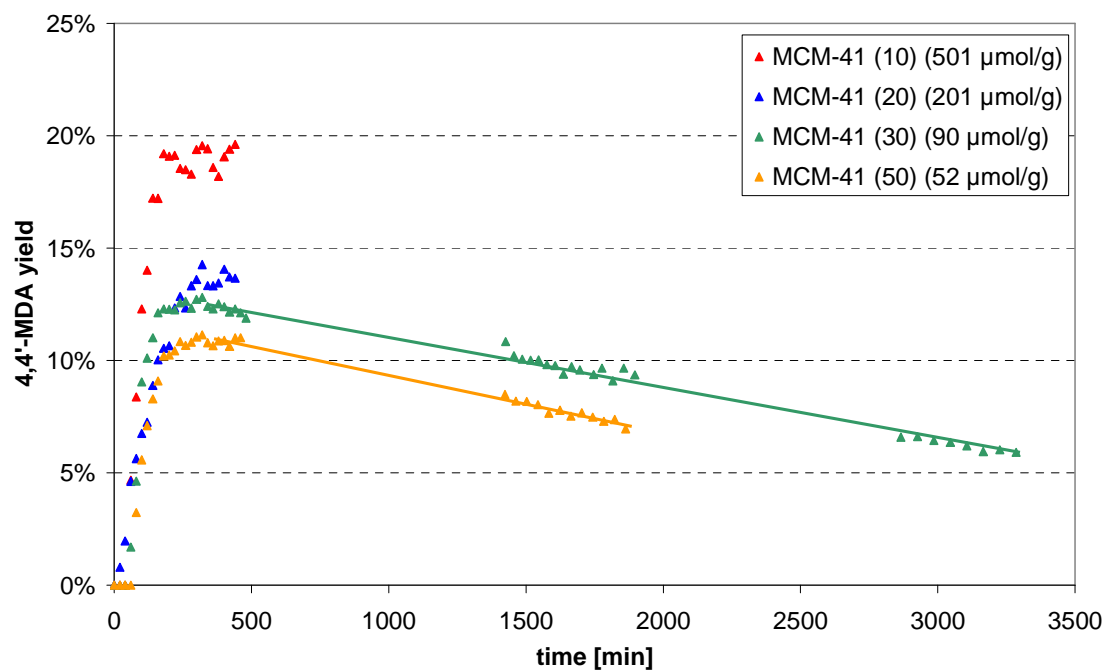


Figure 4.13: Deactivation behavior of MCM-41 materials.

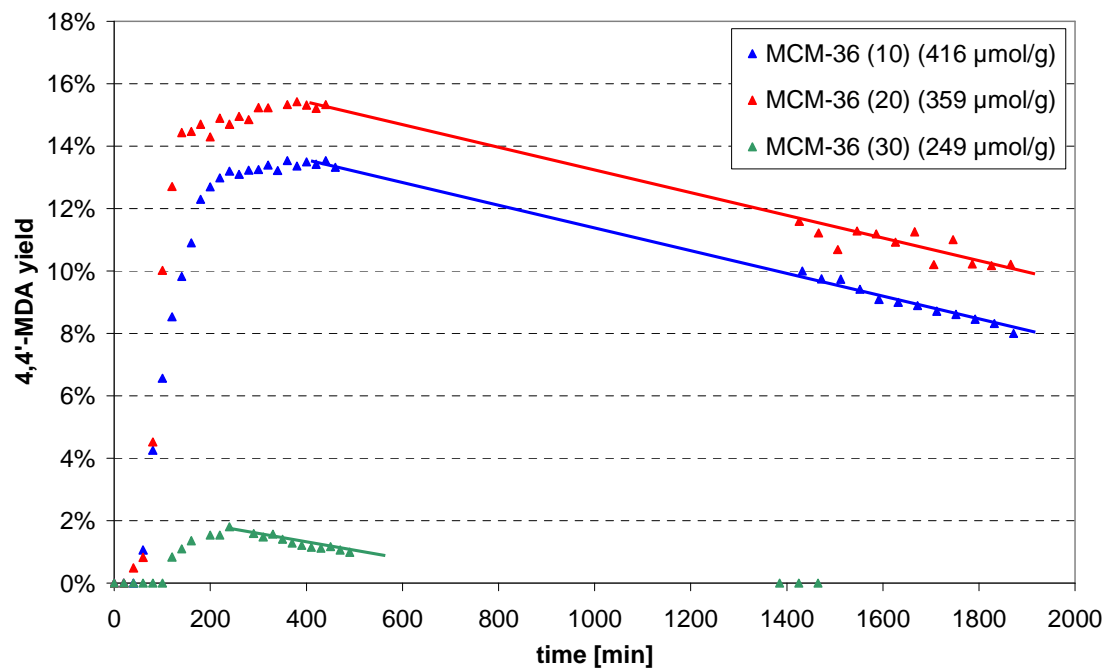


Figure 4.14: Deactivation behavior of MCM-36 materials.

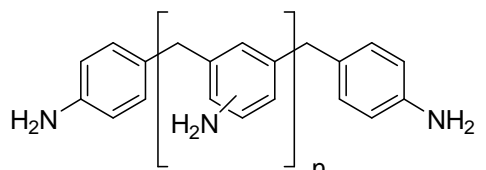
Table 4.2: *Determined deactivation rates.*

Material	Deactivation rate [% min ⁻¹]
H-BEA 25	0.021
H-BEA 35	0.012
H-BEA 150	0.006
H-CBV 720	0.045
H-CBV 740	0.047
H-CBV 760	0.047
H-CBV 780	0.046
H-MCM-41 (10)	n.n.
H-MCM-41 (20)	n.n.
H-MCM-41 (30)	0.002
H-MCM-41 (50)	0.003
H-MCM-36 (10)	0.004
H-MCM-36 (20)	0.004
H-MCM-36 (30)	0.003 ^a
H-MCM-36 (50)	n.n.

^a) 0.104 g catalyst

4.4 Discussion

The analytical data of the viscous oil, isolated out of a deactivated zeolite, is in accordance with the postulated structure of a heavy pMDA species. Carbon, Hydrogen and Nitrogen contents are in very good agreement with the hypothetical composition of the postulated species.



Element	Calculated [wt.%]	Measured [wt.%]
C	79	77
H	7	7
N	14	13

Figure 4.15: Postulated pMDA structure, theoretical and measured composition.

$^1\text{H-NMR}$ is also supporting the postulated structure. As the connectivity on the ring system can vary between the pMDA molecules, also the multitude of diffuse signals can be explained, especially of the undissolved multiplet in the region of aromatic protons, which originate from the differently substituted ring systems of the polymer. The signals of the $-\text{NH}_2$ protons could also be identified, the signal of the $-\text{CH}_2-$ units linking the monomer units could also be assigned. As the connectivity, and therefore the electronic structure, differs between the monomers, multiple singulets of similar but not identical chemical shift are to be expected and are also observed.

However, MALDI-TOF provides the most solid proof of the polymer's structure. The spacing of the observed signals is very close to the mass of one monomer unit (105 m/z). The dispartment of the signals into smaller signals with a spacing of about 15 m/z indicates the loss of amino-fragments either during the severe HF treatment or due to the exposure to the primary laser beam, as the measurements were performed in substance without the aid of a matrix. The most dominant signal at 288 m/z can be assigned to the trimer with $n = 3$, which has lost one amino function. The signal belonging to the trimer still carrying all three amino-function can be observed at 302 m/z. The signals of polymers consisting of $n = 3 - 15$, which have partially lost their $-\text{NH}_2$ functions, can be observed up to 1500 m/z. Therefore the presence of heavy pMDA

species, carrying up to 15 monomer units, in the pore system of a deactivated zeolite is proven. Due to their high molecular mass and the multiple basic binding sites ($-\text{NH}_2$ functions) these polymers adsorb strongly on the catalyst surface and the active (Brønsted acid) sites. Because of their strong bonding to the surface, desorption of such heavy pMDA is almost impossible under reaction conditions. In fact, it is a valid assumption that the polymers will bind stronger the heavier they are, making desorption more and more difficult as they get heavier. A pMDA species is also a valid nucleophile in the reaction mechanism and can be subject to further attacks as long as it is close to another Brønsted acid site and fresh monomer units (from e.g. PABA). Therefore, a once adsorbed species keeps growing until it can be desorbed from the surface. However, as the polymer grows, desorption becomes less and less likely, resulting in a speeding deactivation of the catalyst.

As already shown in previous publications^{1,2} the TOFs of the parent BEA type materials (about 25 min^{-1}) are very poor compared to the dealuminated Y-type materials (400 min^{-1}). These differences are attributed to the presence of mesopores in the dealuminated materials, which provide easier access to the Brønsted acid sites, thus avoiding pore diffusion limitation, which is limiting the reaction rate over strictly microporous materials, such as the parent BEA type zeolites. The determined TOF for MCM-36 (50) is zero as, due to the very low Al-content, the synthesis yielded ZSM-12 instead of MCM-22(P). ZSM-12 is inactive for the production of MDA as its pores and cavities are too small for the reactants to enter. In contrast to this the “cups” in the MWW layers of MCM-36 are a possible reaction site for the formation of MDA, as illustrated by the determined TOFs of up to 300 min^{-1} . The MCM-36 (10) sample shows a significantly lower activity, which can be explained by the smaller mesopore volume and more distorted structure due to the very high Al-content. The TOFs of the MCM-41 materials are obviously linked to the crystallinity of the material, as the TOFs are increasing with increasing crystallinity. Therefore, ordered mesoporous structures seem to be beneficial for high activity towards MDA formation, as the TOFs of the ordered mesoporous MCM-41 samples are about 25% higher as those of the dealuminated Y-type materials, which display randomly distributed (both in size and arrangement) mesopores.

The loss of activity of all tested catalysts proceeds linearly with reaction time. This indicates that both 4,4'-MDA formation and deactivation by pMDA formation follow the same kinetics and occur on the same active sites. Whatever influences one of the reactions has an identical impact on the other reaction, resulting in the observed linear trend. This is in agreement with our proposed mechanism for catalyst deactivation.

The deactivation rate of the dealuminated Y-type catalysts is identical, regardless of their acid site density. The same observation holds true within the MCM-41 and MCM-36 series. Only the deactivation rates over parent BEA vary within the series. Whether this is caused by differences in particle size or the amount of extra-framework Al is subject to further investigations. The negligible impact of acid site density on deactivation contradicts our first hypothesis about the positive influence of lower acid site density on catalyst lifetime. As all tested materials have Si/Al ratios between 5 and 80, this can be explained considering that in order to achieve sufficient spacing between acid sites (assuming one T-site has about 50 “neighboring” T-sites; for an isolated site there may only be one Al within these 51 sites) Si/Al ratios of at least 90 or higher are necessary. As catalytic activity is inherently linked with the amount of acid sites, the activity of such low Al samples is too low for catalytic testing.

Comparison between the different structures (at similar Si/Al ratio) revealed drastic differences in the deactivation rates of the tested materials. While the microporous materials (BEA and FAU) deactivated extremely fast, materials without micropores (MCM-36 and MCM-41) deactivated about 10 times slower. The resistance these materials possess against deactivation is attributed to solvent effects in their mesopores, enabling desorption of pMDA species from the acid sites before their length and sorption strength reaches a level that makes desorption impossible. As the acid sites in dealuminated FAU are located in the micropores (the mesopores only shorten the diffusion pathway to these active sites, thus decreasing mass transport limitation), solvent molecules cannot reach the blocked acid sites, because they are completely shielded off by the growing polymer. The absence of micropores in MCM-41 and MCM-36 is therefore the reason for their increased lifetime. IR spectroscopy of adsorbed pyridine and di-*tert*-butylpyridin will be necessary to verify that the acid sites are indeed located in the

micropores in BEA and dealuminated FAU, mainly located in mesopores in MCM-36 and exclusively in mesopores in MCM-41.

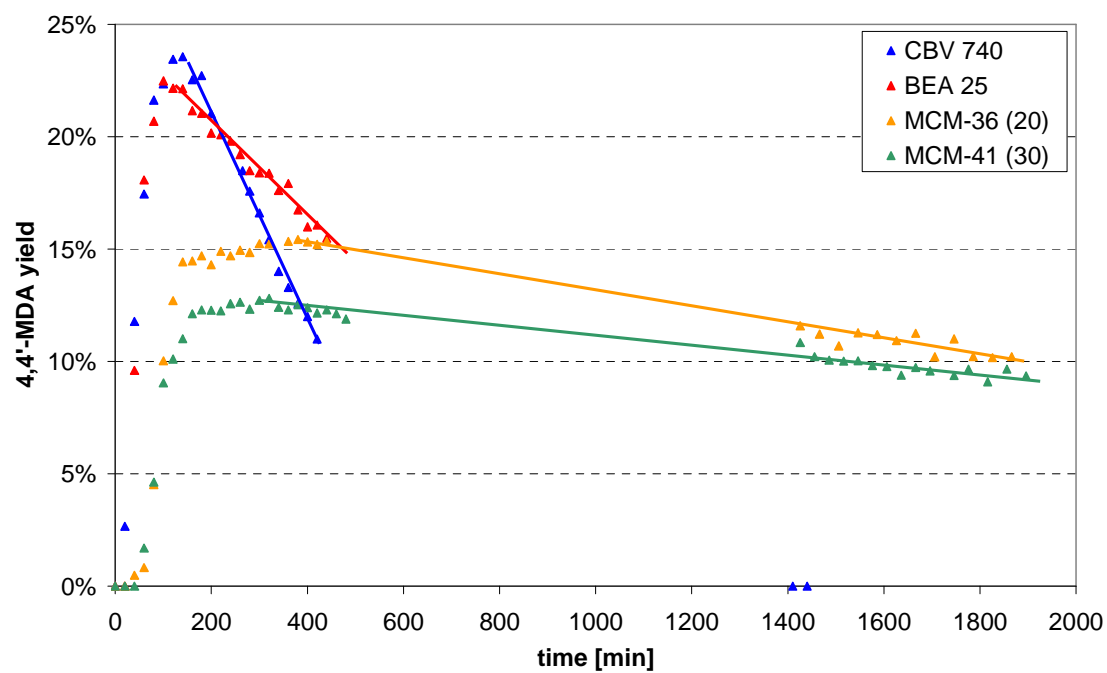


Fig. 4.16: Comparison of deactivation behavior of different catalysts.

4.5 Conclusion

Catalyst deactivation during MDA synthesis is caused by the formation of a polymeric MDA species on the catalyst surface. Due to its high molecular mass and (basic) amino-functions this species is a strong poison for solid Brønsted acidic catalysts. As the loss of catalytic activity is a linear function of time it stands to reason that both MDA formation and catalyst deactivation follow the same kinetics and are occurring on the same active sites. This observation is in line with our proposed deactivation mechanism. As the formation of this oligomer is an intrinsic part of the reaction mechanism, it is not possible to completely avoid its formation during catalysis.

Comparison of parent zeolite BEA, dealuminated FAU, MCM-41 and MCM-36 with varying Si/Al ratio showed that, while acid site density has next to none influence on a catalysts deactivation behavior, pore structure and geometry have a pronounced impact on catalyst lifetime. Materials, whose acid sites are (mainly) located in micropores, such as BEA and FAU, are subject to rapid deactivation. MCM-41, which has no micropores at all, displays significantly improved lifetime behavior. Although deactivation is still notable under the chosen reaction conditions, it proceeds more than ten times slower compared to the microporous materials. MCM-36, which also has no micropores, but consist of cups and cavities of similar size, likewise shows improved lifetime behavior, but not to the same extend as MCM-41. We suggest that solvent effects in mesopores allow desorption of pMDA species from the acid sites before their length and sorption strength reaches a level that makes desorption impossible. This is of course not possible in microporous materials, causing them to deactivate rapidly.

Overall, MCM-41 seems to be a very promising catalyst for MDA production as it displays both high activity and significantly improved lifetime compared to other materials, e.g. zeolite BEA and dealuminated FAU. Further experiments with MCM-41 samples with even larger mesopores are currently in progress in order to verify whether it is possible to decrease the rate of deactivation even further.

ACKNOWLEDGMENTS

The authors are grateful to X. Hecht for BET measurements, M. Neukamm for AAS measurements and S. Scholz and S. Wyrzgol for TEM images. MALDI-TOFTOF measurements were performed by H. Krause at the Institute of Biotechnology of the Technische Universität München. Financial and material support of the Dow Chemical Company are gratefully acknowledged. Furthermore the work at the Technische Universität München was funded by the DOW Chemical Company.

REFERENCES

- [1] M. Salzinger, M.B. Fichtl, J.A. Lercher, *Appl. Catal. A*, paper submitted.
- [2] M. Salzinger, J.A. Lercher, *Green Chemistry*, paper submitted.
- [3] T. Kugita, S. Hirose, S. Namba, *Catal. Today* **2006**, *111*, 275.
- [4] P. Botella Asuncion, J.K.P. Bosman, A. Corma, C.J. Mitchell, *US Patent 7,238,840 B2* **2007**.
- [5] A. de Angelis, P. Ingallina, C. Perego, *Ind. Eng. Chem. Res.* **2004**, *43*, 1169.
- [6] C. Perego, A. de Angelis, A. Carati, C. Flego, R. Villini, C. Rizzo, G. Bellussi, *Appl. Catal. A* **2006**, *307*, 128.
- [7] A. Corma, P. Botella, C. Mitchell, *Chem. Comm.* **2004**, *17*, 2008.
- [8] A. Corma, V. Fornes, S.B. Pergher, Th.L.M. Maesen, J.G. Buglass, *Nature* **1998**, *396*, 353.
- [9] Y.J. He, G.S. Nivarthi, F. Eder, K. Seshan, J.A. Lercher, *Microporous Mesoporous Mat.* **1998**, *25*, 207.
- [10] G.M. Kumaran, S. Garg, K. Soni, M. Kumar, J.K. Gupta, L.D. Sharma, K.S. Rama Rao, G. Murali Dhar, *Microporous Mesoporous Mat.* **2008**, *114*, 103.
- [11] B.C. Lippens, B.G. Linsen, J.H. de Boer, *J. Catal.* 1964, *3*(1), 32.
- [12] G. Hasely, *J. Chem. Phys.* **1948**, *16*(10), 932.
- [13] E.P. Barret, L.G. Joiyner, P.P. Halenda, *J. Am. Chem. Soc.* **1953**, *73*, 373.
- [14] L. Teyssier, M. Thomas, C. Bouchy, J.A. Martens, E. Guillon, *Microporous Mesoporous Mat.* **2006**, *100*, 6.
- [15] S.M. Maier, A. Jentys, J.A. Lercher, *J. Phys. Chem. C*, paper submitted.
- [16] L. Capek, J. Dedecek, B. Wichterlová, *J. Catal.* **2004**, *227*, 352.

Chapter 5

Summary / Zusammenfassung

Summary

Methylenedianiline (MDA) is an important raw material for the production of polyurethanes. It is produced from aniline and formaldehyde by an acid catalyzed reaction, for which HCl is currently applied as catalyst. Replacing mineral acids by solid acid catalysts is of considerable commercial and environmental interest. Over the last 30 years a broad variety of materials, such as ion exchange resins, clays and zeolites, were proposed as catalyst for the production of MDA. The activity of these materials for the reaction, however, was poor compared to the current HCl catalyzed process. Recently, mesoporous materials, such as ITQ-2, were tested in MDA production with promising results. Although the activity of these mesoporous materials is greatly enhanced compared to the previously tested, mostly microporous, materials deactivation of the catalyst during the synthesis is still a major problem.

In order to design a novel catalyst and to identify optimum reaction parameters a profound understanding of the underlying reaction mechanism, surface reactions and deactivation processes is vital. However, up until now the nature of these processes is unknown. It is the aim of this work to 1) clarify the reaction network and mechanism involved in the formation of MDA over solid acid catalysts, 2) to reveal the influence of pore size and geometry on catalytic activity, 3) to identify the processes leading to catalyst deactivation and 4) to develop an improved catalyst and process conditions based on this knowledge.

We were able to derive a S_N2 -type reaction mechanism and a complex reaction network from kinetic data of the reaction. Simulated concentration profiles, based on a set of differential equations describing the above mentioned reaction network and mechanism, fit the experimental data with high accuracy. The fact that the simplified reaction network is able to simulate the experimental data at different temperatures and concentrations provides solid evidence that the proposed reaction mechanism and network are indeed valid. By comparison of a non-mesoporous material (zeolite BEA) and a mesoporous catalyst (dealuminated FAU) it could be shown that the formation of MDA is limited by pore diffusion over materials without mesopores. Introducing mesoporosity into a solid

acid catalyst therefore greatly increases its activity for MDA production by avoiding mass transport limitation.

By comparing the activity of different zeolite and aluminosilicate frameworks for MDA production we were able to further demonstrate the positive impact of mesoporosity on a materials activity for MDA formation. Furthermore, it was shown that materials with pore sizes below about 6 - 7 Å, such as ZSM-5 and MCM-22, display very poor activity towards MDA formation, as the reactants are too large to enter the pore system and can not reach the acid sites located in the micropore system of the catalyst. The little activity they display can be attributed to acid sites in the pore openings. Zeolites with larger pores and possible S_N2 reaction sites (pore intersections or supercages), such as zeolite BEA and FAU, display some activity for the reaction. However, the reaction is heavily limited by pore diffusion over these materials. Zeolites that poses pores larger than 6 Å, but contain no possible S_N2 reaction sites, such as MOR, which only has a one dimensional pore system, are also inactive for MDA formation. This last observation is further proof for the proposed S_N2 -type reaction mechanism. Furthermore, it was shown that all Brønsted acid sites contribute equally to the reaction rate, regardless of their acid strength. This is plausible as their function during catalysis is to protonate the intermediate amines, thus weakening the C-N bond. The protonation of an amine is readily achieved also by weak acids. The most promising materials in terms of activity are MCM-41, SBA-15, dealuminated FAU and MCM-36.

The formation of a high molecular poly-MDA species (up to 17 phenyl units) inside the pore system was found to be the major source of catalyst deactivation. Due to its high molecular weight and multiple basic amino-functions it presents a very strong poison for the Brønsted acid sites of a solid acid catalyst. Continuous deactivation experiments with series of parent BEA, dealuminated FAU, MCM-41 and MCM-36 with different Si/Al ratio showed that acid site density has no influence on the lifetime of a catalyst. Deactivation over MCM-41 and MCM-36 is more than ten times slower compared to BEA or dealuminated FAU. This drastic gain in lifetime is caused by the absence of micropores in MCM-41 and MCM-36. We suggest that solvent effects in mesopores allow desorption of pMDA species from the acid sites before their length and sorption

strength reaches a level that makes desorption impossible. This is of course not possible in microporous materials, causing them to deactivate rapidly.

Zusammenfassung

Methyldianilin (MDA) ist ein wichtiges Rohmaterial für die Herstellung von Polyurethan. MDA wird über eine säurekatalysierte Reaktion aus Anilin und Formaldehyd gewonnen. Stand der Technik wird HCl als Katalysator eingesetzt. Es ist von großem kommerziellem und ökologischem Interesse Mineralsäuren, wie z.B. HCl, durch feste saure Katalysatoren zu ersetzen. In den letzten 30 Jahren wurde eine breite Palette an Materialien, wie z.B. Ionentauscher-Polymere, Tonerden und Zeolithe, als mögliche Katalysatoren für die Produktion von MDA vorgeschlagen. Keinem dieser Ansätze war aber Erfolg beschert, da die Reaktivität dieser Katalysatoren im Vergleich zum HCl-katalysierten Prozess zu niedrig war. Vor kurzem wurden mesoporöse Materialien, wie z.B. ITQ-2, mit viel versprechenden ersten Ergebnissen für die Produktion von MDA getestet. Obwohl diese neuen Materialien den bisherigen, großteils mikroporösen, Materialien in Punkto Aktivität deutlich überlegen sind, ist die rasche Deaktivierung der Katalysatoren während der Reaktion immer noch ein großes Problem.

Um neuartige Katalysatoren zu entwickeln und die optimalen Prozessbedingungen zu ermitteln ist es notwendig, den zugrunde liegenden Reaktionsmechanismus, Oberflächenreaktionen und Deaktivierungsprozesse zu verstehen. Leider sind diese wichtigen Eckdaten bis heute nicht bekannt. Ziel dieser Arbeit ist es 1) das Reaktionsnetzwerk und den Reaktionsmechanismus der Bildung von MDA über festen sauren Katalysatoren aufzuklären, 2) den Einfluss von Porengröße und -geometrie auf die katalytische Aktivität aufzudecken, 3) diejenigen Prozesse aufzuklären die zur Deaktivierung führen und 4) basierend auf diesen Daten einen verbesserten Katalysator und optimale Reaktionsbedingungen zu entwickeln.

Ausgehend von kinetischen Daten aus Konzentrations-Zeitprofilen der Reaktion konnten wir den S_N2 -artigen Reaktionsmechanismus und ein komplexes Reaktionsnetzwerk aufdecken. Ein Satz von Differentialgleichungen, basierend auf dem Reaktionsmechanismus und -netzwerk, ist in der Lage die beobachteten Konzentrationsverläufe mit hoher Genauigkeit wiederzugeben. Die Tatsache, dass die berechneten Konzentrationsverläufe die gemessenen Verläufe bei beliebigen Temperaturen und Konzentrationen in sehr guter Näherung simulieren beweist, dass das

zugrunde liegende Model valide ist. Durch Vergleich der Kinetik über einen nicht-mesoporösen (BEA) mit einem mesoporösen (dealuminiertes FAU) Katalysator konnte gezeigt werden, dass die Bildung von MDA über mikroporösen Materialien durch Stofftransport in Form von Porendiffusionslimitierung gehemmt wird. Durch die Verwendung von mesoporösen Katalysatoren kann die Aktivität für die MDA Herstellung durch das Ausschalten von Porendiffusionslimitierung deutlich gesteigert werden.

Diese Beobachtung konnte durch Vergleich verschiedener Zeolith- und Aluminosilikat-Gerüststrukturen belegt werden. Des Weiteren konnte gezeigt werden, dass Materialien mit Porengrößen unter 6 - 7 Å, wie z.B. ZSM-5 und MCM-22, nahezu inaktiv für die MDA Produktion sind, da die Reaktanden zu groß sind um in das Porensystem einzudringen und deshalb die Brønsted-Zentren in den Mikroporen nicht erreichen können. Zeolithe mit potentiellen S_N2 Reaktionsplätzen (Porenkreuzungen oder Superkäfige), wie z.B. BEA und FAU, zeigen messbare Aktivität für die MDA Darstellung. Die Reaktion ist aber, wie zu erwarten, stark durch Porendiffusionslimitierung gehemmt. Zeolithe, die zwar Poren von mehr als 6 Å Durchmesser, aber keine S_N2 Reaktionsplätze aufweisen, wie z.B. MOR, der nur ein eindimensionales Porensystem besitzt, zeigen ebenfalls nahezu keine Aktivität. Dies ist ein weiterer Beweis für den vorgeschlagenen S_N2 -artigen Reaktionsmechanismus. Außerdem konnte bewiesen werden, dass alle Brønsted-Zentren gleichermaßen zur Aktivität beitragen, unabhängig von ihrer Säurestärke. Dies erscheint plausibel, da die Rolle der Brønsted-Zentren im Katalysezyklus darin besteht die Amin-Intermediate zu protonieren und somit die C-N Bindung zu schwächen. Die Protonierung einesamins ist problemlos auch mit schwachen Säuren möglich.

Die Bildung hochmolekularer poly-MDA Spezies (bis zu 17 Phenyleinheiten) im Porensystem der Katalysatoren wurde als Hauptquelle der Katalysatordeaktivierung erkannt. Aufgrund ihrer hohen molekularen Masse und zahlreicher basischer Aminofunktionen stellen diese pMDA Spezies starke Gifte für die verwendeten sauren Katalysatoren dar. Durch Vergleich des Deaktivierungsverhaltens von Zeolith BEA, dealuminierten FAU, MCM-41 und MCM-36 mit verschiedenen Si/Al Verhältnissen konnte gezeigt werden, dass die Säuredichte keinen merklichen Einfluss auf die

Deaktivierung eines Katalysators hat. Die Deaktivierung von MCM-41 und MCM-36 verläuft allerdings mehr als zehnmals langsamer als von BEA und dealuminierten FAU. Dieser Unterschied ist in der Abwesenheit von Mikroporen in MCM-41 und MCM-36 begründet. Wir nehmen an, dass Lösungsmittelleffekte, die in Mesoporen eine Rolle spielen, es erlauben pMDA Spezies von der Oberfläche zu desorbieren, bevor diese eine kritische Masse (und damit Sorptionsstärke) erreichen, die eine Desorption unmöglich machen. Solche Lösungsmittelleffekte sind in Mikroporen allerdings nicht möglich, was die rasche Deaktivierung mikroporöser Materialien erklärt.